NASA Contractor Report 3968

Extensions to PIFCGT: Multirate Output Feedback and Optimal Disturbance Suppression

John R. Broussard

CONTRACT NAS1-17493
MARCH 1986

NASA

NASA Contractor Report 3968

Extensions to PIFCGT: Multirate Output Feedback and Optimal Disturbance Suppression

John R. Broussard
Information & Control Systems, Incorporated
Hampton, Virginia

Prepared by
Langley Research Center
under Contract NAS1-17493

National Aeronautics
and Space Administration

**Scientific and Technical
Information Branch**

1986

FOREWORD

The investigation described in this report was performed by Information & Control Systems, Incorporated (ICS) under Contract Number NAS1-17493 for the National Aeronautics and Space Administration, Langley Research Center, Hampton, Virginia. This work was sponsored by the Applied Controls Branch of the Flight Control Systems Division. Mr. Richard M. Hueschen served as Technical Representative monitoring this contract.

ABSTRACT

This report contains the theoretical development and the practical application of new control synthesis procedures for digital flight control systems. The new theoretical developments are the solution to the optimal multi-rate sensor output feedback problem and the solution to the problem of optimal disturbance suppression in the presence of windshear. Control synthesis is accomplished using a linear quadratic cost function, the command generator tracker for trajectory following and the proportional-integral-filter control structure for practical implementation. Extensions are made to the optimal output feedback algorithm for computing feedback gains so that the multi-rate and optimal disturbance control designs are computed and compared for the Advanced Transport Operating System (ATOPS). The performance of the designs is demonstrated using closed-loop poles, frequency domain multi-input sigma and eigenvalue plots and detailed nonlinear 6-DOF aircraft simulations in the terminal area in the presence of windshear.

ACKNOWLEDGEMENT

The author would like to thank Dr. Nesim Halyo for numerous stimulating discussions and suggestions, and in particular, for developing the convergent algorithm to solve the Generalized Riccati Equation given in Appendix A.

TABLE OF CONTENTS

TABLE OF CONTENTS

LIST OF TABLES

LIST OF FIGURES

LIST OF SYMBOLS

In general, matrices are represented by capital letters and vectors are underscored; exceptions to these rules are only made when they are contradicted by standard aerodynamic notation.

VARIABLE	DESCRIPTION
A	Discrete time feedforward matrix Fundamental matrix (continuous-time system)
a	Acceleration
a_h	Component of the vehicle acceleration normal to the local level plane
B	Control effect matrix (continuous-time system). Feedforward matrix for measurement noise sources
b	Bias estimate
C	Control law feedback gains Feedforward matrix for disturbance noise
D	Control observation matrix
D_w	Windshear to aircraft state distribution matrix
E	Disturbance effect matrix (continuous-time system)
e	2.71828 ...
f	Vector-valued nonlinear function
G(s)	Plant transfer function
g	Magnitude of gravitational acceleration vector
H	Command observation matrix
H_1^2	Euler angle transformation from Frame 1 axes to Frame 2 axes
h	Distance from the aircraft's cg to the Earth's surface, positive down

VARIABLE	DESCRIPTION
I	Identity matrix
i	Index integer
J	Cost functional matrix
j	$\sqrt{-1}$
K	Gain value
k	Index integer
L	skew symmetric matrix
ℓ	Number of commands
$\hat{M}$	Cross weighting matrix in Linear Quadratic Regulator cost function
m	Mass of the vehicle Number of controls Meters
N	Number of time steps
n	Number of states
P	Riccati matrix in the optimal limited state feedback regulator problem
p	Rotational rate about the body x-axis
Q	State weighting matrix
q	Rotational rate about the body y-axis
R	Control weighting matrix
r	Rotational rate about the body z-axis Number of fast rate samples in the slowest rate
S	Covariance matrix in the optimal limited state feedback regulator problem Feedforward matrix with disturbances present
s	Laplace transform variable Windshear gradient

VARIABLE	DESCRIPTION
T	Thrust
T_L	Time-to-go to an end of segment
t	Time
U	Windshear x-axis velocity
u	Body x-axis velocity component Control Vector
V	Velocity magnitude Measurement noise covariance matrix
v	Body y-axis velocity component Control difference
W	Process noise covariance matrix Windshear z-axis velocity
w	Body z-axis velocity component White noise Gaussian vector
X_o	Covariance matrix of state initial conditions
x	Position along the x-axis State vector
y	Position along the y-axis Observation vector
z	Position along the z-axis

VARIABLE (GREEK)	DESCRIPTION
α	Wind-body pitch Euler Angle (angle of attack)
β	Negative of wind-body yaw Euler angle (sides-slip angle)
Γ	Discrete time control effect matrix
γ	Inertial-velocity axis pitch Euler angle (flight-path angle)
Δ	Periodically time-varying multi-rate matrix
δ	Delta function

VARIBLE (GREEK)	DESCRIPTION
δ_E	Elevator deflection
δ_{EC}	Elevator command
δ_e	Elevator state
δ_T	Throttle deflection
δ_{TC}	Throttle command
ζ	Damping ratio
η	Gaussian noise
θ	Inertial-body pitch Euler angle
λ	Eigenvalue
ν	Measurement Gaussian noise
ξ	Integrator state
ρ	Air density
Σ	Summation
σ	Real part of an eigenvalue in radians/sec Singular value
Φ	Discrete-time system matrix
ϕ	Inertial-body axis roll Euler angle
Ω	Quad matrix inverse partition
ω	Frequency in radians/sec Imaginary part of an eigenvalue

SUBSCRIPTS	DESCRIPTION
a	Accommodate disturbance
B	Body axis
b	Bias
C	Command value

SUBSCRIPTS	DESCRIPTIONS
CL	Closed-loop
E	Earth-relative axis
e	Error quantity
f	Full state feedback Fast rate sample
GS	Ground speed
g	Gust
H	Horizontal
i	Element index for vectors and matrices
j	Element index for vectors and matrices
k	Sampling instant index
L	Lagrange
m	Model variable
o	Nominal value
s	Stochastic Slow rate sample
t	Transient
u	Velocity component along body x-axis
v	Velocity component along body y-axis
w	Velocity component along body z-axis Windshear
x	Horizontal perpendicular to y and z
y	Horizontal perpendicular to x and z
z	Vertical perpendicular to x and y

SUPERSCRIPTS	DESCRIPTION
E	Earth (inertial) axis
T	Transpose of matrix
-1	Inverse of matrix

PUNCTUATION	DESCRIPTION
$(\dot{})$	Derivative of quantity with respect to time
$(\bar{})$	Combined variable
$\partial(\ )/\partial(\ )$	Partial derivative of one variable with respect to another
$E\{\ \}$	Expected value
$\Delta(\ )$	Perturbation variable
$(\ )^*$	Star trajectory
$(\hat{})$	Estimated quantity Discrete cost function weighting matrix
∞	Infinity
$\int$	Integral
$(\tilde{})$	Difference between variable and star trajectory
$\otimes$	Kronecker product

ACRONYM	CORRESPONDING PHRASE
ATOPS	Advanced Transport Operating Systems
CAS	Calibrated Airspeed
CGT	Command Generator Tracker
DIALS	Digital Integrated Automatic Landing System
DOF	Degrees of Freedom
dB	Decibels
EPR	Engine Pressure Ratio
GPS	Global Positioning System
INS	Inertial Navigation System
kt	Knot
LQR	Linear Quadratic Regulator
lim	Limit
lb	Pound

ACRONYM	CORRESPONDING PHRASE
ln	Natural log
MAX	Maximum
MEAS	Measurement
MLS	Microwave Landing System
MIN	Minimum
MXEPR	Maximum Engine Pressure Ratio
NASA	National Aeronautics and Space Administration
PIF	Proportional Integral Filter
RNAV	Area Navigation
rad	Radians
SIGN	Signum Function
sec	Seconds
Tas	True Airspeed
tr	Trace Function

1. INTRODUCTION

The proportional-integral-filter (PIF) control system is an established control structure which can be used to design and implement digital flight control systems for aircraft. The theoretical developments for the PIF design using an infinite time quadratic cost function, one sample rate and full state feedback is presented in Refs. 1-3. Successful flight tests of a PIF-like structure in position form is presented in Ref. 4.

The PIF control system in a state space representation integrates well with the command generator tracker (CGT). The CGT, discussed in Refs. 5, 6 and 7 is a method for computing the trajectory plant states and controls follow when the output of a plant is tracking the output of a model. The command model can be used to generate coordinated turn paths for heading changes, smooth vertical height transfer paths for height changes or a complete three dimensional trajectory for curved path tracking.

At present, all flight tested PIF control laws have been designed using full state feedback and the Linear Quadratic Regulator (LQR) approach. Problems have occurred due to the inability to accurately represent the actual aircraft dynamics and flight control system in the design aircraft model. For example, aircraft actuator dynamics, disturbance dynamics (gusts, wind shear), complementary filter states, and analog prefilter states have not been included in PIF design models used to determine the full state feedback control law gains. The LQR approach would require feedback of all these states as well as the orginal aircraft states in an attempt to favorably, but impractically, alter filter and actuator dynamics as well as the aircraft's response to disturbances. The LQR approach guarentees $\pm$ 60 DEG of phase margin and -6dB to + ∞ dB gain margin, but may require feedback loops that are not practical to implement.

The difficulties with full state feedback have been partially alleviated by extensive simulation of the PIF control system using a realistic truth model and iterative adjustment of quadratic weights in a more simple synthesis model.

A fundamentally better approach is to use limited state or output feedback in the PIF synthesis procedure. The realistic truth model can be used as the design synthesis model. Only practical measurements and feedback paths are used to design the PIF control gains.

Until recently, the main obstacle to the use of the limited state feedback approach has been the unavailability of a fast, reliable algorithm to compute the output feedback gains. This obstacle was recently removed by an algorithm whose derivation is presented in Ref. 8. This algorithm provides a fast, efficient and reliable method to obtain optimal output feedback gains for large order systems.

Some progress in the use of output feedback, PIF and the CGT has been made in Ref. 3. Chapter 2 in the report begins with a more complete derivation of PIF with output feedback. The discussion in Chapter 2 provides the basic developments that the rest of this report will further investigate and generalize.

The first generalization, discussed in Section 2A, is the use of the hierarchical or nested approach to design the feedback gains using optimal optimal output feedback. In the nested approach, one control loop can be designed with specific feedback paths, the designed control loop is closed, then the next control loop can be designed with a different configuration of feedback paths. Only a few small changes are required to convert the output feedback PIF design procedure to use the nested approach. The nested approach is a form of decentralized control, Ref. 9.

The theory of digital control design using PIF/CGT currently includes only the case where control effectors and sensor are all operating or sampled at the same rate. Due to practical considerations, sensor measurements, such as INS (Inertial Navigation System) signals, and external position measurements such as MLS (Microwave Landing System), GPS (Global Positioning System) and ILS (Instrument Landing System) may be available only at sample rates slower than the rates of onboard sensors used to stabilize inner loops. The space shuttle is an example of a vehicle which had to contend with sensor measurements available at different rates. An important problem is to extend the PIF/CGT output feedback approach to the multi-rate sensor measurement case. The multi-rate sensor approach is particularly useful in designing inner-loop/outer-loop sensor control systems. The optimal multi-rate limited state feedback approach is derived in Chapter 3 and represents an important new contribution to multi-rate control synthesis.

A contribution to the theory of control system design using the CGT was made in Ref. 5 in the research area of model following, and in the research area of disturbance suppression. Thus far, no flight tested PIF/CGT control systems have exploited the disturbance suppression aspects of the CGT theory.

An aircraft disturbance that has received considerable attention recently is windshear. In some types of windshear in the aircraft landing approach, the aircraft encounters a head wind, then a strong vertical downdraft, then a tail wind. Windshear is a type of disturbance that a flight control system must safely accommodate.

A number of questions arise, however, that must be resolved in order to design a PIF/CGT control system with windshear disturbance assommodation. CGT theory assumes that the plant dynamics do not affect the disturbance dynamics.

Windshear disturbance models are different, in that certain aircraft states (height) affect the windshear dynamics. The first problem to be resolved then is to rederive CGT theory with the aircraft states coupled to the disturbance states. This derivation of a more advanced version of CGT theory is presented in Section 4B. A new type of matrix algebraic equation occurs during the development of the advanced CGT and is recognized as a generalized matrix Riccati equation. A new, globally stable algorithm which finds a solution to the generalized matrix Riccati equation is presented in Appendix A.

Another CGT problem concerns the fact that the theory solves the disturbance problem for perfect accommodation. Perfect or ideal disturbance accommodation is accommplished by feeding forward the disturbance states in the control system. The disturbance states are not usually all exactly measured and the disturbance states not measured are sometimes difficult to estimate. A third question regarding the use of CGT theory concerns the use of imperfect, but adequate and practical, disturbance suppression. Given a PIF/CGT control system, which does not perfectly accommodate windshear, what is the effect of windshear on the aircraft states and how does changing the control gains alter the aircraft closed-loop windshear response? This question is resolved in Section 4C.

The steady state effect of stochastic disturbances on the closed-loop system is solved in Section 4C using a new concept called the stochastic star trajectory. The stochastic star trajectory shows that the steady state reponse of a plant driven by deterministic and stochastic disturbances decomposes into a deterministic plant response and a random or stochastic plant response. In Section 4D, a new type of optimal output feedback cost function is created using the stochastic star trajectory. The quadratic cost is used to minimize the zero mean stochastic component and an algebraic matrix cost is added to

the quadratic cost in order to minimize the deterministic component of the steady state plant response.

The last section in the report applies the new theories of multi-rate output feedback and disturbance accommodation to the design of an ATOPS aircraft path tracking autopilot. Nonlinear six degree of freedom simulations are made with the aircraft flying through wind shears. The energy probe sensor, Refs. 10 and 11, is included in the measurement vector and the effect on the design is presented.

2. OPTIMAL LIMITED STATE FEEDBACK PROPORTIONAL-INTEGRAL-FILTER/COMMAND GENERATOR TRACKER

A derivation of the discrete-time output feedback proportional-integral-filter (PIF) control system combined with the command generator tracker (CGT) is presented in this chapter. A full state feedback derivation of the PIFCGT control system is presented in Ref. 2. The first derivation uses the usual integrated optimal output feedback approach. The nested approach, which takes advantage of the structure flexibility offered by output feedback is presented in the second section. In the nested approach, each control loop is designed individually in a sequential order. Each designed control loop is closed before the feedback gains for the next controller is computed.

A. Integrated Approach

The perturbation state vector, Δx, of the aircraft dynamics driven by control inputs, Δu, and white Gaussian noise Δw is augmented to contain the perturbation control driven by the control rate, Δv. Integral states $\Delta\xi$ are augmented to the state vector to operate on the aircraft output, Δy,

$$\begin{bmatrix} \Delta\dot{x} \\ \Delta\dot{\xi} \\ \Delta\dot{u} \end{bmatrix} = \begin{bmatrix} A & 0 & B \\ H & 0 & D \\ 0 & 0 & 0 \end{bmatrix} \begin{bmatrix} \Delta x \\ \Delta\xi \\ \Delta u \end{bmatrix} + \begin{bmatrix} 0 \\ 0 \\ I \end{bmatrix} \Delta v + \begin{bmatrix} \Delta w \\ 0 \\ 0 \end{bmatrix} \tag{1}$$

The control, Δv, is used to optimize the quadratic cost function

$$J = \int_0^\infty [\Delta x \ \Delta\xi \ \Delta u]^T Q \begin{bmatrix} \Delta x \\ \Delta\xi \\ \Delta u \end{bmatrix} + \Delta v^T R \Delta v dt \tag{2}$$

The control rate, Δv, is assumed to be constant over the sample interval, Δt. The continuous-time optimization problem is converted to the equivalent

discrete optimization problem using the sampled data regulator, Ref. 12.

After converting the system dynamics and cost function, further simplifying assumptions and objectives are introduced into the optimization problem. Both the control position, Δu, and control rate, Δv, are required to be constant over the sample period. The discrete integrator $\Delta\xi_k$ is to be implemented digitally using Euler integration. The measurement noise present in the integration of Δy by the integrator is neglected. The objective of the control, Δv, is changed from driving aircraft states to zero, to driving Δy, used in the integrator, to track the output, Δy_m, of the command model:

$$\Delta x_{mk+1} = \Phi_m \Delta x_{mk} + \Gamma_m \Delta u_{mk+1} \tag{3}$$

$$\Delta y_{mk} = H_m \Delta x_{mk} + D_m \Delta u_{mk+1} \tag{4}$$

In the derivation to follow, Δu_m is assumed to change once at t_o and remain constant thereafter. In implementation, the command model control input is not constant and the command model dynamics are nonlinear. When Δu_m is changing, Δy and Δy_m become mismatched and their error is governed by the closed-loop dynamics and the integrator. When Δu_m is constant, Δy eventually tracks Δy_m along the star trajectory, Δx^* and Δu^* (assuming no plant parameter variations). The star trajectory is discussed in Refs. 1 to 3. The star trajectory is a linear system version of the nominal trajectory which is used when discussing tracking for nonlinear systems.

The star trajectory for discrete-time systems with a constant command model input is determined from

$$\begin{bmatrix} \Delta x_k^* \\ \Delta u_k^* \end{bmatrix} = \begin{bmatrix} A_{11} & A_{12} \\ A_{21} & A_{22} \end{bmatrix} \begin{bmatrix} \Delta x_{mk} \\ \Delta u_m \end{bmatrix} \tag{5}$$

The feedforward matrices A_{ij} satisfy

$$\begin{bmatrix} (\Phi-I) & \Gamma \\ H & D \end{bmatrix} \begin{bmatrix} A_{11} & A_{12} \\ A_{21} & A_{22} \end{bmatrix} = \begin{bmatrix} A_{11} & (\Phi_m - I) & A_{11}\Gamma_m \\ & H_m & D_m \end{bmatrix} \tag{6}$$

which is a solvable matrix algebraic equation. The star trajectory is a convenient notational abstract and is not generated in implementation.

The tracking objective of the control law is introduced into the design by defining the variables

$$\Delta\tilde{x}_k = \Delta x_k - \Delta x_k^* \; ; \quad \Delta\tilde{u} = \Delta u_k - \Delta u_k^* \tag{7a,b}$$

$$\Delta\tilde{v}_k = \Delta v_k - A_{21}\,(\Delta x_{m,k+1} - \Delta x_{m,k})/\Delta t \tag{8}$$

$$\Delta\tilde{\xi}_k = \Delta\xi_k - \Delta\xi_k^* \; ; \quad \Delta\bar{x}_k^T = \left[\Delta\tilde{x}_k^T \;\; \Delta\tilde{u}_k^T \;\; \Delta\tilde{\xi}_k^T\right] \tag{9a,b}$$

and the discrete cost function,

$$J = \sum_{k=-1}^{\infty} \left\{ \Delta\bar{x}_k^T \hat{Q}\Delta\bar{x}_k + 2\Delta\bar{x}_k^T \hat{M}\Delta\tilde{v}_k + \Delta\tilde{v}_k^T \hat{R}\Delta\tilde{v}_k \right\} \tag{10}$$

At this stage, the star trajectory for the integrator is undefined, but is chosen as part of the optimization process.

The star trajectory, by definition, must satisfy the plant dynamics with noise sources set to zero. Subtracting the star trajectory dynamics from the plant dynamics and using Eqs. 7 to 9 yields

$$\begin{bmatrix} \Delta\tilde{x}_{k+1} \\ \Delta\tilde{\xi}_{k+1} \\ \Delta\tilde{u}_{k+1} \end{bmatrix} = \underbrace{\begin{bmatrix} \Phi & 0 & \Gamma \\ \Delta t H & I & \Delta t D \\ 0 & 0 & I \end{bmatrix}}_{\bar{\Phi}} \begin{bmatrix} \Delta\tilde{x}_k \\ \Delta\tilde{\xi}_k \\ \Delta\tilde{u}_k \end{bmatrix} + \underbrace{\begin{bmatrix} 0 \\ 0 \\ I\Delta t \end{bmatrix}}_{\bar{\Gamma}} \Delta\tilde{v}_k + \underbrace{\begin{bmatrix} w_k \\ 0 \\ 0 \end{bmatrix}}_{\bar{w}_k} \tag{11}$$

The plant is assumed to be tracking the model for constant Δu_m previous to $t_o=0$. The cost function starts at -1 since Δu , and $\Delta\xi^*_{-1}$ are to be determined. The quantities, Δu^*_{-1} and Δx^*_{-1} are defined in Eq. 10 using $\Delta u_{m,o}$ instead of $\Delta u_{m,-1}$. The standard use of the linear quadratic cost function is to regulate nonzero initial condition states to zero. The cost function in Eq. 10 is constructed so that the non-zero initial conditions in $\Delta\bar{x}_{-1}$ are caused by the change in the command input at $t_o=0$. The control law optimally transfers the system between star trajectories for a step change in u_m. In practice, the control law performs well if u_m changes intermittently or "slowly" varies.

To clarify the construction of the cost function, a brief scenario of a step change in Δu_m is presented. At k=-2, the plant is tracking the star trajectory and the error quantities $\Delta\tilde{x}_{-2}$ and $\Delta\tilde{u}_{-2}$ are zero. At k=-1, the star trajectory for Δx^*_{-1} and Δu^*_{-1} is switched to the trajectory being generated by the new Δu_m which will occur at k=0. The command model is chosen so that the command model states at time k=0 are immediately affected by the command model control at k=0 as shown in Eqs. 3 and 4. The new star trajectory causes large errors to appear in $\Delta\bar{x}_{-1}$ which is being weighted in the cost function. The control increment, $\Delta\tilde{v}_{-1}$, a variable to be optimally chosen, feeds back the large errors to generate $\Delta\tilde{u}_o$. The control $\Delta\tilde{u}_o$, generated from $\Delta\tilde{u}_{-1}$ and $\Delta\tilde{v}_{-1}$, immediately moves in a direction to reduce the tracking error when Δu_m is changed at k=0. What this means in implementation, as shown in Eq. 3 and Eq. 40, is that $u_{m,k}$ is fed forward and directly affects u_k. Similarly, starting the cost function at k=-1 and computing the star trajectory at k=-1, using Δu_m at k=0, aids in choosing $\Delta\xi^*_{-1}$ as discussed in the next paragraph. If the cost function were to start at k=0, (the standard optimal control starting point for the non-zero initial condition problems), then $\Delta\tilde{v}_o$ would be optimally chosen to affect Δu_1.

The proper optimal value for Δu_o and $\Delta \xi_o$ would be unclear; Δu_o and $\Delta \xi_o$ would become unknown initial conditions in the plant state vector.

The next assumption used is that not all aircraft states are available for feedback. The states that are available for feedback are represented as

$$\begin{bmatrix} \Delta\tilde{y}_{MEAS} \\ \Delta\tilde{u} \\ \Delta\tilde{\xi} \end{bmatrix}_k = \underbrace{\begin{bmatrix} C & 0 & 0 \\ 0 & I & 0 \\ 0 & 0 & I \end{bmatrix}}_{\bar{C}} \begin{bmatrix} \Delta\tilde{x} \\ \Delta\tilde{u} \\ \Delta\tilde{\xi} \end{bmatrix}_k + \underbrace{\begin{bmatrix} \Delta v_k \\ 0 \\ 0 \end{bmatrix}}_{\bar{v}_k} \tag{12}$$

The states observed from the aircraft model are corrupted by white Gaussian measurement noise $\Delta\bar{v}_k$ with covariance, $\bar{V}$. The control internal states Δu and $\Delta\xi$ are noise free.

The globally optimum solution for the problem construced thus far is a singular Kalman filter combined with the full state feedback gain from the linear quadratic regulator, Ref. 13. The globally optimum solution is not necessarily robust, Ref. 14, or straightforward to implement. Greater flexibility in the control design process is obtained if the quadratic cost is minimized using a prespecified control structure. The class of control laws considered in this chapter are restricted to be of the form

$$\Delta\tilde{v}_k = -\,[K_y \; K_u \; K_\xi] \begin{bmatrix} \Delta\tilde{y}_{MEAS} \\ \Delta\tilde{u} \\ \Delta\tilde{\xi} \end{bmatrix}_k = -\,\bar{K}\,\bar{y}_k \tag{13}$$

For the plant dynamics shown in Eq. 11, the feedback gain constraint shown in Eq. 13 and the following conditions:

$$E\left\{\Delta\bar{w}_k\right\} = 0 \qquad E\left\{\Delta\bar{w}_k\ \Delta\bar{w}_k^T\right\} = W\delta_{kj} \tag{14a,b}$$

$$E\left\{\Delta\bar{v}_k\right\} = 0 \qquad E\left\{\Delta\bar{v}_k\ \Delta\bar{v}_j^T\right\} = V\delta_{kj} \tag{15a,b}$$

$$E\left\{\Delta\bar{x}_{-1}\ \Delta\bar{x}_{-1}^T\right\} = X_o \tag{16}$$

$$E\left\{\Delta\bar{w}_k\ \Delta\bar{v}_j^T\right\} = E\left\{\Delta\bar{w}_k\ \Delta\bar{x}_{-1}^T\right\} = E\left\{\Delta\bar{v}_k\ \Delta\bar{x}_{-1}^T\right\} = 0 \tag{17}$$

the cost function in Eq. 10 is modified as follows (Ref. 15):

$$J(\bar{K}) = \frac{1}{2}\left(J_t + J_s\right) \tag{18}$$

$$J_t = \sum_{k=-1}^{\infty} \Delta\bar{x}_{tk}^T\ \hat{Q}\ \Delta\bar{x}_{tk} + 2\ \Delta\bar{x}_{tk}^T\ \hat{M}\ \Delta\tilde{v}_{tk} + \Delta\tilde{v}_{tk}^T\ \hat{R}\ \Delta\tilde{v}_{tk} \tag{19}$$

$$J_s = \lim_{N\to\infty} \frac{1}{N+1}\ E\left\{\sum_{k=-1}^{N} \Delta\bar{x}_{sk}^T\ \hat{Q}\ \Delta\bar{x}_{sk} + 2\ \Delta\bar{x}_{sk}^T\ \hat{M}\ \Delta\tilde{v}_{sk} + \Delta\tilde{v}_{sk}^T\ \hat{R}\ \Delta\tilde{v}_{sk}\right\} \tag{20}$$

$$J(\bar{K}) = \frac{1}{2}\ tr\left\{P(W + X_o)\right\} + \frac{1}{2}\ tr\left\{\bar{K}^T\ (\bar{\Gamma}^T\ P\bar{\Gamma} + \hat{R})\ \bar{K}\ V\right\} \tag{21}$$

The notation "tr" denotes the trace of a matrix. J_t is the transient cost with noise sources set to zero while J_s is the average stochastic cost. The trade-off between J_t and J_s is accomplished by varying X_o with respect to W. The effect of X_o is like adding pseudo process noise to the plant to improve control system robustness. The benefits of using Eq. 18 as the cost function are discussed further in Ref. 15.

The matrix, P, in Eq. 21, satisfies the Riccati-like equation

$$P = \bar{\Phi}_{CL}^T\ P\ \bar{\Phi}_{CL} + \bar{C}^T\ \bar{K}^T\ \hat{R}\ \bar{K}\ \bar{C} + \hat{Q} - \hat{M}\ \bar{K}\ \bar{C} - \bar{C}^T\ \bar{K}^T\ \hat{M}^T \tag{22}$$

Φ_{CL} is the stable closed-loop plant matrix,

$$\Phi_{CL} = \bar{\Phi} - \bar{\Gamma}\,\bar{K}\,\bar{C} \tag{23}$$

The necessary conditions for $J(\bar{K})$ to have a minimum, are derived in Ref. 8 The necessary conditions are:

- o There must exist a gain $\bar{K}$ so that $\bar{\Phi}_{CL}$ is stable.
- o The gain $\bar{K}$ must satisfy

$$\left(\bar{\Gamma}^T P \bar{\Gamma} + \hat{R}\right)\bar{K}\left(\bar{C}\,S\,\bar{C}^T + V\right) = \left(\bar{\Gamma}^T P \bar{\Phi} + \hat{M}^T\right) S\bar{C}^T \tag{24}$$

where

$$S = \bar{\Phi}_{CL}\, S\bar{\Phi}_{CL}^T + (W + X_o) + \bar{\Gamma}\,\bar{K}\,\bar{V}\,\bar{K}^T\,\bar{\Gamma}^T \tag{25}$$

A gain which satisfies the necessary conditions is not necessarily unique.

The next objective is to determine $\Delta\xi^*$. The choice of $\Delta\xi^*$ has a strong effect on Δu_o, the first control effort that occurs when it is learned the Δu_m has changed. From a purely tracking viewpoint, the noise sources cause the states and controls to vary with zero mean about a trajectory which transfers the states and controls between star trajectories. The cost minimized to determine the state and control trajectory which intercepts the star trajectory is given by Eq. 19 where the noise sources are zero. Substituting the control system into the cost, J_t, yields,

$$J_t = \sum_{k=-1}^{\infty} \Delta\bar{x}_{tk}^T \overbrace{\left[\hat{Q} - \hat{M}\,\bar{K}\,\bar{C} - \bar{C}^T\,\bar{K}^T\,\hat{M}^T + \bar{C}^T\,\bar{K}^T\,\hat{R}\,\bar{K}\,\bar{C}\right]}^{\bar{Q}} \Delta\bar{x}_{tk} \tag{26}$$

Only the initial value of the state vector is unknown in the transient cost,

$$J_t = \sum_{k=-1}^{\infty} \Delta\bar{x}^T_{t,-1} \left(\bar{\Phi}^T_{CL}\right)^{k+1} \bar{Q} \left(\bar{\Phi}_{CL}\right)^{k+1} \Delta\bar{x}_{t,-1} \tag{27}$$

The infinite sum converges to a matrix, $\bar{P}$, if Φ_{CL} is stable. The matrix $\bar{P}$ is the same as the matrix P shown in Eq. 22, hence;

$$J_t = \Delta\bar{x}^T_{-1} \bar{P} \Delta\bar{x}_{-1} = \Delta\bar{x}^T_{-1} \begin{bmatrix} P_{xx} & P_{xu} & P_{x\xi} \\ P^T_{xu} & P_{uu} & P_{u\xi} \\ P^T_{x\xi} & P^T_{u\xi} & P_{\xi\xi} \end{bmatrix} \Delta\bar{x}_{-1} \tag{28}$$

For tracking without noise, $\Delta\bar{x}_{-1}$ is given by

$$\Delta\bar{x}_{-1} = \begin{bmatrix} \Delta x_{-1} \\ \Delta u_{-1} \\ \Delta\xi_{-1} \end{bmatrix} - \begin{bmatrix} \Delta x^*_{-1} \\ \Delta u^*_{-1} \\ \Delta\xi^*_{-1} \end{bmatrix} \tag{29}$$

but

$$\begin{bmatrix} \Delta\bar{x}_{-1} \\ \Delta u_{-1} \end{bmatrix} = \begin{bmatrix} A_{11} & A_{12} \\ A_{21} & A_{22} \end{bmatrix} \begin{bmatrix} \Delta x_{m-1} \\ \Delta u_{m-1} \end{bmatrix} \tag{30}$$

hence

$$\Delta\bar{x}_{-1} = \begin{bmatrix} A_{12}(u_{m-1} - u_{mo}) \\ A_{22}(u_{m-1} - u_{mo}) \\ \Delta\xi^*_{-2} - \Delta\xi^*_{-1} \end{bmatrix} \tag{31}$$

Treating the increment in the integrator as an unknown, $\bar{\xi} = \Delta\xi^*_{-2} - \Delta\xi^*_{-1}$, the value for $\bar{\xi}$ that minimizes J is given by

$$\partial J/\partial\bar{\xi} = 0 \tag{32}$$

The solution is

$$P_{22}\,\bar{\xi} + (P^T_{x\xi}\,A_{12} + P^T_{u\xi}\,A_{22})\,(\Delta u_{m-1} - \Delta u_{mo}) = 0 \tag{33}$$

From Eq. 33, the value for $\Delta\xi^*_k$ must be given by

$$\Delta\xi^*_k = \begin{bmatrix} 0 & A \end{bmatrix} \begin{bmatrix} \Delta x_{mk} \\ \Delta u_{mk+1} \end{bmatrix} \tag{34}$$

where

$$A = -P^{-1}_{\xi\xi}\left[P^T_{x\xi}\,A_{12} + P^T_{u\xi}\,A_{22}\right] \tag{35}$$

Evaluating Eq. 34 at k=-1 and k=0 and substituting into Eq. 33 demonstrates that the solution is correct. Using the feedback gain in Eq. 13, the perturbation control system is

$$\Delta\tilde{u}_k = \Delta\tilde{u}_{k-1} + \Delta t\,\Delta\tilde{v}_{k-1} \tag{36}$$

$$\Delta\tilde{v}_{k-1} = (I - \Delta t\,K_u)\,\Delta\tilde{v}_{k-2} - K_y\,(\Delta y_{k-1} - \Delta y_{k-2}) - K_\xi\,(\Delta\tilde{\xi}_{k-1} - \Delta\tilde{\xi}_{k-2}) \tag{37}$$

The previous value, $\Delta\tilde{v}_{k-2}$, is subtracted from $\Delta\tilde{v}_{k-1}$ to obtain the incremental expression in Eq. 37. The perturbation variables and trim variables are eliminated from the incremental expression using a large number of substitutions

and cancellations (discussed in Ref. 2). The use of output feedback in Eq. 37 does not significantly alter the derivation in Ref. 2, which is for full state feedback. The implementable equations for the PIFCGT control law become,

$$u_k = u_{k-1} + \Delta t\, v_{k-1} + A_{21}\,(x_{m,k} - x_{m,k-1}) \tag{38}$$

$$e_{k-1} = y_{MEAS,k-1} - C\,A_{11}\,x_{m,k-1} \tag{39}$$

$$v_{k-1} = (I - \Delta t\, K_u)\, v_{k-2} - K_y(e_{k-1} - e_{k-2}) - \Delta t\, K_\xi(y_{k-2} - y_{m,k-2})$$

$$+ (\overbrace{K_\xi\, A + K_y\, C\, A_{12} + K_u\, A_{22}}^{K_{um}})(u_{m,k} - u_{m,k-1}) \tag{40}$$

The gain, K_{um}, which feeds forward the command generator forcing function increment, is a linear combination of feedback and feedforward gains. The effect of K_{um} is to improve the transient response of the outer-loop control system by changing closed-loop system zeroes without affecting closed-loop poles.

B. Nested Design Approach

The output feedback control synthesis approach discussed in the previous section is an integrated control design. Each measurement is fed back to every controller. The feedback gains from measurements to controllers are all computed simultaneously. If a control actuator fails or a control actuator saturates, and becomes inoperative for a length of time, the control feedback network undergoes a structural change. The feedback gains designed simultaneously do not guarantee that the reduced controller situation will remain stable.

Situations also occur where it is not desirable to feedback every measurement to every controller. In a jet transport, for example, feeding back pitch rate, normal acceleration and the height integrator output to the elevator, but

not to the throttle, can be a reasonable design constraint.

The nested design approach allows the designer to specify the measurement vector for each controller. In addition, each control loop is designed in a sequential hierarchical manner with critical control loops designed first. The design of the nested approach begins by choosing a controller and the corresponding desired measurement vector. The optimal output feedback optimization problem is solved to obtain the feedback gain. The control loop is closed to create a new plant model. The next controller in the hierarchy is used for design with a new measurement vector and the process is repeated. The controllers can fail or saturate in a particular order from the outer most controller loop to the inner loop and the closed-loop system remains stable.

Since the development of the nested approach, two alternative techniques have been developed that are considered to be more useful for designing decentralized measurement feedback loops and accommodating control surface failure. An integrated approach to the decentralized measurement feedback loop problem is presented in Ref. 16. An integrated appraoch to the combined decentralized control and control surface failure problem is solved in Ref. 17.

The nested approach applied to the PIFCGT design begins as in Section 2A up to Eq. 21. Computational considerations require that the design should proceed from control loop to control loop with no change to matrix dimensions. The design matrices $\bar{\Phi}$, $\bar{\Gamma}$, $\bar{C}$, $\hat{Q}$, $\hat{M}$, $\hat{R}$, $\hat{W}$, $\bar{V}$ are used to form a second group of design matrices where one controller is used for design and there are other controllers that have not been designed yet. Controllers not designed yet and integrators not used for feedback yet, cause $\bar{\Phi}$ to have uncontrollable states with eigenvalues at 1.

The following operations are performed on the second group of design matrices ($\bar{\Phi}_1$, $\bar{\Gamma}_1$, $\bar{C}_1$, $\hat{Q}_1$, $\hat{M}_1$, $\hat{W}_1$, $\bar{V}_1$) to create a stabilizable optimization problem:

$\bar{\Gamma}_1$ - null columns in Γ for controls not being used

$\bar{C}_1$ - null rows in $\bar{C}$ for measurements not being used. These measurements include controls and integrators not desired.

$\hat{Q}_1$ - not changed from $\hat{Q}$

$\hat{M}_1$ - not changed from $\hat{M}$

$\hat{R}_1$ - not changed from $\hat{R}$ but must have full rank

$\bar{\Phi}_1$ - Diagonal elements of $\bar{\Phi}$ for control states not previously designed; integrator states not being used, are artifically stabilized by placing a small negative number in the diagonal position.

$\hat{W}_1$ - Positive scalars are added to diagonal elements of W for the same control and integrator states stabilized in $\bar{\Phi}_1$

$\bar{V}_1$ - Positive scalars are added to diagonal elements of $\bar{V}$ for measurements whose rows are nulled in $\bar{C}_1$

The changes cause $\bar{\Phi}_1$ to be stabilizable; control states and integrator states which are neutrally stable and not used in the design are made unobservable, uncontrollable and stable. The states that are uncontrollable and unobservable do not cause P and S to reduce in rank. The changes to $\bar{V}_1$ and $\hat{R}$ (if required) cause $\bar{\Gamma}_1^T P \bar{\Gamma}_1 + \hat{R}$ and $\bar{C}\ S\ \bar{C}^T + V_1$ to be invertible so that Eq. 24 has a solution. None of the changes adversly affect the design of the control gains for the nested loop being synthesized. An alternative, but computationally unattractive approach, would be to reduce the dimensions of the design matrices to eliminate unobservable and uncontrollable states.

After a design for one control loop is completed the system matrices are altered as follows:

$$\bar{\Phi} = \bar{\Phi} - \bar{\Gamma}_1\ K_1\ \bar{C}_1 \tag{41}$$

$$\hat{Q} = \hat{Q} + \bar{C}_1^T\ K_1^T\ \hat{R}\ K_1\ \bar{C}_1 - \hat{M}\ K_1\ \bar{C}_1 - \bar{C}_1^T\ K_1^T\ \hat{M}^T \tag{42}$$

$$\hat{W} = \hat{W} + \bar{\Gamma}_1 K_1 V K_1^T \bar{\Gamma}_1^T \tag{43}$$

The alterations reflect the fact the K_1 is now a known matrix and must be absorbed into the design. Using the new system matrices, $\bar{\Phi}_2$, $\bar{\Gamma}_2$, $\bar{C}_2$, ... etc. can be computed for the second controller in the hierarchy. The operations continue until all control loops are designed. When the nested design is completed by solving m different optimal output feedback problems, the total control system is

$$v_k = \left[K_1 \bar{C}_1 + K_2 \bar{C}_2 + \ldots K_m \bar{C}_m\right] \bar{x}_k = \bar{K} \bar{C} \bar{x}_k \tag{44}$$

The PIFCGT design requires that the $\bar{P}$ matrix defined in Eq. 28 be used to find $\Delta\xi^*$. The $\bar{P}$ matrix in Eq. 28 is equal to the $\bar{P}_m$ cost matrix obtained in the last nested design performed to obtain K_m.

3. OPTIMAL MULTI-RATE LIMITED STATE FEEDBACK

A multi-rate control system has sensor measurements, computer calculations and control commands performed at a variety of different sampling intervals. The advantage of using a multi-rate control system is to better utilize the computational capability of the on-board computer. Critical control loops with fast dynamics can operate at fast sampling rates, while less critical control loops with slow dynamics can be processed at slow rates with little degradation in overall performance. Multi-rate control designs have been incorporated in a number of digital flight control systems for aircraft.

Computational capacity is continually improving, making the need for multi-rate controls less attractive. A problem that will persist, however, is that all sensor measurements will propoably not be available at the fastest computational rate of the control computer.

An aircraft, for example, using a full complement of on-board and external sensors, (such as the microwave landing systems (MLS)), often does not have these sensors all sampled at the same rate. Body mounted sensors are available, or may have the equipment potential to be available, at a fast sample rate, while INS and aircraft geographical position measurements are available at slower rates.

A procedure that allows each sensor to be feed back at the sensor's sample rate is developed in this chapter using an optimal, multi-rate output feedback synthesis approach. The increased computational capacity available when control commands are computed at different rates is also a feature of multi-rate sensor feedback. The control computations for slow rate sensors need only be performed at the sample rate of the sensor. The control calculations for control commands to the actuators are assumed to be performed at the fastest control rate. Each sample rate of the different sensors is assumed to be an integer multiple of the fastest control rate. The assumption placed on

the sensors sample rate guarantees that the design model and cost function for the control design problem are periodic in time.

Optimal multi-rate limited state feedback does not appear to have been previously investigated in the literature. The optimal full state feedback multi-rate control problem has been investigated in Ref. 18 using a state-space approach. The optimal control solution in Ref. 18 is a periodic sequence of full state feedback gains. The derivation in this report will take advantage of the structure flexibility offered by optimal limited state feedback and require that the multi-rate gain which minimizes the quadratic cost function be constant. A constant feedback gain reduces implementation complexity over a periodic sequence of feedback gains, particularly as the number of cycles in the period increases.

A. Aircraft System Model and Cost Function

The measurement vector is assumed to be separable into two groups, y_f and y_s. The y_f measurements are sampled at the fast rate r_f. The y_s vector is the collection of sensors sampled at rates slower than the fast rate. The number of slower rates is assumed to be n. The n slow rates are grouped into the ordered sequence r_{s1}, r_{s2}, ... r_{sn}. The fast rate divided by the slowest rate, r_f/r_{sn}, is an integer r. The sequence of fast and slow measurements repeats itself every r samples in a periodic fashion. A slow rate sensor output is held constant at the last sampled value during the fast sample times when the slow rate sensor is not being measured.

The linear time-invariant model of the dynamics of the plant is represented at the fastest rate as follows:

$$\bar{x}_{k+1} = \Phi \bar{x}_k + \Gamma u_k + w_k \tag{45}$$

The control is u_k and $\bar{x}_k$ is the state vector of the plant model. The white, zero mean Gaussian process noise disturbing the plant is w_k with covariance W. The control system is assumed to have the fixed structure,

$$u_k = - \begin{bmatrix} K_f & K_s \end{bmatrix} \begin{bmatrix} y_{f,k} \\ y_{s,k} \end{bmatrix} \tag{46}$$

K_f and K_s are, respectively, the fast rate constant feedback gain and the slow rate constant feedback gain. The measurement vectors are represented as

$$y_{f,k} = C_f \bar{x}_k + v_{f,k} \qquad k = 1, 2, 3 \ldots \tag{47}$$

$$i = 1, 2, \ldots, n$$

$$y_{si,k} = C_{si} \bar{x}_k + v_{si,k} \qquad k = 1, \; r_f/r_{si} + 1 \; , \; 2 \; r_f/r_{si} + 1 \; , \; \ldots \tag{48}$$

$$y_{si,k} = y_{si,k-1} \qquad k \neq 1, \; r_f/r_{si} + 1 \; , \; 2 \; r_f/r_{si} + 1 \; , \; \ldots \tag{49}$$

The vector y_{si} is composed of the slow sensor measurements that are available at the slow rate r_{si}. At the fast rate, Eq. 48 represents time samples when the y_{si} slow rate sensors are measured. The y_{si} measurement is held constant for all other fast sample times as shown in Eq. 49. The white Gaussian measurement noise sources are $v_{f,k}$ and $v_{si,k}$ with covarances V_f and V_{si}.

Equations 47 to 49 can be combined with the system model dynamics in Eq. 45 using the periodically time-varying matrix Δ_k. The periodically time-varying matrix Δ_k is given by

$$\Delta_k = \begin{bmatrix} \delta_{s1,k} & & & 0 \\ & \delta_{s2,k} & & \\ & & \ddots & \\ 0 & & & \delta_{sn,k} \end{bmatrix} \tag{50}$$

where

$$i = 1, 2, \ldots, n$$

$$\delta_{si,k} = \begin{array}{l} I;\ k = 1,\ r_f/r_{si} + 1,\ 2\,r_f/r_{si} + 1, \ldots \\ 0;\ k \neq 1,\ r_f/r_{si} + 1,\ 2\,r_f/r_{si} + 1, \ldots \end{array} \tag{51}$$

Using the periodic matrix, Δ_k, the slow measurements can be combined into the measurement vector y_s and represented at the fast rate as follows:

$$y_{s,k+1} = \Delta_{k+1}\,(C_s\,\bar{x}_{k+1} + v_{s,k+1}) + (I - \Delta_{k+1})\,y_{s,k} \tag{52}$$

The combined plant and slow rate measurement periodic model has the following state space representation:

$$\begin{bmatrix} I & 0 \\ -\Delta_{k+1}\,C_s & I \end{bmatrix} \begin{bmatrix} \bar{x}_{k+1} \\ y_{s,k+1} \end{bmatrix} = \begin{bmatrix} \Phi & 0 \\ 0 & (I-\Delta_{k+1}) \end{bmatrix} \begin{bmatrix} \bar{x}_k \\ y_{s,k} \end{bmatrix} + \begin{bmatrix} \Gamma \\ 0 \end{bmatrix} u_k + \tag{53}$$

$$\begin{bmatrix} I & 0 \\ 0 & \Delta_{k+1} \end{bmatrix} \begin{bmatrix} \bar{w}_k \\ v_{s,k+1} \end{bmatrix}$$

The diagonal elements of Δ_k switch between zero and one depending on whether the slow measurement should be represented by Eq. 48 or Eq. 49 at the kth sampling interval. The Δ_k matrix repeats itself every r samples. One cycle of Δ_k matrices are written as Δ_1, Δ_2, ... Δ_r. The slow measurement observation matrix C_s is composed of the matrices C_{s1} to C_{sn} packed rowwise,

$$C_s = \begin{bmatrix} C_{s1} \\ C_{s2} \\ \vdots \\ C_{sn} \end{bmatrix} \tag{54}$$

Multiplying Eq. 53 by the matrix $\begin{bmatrix} I & 0 \\ \Delta_{k+1} C_s & I \end{bmatrix}$, the inverse of the left partition matrix in Eq. 53, changes the plant representation to a standard time-varying difference equation format:

$$\underbrace{\begin{bmatrix} \bar{x}_{k+1} \\ y_{s,k+1} \end{bmatrix}}_{x_{k+1}} = \underbrace{\begin{bmatrix} \Phi & 0 \\ \Delta_{k+1} C_s \Phi & I-\Delta_{k+1} \end{bmatrix}}_{\Phi_k} \underbrace{\begin{bmatrix} \bar{x}_k \\ y_{s,k} \end{bmatrix}}_{x_k} + \underbrace{\begin{bmatrix} \Gamma \\ \Delta_{k+1} C_s \Gamma \end{bmatrix}}_{\Gamma_k} u_k +$$

$$\underbrace{\begin{bmatrix} I & 0 \\ \Delta_{k+1} C_s & \Delta_{k+1} \end{bmatrix}}_{E_k} \underbrace{\begin{bmatrix} \bar{w}_k \\ v_{s,k+1} \end{bmatrix}}_{w_k} \tag{55}$$

The feedback control system is represented as follows using the periodic model states:

$$u_k = -\underbrace{\begin{bmatrix} K_f & K_s \end{bmatrix}}_{K} \underbrace{\begin{bmatrix} C_f & 0 \\ 0 & I \end{bmatrix}}_{C} \begin{bmatrix} \bar{x}_k \\ y_{s,k} \end{bmatrix} - \underbrace{\begin{bmatrix} K_f & K_s \end{bmatrix}}_{K} \underbrace{\begin{bmatrix} v_{f,k} \\ 0 \end{bmatrix}}_{v_k} \tag{56}$$

The cyclic nature of the matrices shown in Eq. 55, means that there are recurring moments in time where the matrix cycle begins and ends. Substituting Eq. 56 into Eq. 55, the periodic closed-loop plant representation for a cycle which begins at index k and ends at index k+r-1 is

$$x_{k+1} = (\Phi_1 - \Gamma_1 KC)\, x_k + E_1\, w_k - \Gamma_1\, Kv_k \tag{57}$$

$$x_{k+2} = (\Phi_2 - \Gamma_2 KC)\, x_{k+1} + E_2\, w_{k+1} - \Gamma_2\, Kv_{k+1} \tag{58}$$

$$\vdots$$

$$x_{k+r} = (\Phi_r - \Gamma_r KC)\, x_{k+r-1} + E_r\, w_{k+r-1} - \Gamma_r\, Kv_{k+r-1} \tag{59}$$

where

$$\Phi_1 = \begin{bmatrix} \Phi & 0 \\ \Delta_2 C_s \Phi & I-\Delta_2 \end{bmatrix};\quad \Phi_2 = \begin{bmatrix} \Phi & 0 \\ \Delta_3 C_s \Phi & I-\Delta_3 \end{bmatrix};\quad \cdots$$

$$\cdots \Phi_{r-1} = \begin{bmatrix} \Phi & 0 \\ \Delta_r C_s \Phi & I-\Delta_r \end{bmatrix};\quad \Phi_r = \begin{bmatrix} \Phi & 0 \\ \Delta_1 C_s \Phi & I-\Delta_1 \end{bmatrix} \tag{60}$$

The other matrices in Eqs. 57 to 59 are similiarly defined.

The multi-rate optimal output feedback cost function can be constructed in a variety of ways. The following simple approach is used in this development. The sampled-data regulator cost function at the fast rate in standard form is given by

$$J = \lim_{N\to\infty} \frac{1}{2N} E \left\{ \sum_{i=0}^{N} \begin{bmatrix} \bar{x}_i^T & u_i^T \end{bmatrix} \begin{bmatrix} \bar{Q} & \bar{M} \\ \bar{M}^T & R \end{bmatrix} \begin{bmatrix} \bar{x}_i \\ u_i \end{bmatrix} \right\} \tag{61}$$

The weighting matrices $\bar{Q}$, $\bar{M}$, and R can be obtained from a continuous quadratic cost and plant model using the fast sample rate and a suitable software package such as ORACLS, Ref. 19. The additional state, y_s caused by the slow measurements, is arbitrarily introduced in the cost with no weight

$$J = \lim_{N\to\infty} \frac{1}{2N} E\left\{ \sum_{i=0}^{N} \begin{bmatrix} x_i^T & u_i^T \end{bmatrix} \begin{bmatrix} Q & M \\ M^T & R \end{bmatrix} \begin{bmatrix} x_i \\ u_i \end{bmatrix} \right\} \tag{62}$$

$$Q = \begin{bmatrix} \bar{Q} & 0 \\ 0 & 0 \end{bmatrix}; \quad M = \begin{bmatrix} \bar{M} \\ 0 \end{bmatrix} \tag{63}$$

The y_s states are a part of $\bar{x}$ and can be weighted using $\bar{Q}$. The design objective is to determine the control system gain shown in Eq. 56 which minimizes the cost shown in Eq. 62.

It can be shown that if a periodic system is stable, then the covariance of the states of the periodic system reach a periodic steady-state. Assuming the periodic system shown in Eq. 55 can be stabilized using Eq. 56, the periodic steady-state covariances are the solution to the following sequence of equations:

$$S_2 = (\Phi_1 - \Gamma_1 K C)\, S_1\, (\Phi_1 - \Gamma_1 K C)^T + E_1 W E_1^T + \Gamma_1 K V K^T \Gamma_1^T \tag{64}$$

$$S_3 = (\Phi_2 - \Gamma_2 K C)\, S_2\, (\Phi_2 - \Gamma_2 K C)^T + E_2 W E_2^T + \Gamma_2 K V K^T \Gamma_2^T \tag{65}$$

$$\vdots$$

$$S_1 = (\Phi_r - \Gamma_r K C)\, S_r\, (\Phi_r - \Gamma_r K C)^T + E_r W E_r^T + \Gamma_r K V K^T \Gamma_r^T \tag{66}$$

The periodicity is shown in Eq. 66 where the covariance matrix equation cycle begins to repeat itself. In periodic steady-state, the cost function can be rewritten as

$$J = \lim_{N_s \to \infty} \frac{1}{2rN_s} \sum_{i=0}^{N_s} J_{cycle} = \frac{1}{2r} J_{cycle} \tag{67}$$

The integer, N_s, is the number of periodic cycles in N. J_{cycle} is the sum of the weighted states and controls for one cycle.

$$J_{cycle} = tr \left\{ \overbrace{(Q - M K C - C^T K^T M^T + C^T K^T R K C)}^{\hat{Q}} \left[S_1 + S_2 + \ldots + S_r \right] \right\}$$

$$+ r \, tr \left\{ K^T R K V \right\} \tag{68}$$

B. Necessary Conditions For An Optimal Controller

Adjoining the equality constraints shown in Eqs. 64 to 66 to Eq. 68 yields,

$$J = \frac{1}{2r} J_{cycle} +$$

$$tr (-S_2 + (\Phi_1 - \Gamma_1 K C) S_1 (\Phi_1 - \Gamma_1 K C)^T + E_1 W E_1^T + \Gamma_1 K V K^T \Gamma_1^T) P_1^T + \ldots$$

$$+ tr (-S_1 + (\Phi_r - \Gamma_r K C) S_r (\Phi_r - \Gamma_r K C)^T + E_r W E_r^T + \Gamma_r K V K^T \Gamma_r^T) P_r^T \tag{69}$$

The Lagrange multipliers are P_1 to P_r. The conditions necessary for J to have a minimum are $\partial J/\partial S_1 = 0 \ldots \partial J/\partial S_r = 0$, $\partial J/\partial P_1 = 0 \ldots \partial J/\partial P_r = 0$, $\partial J/\partial K = 0$. The $\partial J/\partial S_i$ sequence determines the equations for P_i:

$$P_r = (\Phi_1 - \Gamma_1 K C)^T P_1 (\Phi_1 - \Gamma_1 K C) + \hat{Q} \tag{70}$$

$$P_1 = (\Phi_2 - \Gamma_2 K C)^T P_2 (\Phi_2 - \Gamma_2 K C) + \hat{Q} \tag{71}$$

$$\vdots$$

$$P_{r-1} = (\Phi_r - \Gamma_r K C)^T P_r (\Phi_r - \Gamma_r K C) + \hat{Q} \tag{72}$$

The necessary condition $\partial J/\partial K$ determines the equation for the feedback gain K:

$$R K (C S_1 C^T + \ldots + C S_r C^T) + (\Gamma_1^T P_1 \Gamma_1 + \ldots \Gamma_r^T P_r \Gamma_r + r R) K V +$$

$$\Gamma_1^T P_1 \Gamma_1 K C S_1 C^T + \ldots + \Gamma_r^T P_r \Gamma_r C S_r C^T = \Gamma_1^T P_1 \Phi S_1 C^T + \ldots +$$

$$\Gamma_r^T P_r \Phi_r S_r C^T + M^T \left[S_1 C^T + \ldots S_r C^T\right] \tag{73}$$

4. NUMERICAL APPROACHES

The numerical solution for S_i and P_i given a feedback gain matrix, K, are obtained by expressing one of the covariance matrices and one of the cost matrices at the slow rate. Starting with Eq. 64, S_2 can be substituted into Eq. 65 and so on until Eq. 66 is reached. When Eq. 66 is reached the only unknown is the matrix S_1,

$$S_1 = \hat{\Phi}_1 \, S_1 \, \hat{\Phi}_1 + W^* \tag{74}$$

where

$$\hat{\Phi}_j = (\Phi_r - \Gamma_r \, K \, C) \, (\Phi_{r-1} - \Gamma_{r-1} \, K \, C) \, \ldots \, (\Phi_j - \Gamma_j \, K \, C) \tag{75}$$

$$\hat{\Phi}_{r+1} = I \tag{76}$$

$$\bar{W}_j = E_j \, W \, E_j^T + \Gamma_j \, K \, V \, K^T \, \Gamma_j^T \tag{77}$$

$$W^* = \sum_{j=1}^{r} \hat{\Phi}_{j+1} \, \bar{W}_j \, \hat{\Phi}_{j+1}^T \tag{78}$$

The covariance equation shown in Eq. 74 is easily solved. Once S_1 is known, the other covariance matrices can be reconstructed from Eqs. 64 to 66. The matrix $\hat{\Phi}_1$ is the representation of the plant at the slowest rate. The periodic system is stable for a given K matrix if $\hat{\Phi}_1$ has eigenvalues within the unit circle.

The solution for the cost matrices, P_i, are similarly determined:

$$P_r = \tilde{\Phi}_r^T \, P_r \, \tilde{\Phi}_r + Q^* \tag{79}$$

$$\tilde{\Phi}_j^T = (\Phi_1 - \Gamma_1 K C)^T (\Phi_2 - \Gamma_2 K C)^T \ldots (\Phi_j - \Gamma_j K C)^T \tag{80}$$

$$\tilde{\Phi}_0^T = I \tag{81}$$

$$Q^* = \sum_{j=1}^{r} \tilde{\Phi}_{j-1}^T \hat{Q} \tilde{\Phi}_{j-1} \tag{82}$$

The remaining numerical problem is the solution for K in Eq. 73. Equation 73 is a Lyapunov-like equation with more than 2 entries, i.e.,

$$A_1 X B_1 + A_2 X B_2 + \ldots A_{r+2} X B_{r+2} = C \tag{83}$$

The method currently being used for finding X is to use Kronecker products,

$$\left[B_1^T \circledast A_1 + B_2^T \circledast A_2 + \ldots + B_{r+2}^T \circledast A_{r+2}\right] \underline{x} = \underline{c} \tag{84}$$

and solve for $\underline{x}$ by inverting the Kronecker product matrix sum. The Kronecker product matrix sum yields a symmetric, positive definite matrix if K is the optimal feedback gain. The vector $\underline{x}$ consists of the columns of the matrix X, stacked. Likewise, the vector $\underline{c}$ is a stacked version of the matrix C.

A. Numerical Algorithm for Solving Necessary Conditions

The proposed algorithm is a straightforward extension of the convergent algorithm discussed in Ref. 8.

1. Choose a starting gain K_o which stabilizes $\hat{\Phi}_1$. Choose a positive scalar $\alpha < 1$, so that $J(K_i)$ is decreasing in the iterative procedure.
2. Solve for S_1 in Eq. 74, then iteratively compute S_2 through S_r starting from S_1.
3. Solve P_r in Eq. 79, then iteratively compute P_{r-1} to P_1 starting from P_r.

4. Solve for K in Eq. 73.

5. Find the next gain in the sequence

$$K_{i+1} = K_i + \alpha\,(K - K_i) \tag{85}$$

6. If $J(K_{i+1}) - J(K_i)$ and $\| \partial J/\partial K_i \|$ are less than some convergence criterion stop, otherwise set i = i+1 and repeat the sequence starting from 2.

If the algorithm has convergence difficulties or the Kronecker product matrix is not positive definite, reduce α and start over from the most recent stabilizing gain as discussed in Ref. 8. At present, conditions which guarantee algorithmic convergence for $\alpha>0$ are unknown.

B. Application To The PIFCGT Design Approach

The multi-rate optimization problem is performed at the fast sample rate. Incorporating the command generator tracker into the design problem along with integrators and control difference weighting requires careful consideration. The derivation which follows results in the PIFCGT control system that can be implemented to control nonlinear dynamics and use multi-rate feedback. Assumptions have been made to determine a solution. The integrator is computed at the fast rate but can use fast or slow measurements in the integration process. The control position is always updated at the fast rate. The command generator tracker and star trajectory are assumed to be computed at the fast rate. The measurement system does not affect the tracking objectives. A multi-rate command generator tracker is possible, but is beyond the scope of this effort.

Starting from the plant dynamics at the fast rate, the dynamic equation for the error variables $\tilde{x}_k$ and $\tilde{u}_k$ is determined exactly as in Eqs. 7a, 7b and the $\tilde{v}_k$ dynamics are adjoined to the model:

$$\begin{bmatrix} \tilde{x} \\ \tilde{u} \end{bmatrix}_{k+1} = \begin{bmatrix} \Phi & \Gamma \\ 0 & I \end{bmatrix} \begin{bmatrix} \tilde{x} \\ \tilde{u} \end{bmatrix}_{k} + \begin{bmatrix} 0 \\ \Delta t I \end{bmatrix} \tilde{v}_k \tag{86}$$

The slow rate measurements tracking command error is defined as follows:

$$\tilde{y}_{sk} = \tilde{y}_{sk-1} + \Delta_k \, (C_s \, \tilde{x}_k - \tilde{y}_{sk-1}) \tag{87}$$

The variable $\tilde{y}_{sk}$ is defined by the above equation. The plant state, y_s, and star trajectory, y_s^*, cannot be separated for the $\tilde{y}_{sk}$ variable because y_s^* is undefined. The state and star trajectory can be separated for $C_{si} \, \tilde{x}_k$,

$$C_{si} \, \tilde{x}_k = C_{si} \, \bar{x}_k - C_{si} \, x_k^*$$

The integrator for slow and fast measurements is

$$\xi_{k+1} = \xi_k + \Delta t \, H_s \, \tilde{y}_{sk} + \Delta t \, (y_{fk} - y_{fk}^*) \tag{89}$$

Subtracting ξ^* from both sides yields

$$\tilde{\xi}_{k+1} = \tilde{\xi}_k + \Delta t \, H_s \, \tilde{y}_{sk} + \Delta t \, H_f \, \tilde{x}_k + \Delta t \, D_f \, \tilde{u}_k \tag{90}$$

where

$$y_{fk} = H_f \, x_k + D_f \, u_k \tag{91}$$

Grouping everything together, the multi-rate PIFCGT design model is

$$\begin{bmatrix} \tilde{x} \\ \tilde{\xi} \\ \tilde{u} \\ \tilde{y}_s \end{bmatrix}_{k+1} = \begin{bmatrix} \Phi & 0 & \Gamma & 0 \\ \Delta t H_f & I & \Delta t D_f & \Delta t H_s \\ 0 & 0 & I & 0 \\ \Delta_{k+1} \, C_s \, \Phi & 0 & \Delta_{k+1} \, C_s \, \Gamma & I - \Delta_{k+1} \end{bmatrix} \begin{bmatrix} \tilde{x} \\ \tilde{\xi} \\ \tilde{u} \\ \tilde{y}_s \end{bmatrix}_{k} + \begin{bmatrix} 0 \\ 0 \\ \Delta t I \\ 0 \end{bmatrix} \tilde{v}_k +$$

$$\begin{bmatrix} I & 0 & 0 \\ 0 & \Delta t H_f & 0 \\ 0 & 0 & 0 \\ \Delta_{k+1} C_s & 0 & \Delta_{k+1} \end{bmatrix} \begin{bmatrix} w_k \\ v_{fk} \\ v_{sk} \end{bmatrix} \tag{92}$$

The cost function is constructed similiar to Eq. 62. The measurement equation is

$$\begin{bmatrix} \tilde{y}_f \\ \tilde{\xi} \\ \tilde{u} \\ \tilde{y}_s \end{bmatrix}_k = \begin{bmatrix} C_f & 0 & 0 & 0 \\ 0 & I & 0 & 0 \\ 0 & 0 & I & 0 \\ 0 & 0 & 0 & I \end{bmatrix} \begin{bmatrix} \tilde{x} \\ \tilde{\xi} \\ \tilde{u} \\ \tilde{y}_s \end{bmatrix}_k + \begin{bmatrix} v_{fk} \\ 0 \\ 0 \\ 0 \end{bmatrix} \tag{93}$$

Optimizing the cost function produces the constant gain feedback control system

$$\underline{v}_k = \begin{bmatrix} K_f & K_{\tilde{\xi}} & K_u & K_s \end{bmatrix} \begin{bmatrix} \tilde{y}_f \\ \tilde{\xi} \\ \tilde{u} \\ \tilde{y}_s \end{bmatrix}_k \tag{94}$$

The next step in the derivation is to increment the measurements. The derivation for incrementing the measurements, which involves simple algebraic manipulations and careful attention to time indexes, becomes lengthy if more than one slow rate is assumed. The derivation continues with only two rates, r_f and r_s where

$$r_s/r_f = r \tag{95}$$

The generalization to more than one slow rate is straightforward. The slow measurement increment for $\tilde{y}_{si}$ using the definition in Eq. 87 is

$$\tilde{y}_{sik} - \tilde{y}_{si,k-1} = (C_s\, x_k - C_s\, x_{k-r}) - (C_s\, x^*_k - C_s\, x^*_{k-r});\ k=1,\ r+1,\ 2r+1 \qquad (96)$$

$$\tilde{y}_{sik} - \tilde{y}_{si,k-1} = 0; \qquad k\neq 1,\ r+1,\ 2r+1 \qquad (97)$$

The error increment

$$\tilde{e}_k - \tilde{e}_{k-1} = \begin{bmatrix} \tilde{y}_{fk} - \tilde{y}_{f,k-1} \\ \tilde{y}_{sk} - \tilde{y}_{s,k-1} \end{bmatrix} \qquad (98)$$

can be expanded to

$$e_k - e_{k-1} = \begin{bmatrix} y_{fk} - y_{f,k-1} \\ \Delta_k\ (y_{sk} - y_{s,k-r}) \end{bmatrix} - \begin{bmatrix} C_f\, A_{11}\ (x_{mk} - x_{m,k-1} \\ \Delta_k\, C_s\, A_{11}\ (x_{mk} - x_{m,k-r}) \end{bmatrix} -$$

$$\begin{bmatrix} C_f\, A_{12}\ (u_{m,k+1} - u_{mk}) \\ \Delta_k\, C_s\, A_{12}\ (u_{m,k+1} - u_{m,k-r+1} \end{bmatrix} \qquad (99)$$

The derivation for finding ξ^* parallels the derivation in Section 2A up to Eq. 33, which becomes

$$\tilde{\xi}_{-1} = -P^{-1}_{\xi\xi} \left[P^T_{x\xi}\ \tilde{x}_{-1} + P_{\xi u}\, \tilde{u}_{-1} + P_{\xi y}\, \tilde{y}_{s,-1} \right] \qquad (100)$$

The star trajectory can be separated from $\tilde{x}_{-1}$ and $\tilde{u}_{-1}$ but not from $\tilde{y}_{s,-1}$:

$$\xi_{-1} - \xi^*_{-1} = -\, P^{-1}_{\xi\xi} \left[P^T_{x\xi}\ (x_{-1} - x^*_{-1}) + P_{\xi u}\ (u_{-1} - u^*_{-1}) + P_{\xi y}\, \tilde{y}_{s,-1} \right] \qquad (101)$$

$$\Delta\tilde{y}_{s,-1} = (I-\Delta_{-1})\ \Delta\tilde{y}_{s,-2} + \Delta_{-1}\ C_s(x_{-1} - x^*_{-1}) \tag{102}$$

Since only two rates are considered, Δ_{-1} is either 0 or I. If the matrices A and B are defined to be

$$A = -P^{-1}_{\xi\xi}\ (P^T_{x\xi}\ A_{12} + P_{\xi u}\ A_{22}) \tag{103}$$

$$B = -P^{-1}_{\xi\xi}\ (P_{\xi y}\ C_s\ A_{12}) \tag{104}$$

then

$$\xi^*_{-1} = \xi^*_{-2} + A\ (u_{mo} - u_{m,-1}) + \Delta_{-1}\ B\ (u_{mo} - u_{m,-1}) \tag{105}$$

If $\Delta_{-1} = I$ then, Eq. 102 is substituted into Eq. 101 to yield the B matrix in Eq. 104. If $\Delta_{-1} = 0$ then, the term $\tilde{y}_{s,-2}$ should be used in Eq. 101, but $\tilde{y}_{s,-2}$ is zero since the control system is assumed to be tracking the star trajectory for k<-1.

Using a time index, the integrator star trajectory is defined using Eq. 105 as

$$\xi^*_k - \xi^*_{k-1} = (A + \Delta_k\ B)\ (u_{m,k+1} - u_{mk}) \tag{106}$$

If u_m is changing then ξ^*_k is periodic if the B matrix is nonzero. If u_m is constant then ξ^*_k is constant.

Incrementing the integrator and using the integrator star trajectory yields

$$\tilde{\xi}_k - \tilde{\xi}_{k-1} = \xi_k - \xi_{k-1} - A\ (u_{m,k+1} - u_{m\ k}) - \Delta_k\ B\ (u_{m,k+1} - u_{m\ k}) \tag{107}$$

where

$$\xi_k - \xi_{k-1} = \Delta t\ H_s\ \tilde{y}_{s,k-1} + \Delta t\ (y_{f,k-1} - y_{mf,k-1}) \tag{108}$$

Defining the variables

$$\tilde{y}_{\xi sk} = H_s\ \tilde{y}_{sk} \tag{109}$$

$$y_{msk} = H_s\ y_{mk} \tag{110}$$

then, from Eq. 87,

$$\tilde{y}_{\xi sk} = (I - \bar{\Delta}_k)\ \tilde{y}_{\xi sk-1} + \bar{\Delta}_k\ (y_{\xi sk} - y_{msk}) \tag{111}$$

where $\bar{\Delta}_k$ is a matrix that satisfies the equation

$$H_s\ \Delta_k = \bar{\Delta}_k\ H_s \tag{112}$$

If Δ_k is a zero matrix then $\bar{\Delta}_k$ is a zero matrix. If Δ_k is a ℓ_s x ℓ_s identity matrix then $\bar{\Delta}_k$ is an m x m identity matrix.

Grouping all the results together the multi-rate output feedback PIFCGT implementation equations are

(from Eq. 86)

$$u_k = u_{k-1} + \Delta t\ v_{k-1} + A_{21}\ (x_{m,k} - x_{m,k-1}) \tag{113}$$

(from Eq. 99)

$$e_{k-1} - e_{k-2} = \begin{bmatrix} y_{f,k-1} - y_{f,k-2} - C_f\ A_{11}\ (x_{m,k-1} - x_{m,k-2}) \\ \Delta_{k-1}\ (y_{s,k-1} - y_{s,k-r-1}) - \Delta_{k-1} C_s A_{11} (x_{m,k-1} - x_{m,k-r-1}) \end{bmatrix} \tag{114}$$

(from Eq. 111)

$$\tilde{y}_{\xi s,k-2} = (I - \bar{\Delta}_{k-2})\, \tilde{y}_{\xi s,k-3} + \bar{\Delta}_{k-2}\, (y_{\xi s,k-2} - y_{ms,k-2}) \tag{115}$$

(from Eqs. 94 and 99)

$$\begin{aligned} \underline{v}_{k-1} = {} & (I + \Delta t\, K_u)\, \underline{v}_{k-2} + \left[K_f \; K_s\right] \left[\underline{e}_{k-1} - \underline{e}_{k-2}\right] + \\ & \Delta t\, K_\xi\, (\tilde{y}_{\xi s,k-2} + (y_{\xi f,k-2} - y_{mf,k-2})) + \\ & (-K_\xi\, A - K_\xi\, \Delta_{k-1}\, B - K_f\, C_f\, A_{12} - K_u\, A_{22})\, (u_{mk} - u_{m,k-1}) + \\ & -K_s\, \Delta_{k-1}\, C_s\, A_{12}\, (u_{mk} - u_{m,k-r}) \end{aligned} \tag{116}$$

Although the feedback gain is constant and the CGT feedforward gains are constant, the implemented feedforward gain is periodic because of the integrator star trajectory.

5. DISTURBANCE ACCOMMODATION FOR WINDSHEAR DYNAMICS

One of the primary purposes of a flight control system is to stabilize the aircraft about a desired trajectory in an enviroment where external disturbances are affecting the aircraft dynamics and sensor measurements. Some of the disturbances are difficult to model and are best characterized by zero-mean Gaussian white noise. Other types of disturbances are best described by differential equations driven by Gaussian noise. Examples of the latter type of disturbance include the well known Dryden model for gusts, steady-state atmospheric wind and windshear. The objective of the control system is to stabilize the plant while having the capability to cope with the disturbances.

Disturbance accommodation has a history of investigation with progress made by a number of researchers. The procedure for computing the control system in this paper is to minimize a linear quadratic cost function. Efforts in this area include Refs. 20 to 23. The objective in the references in to construct two signals in the control variable, u, i. e.,

$$\Delta u = \Delta u_f + \Delta u_a \tag{117}$$

where, Δu_f, is designed to stabilize the plant while the other signal, Δu_a, is chosen to accommodate the disturbance. One method for determining Δu_a exactly using feedforward control is discussed in Refs. 5 and 24. The effect of the disturbance is eliminated on selected system outputs. Feeding forward the disturbance in Δu_a usually requires some form of dynamic compensator (observer, servo compensator), since the disturbance is rarely measured. The feedback system for Δu_f usually does not contribute towards steady-state disturbance suppression.

An alternative to Eq. 117 is investigated in Refs. 25, 26, and 27 where only the Δu_f signal is used to stabilize the plant and eliminate the effects of the disturbances on selected system outputs. The disturbances are suppressed using feedback gain eigenstructure assignment.

An alternative to the approaches just discussed (which can be considered more practical) consists of constructing a feedback controller which strives to minimize, rather than completely eliminate, the effect of disturbances on selected system outputs. Investigations into the more practical approach have been made in Ref. 27 using pole assignment to achieve stability and Ref. 28.

The disturbance accommodation procedures in Refs. 21 to 28 all assume that the disturbance dynamics are not affected by the plant dynamics. Models for aircraft windshear have a plant representation where the aircraft plant states affect the windshear dynamics as discussed in Ref. 29 and presented in the next section. Changes in aircraft height cause the windshear state to change in value.

In the rest of this chapter a new tack is pursued for computing disturbance suppression control systems using the optimal control approach. The designer can specify any control structure that can be modeled using output or limited state feedback. The chosen control structure may or may not be able to exactly suppress the deterministic disturbance. The plant model and disturbance model are expressed in discrete time. The plant model and disturbance model can be completely coupled and each model can be driven by Gaussian white noise. The objective is to design the control system gains optimally so as to minimize the stochastic effects of the disturbances on the plant states and minimize the deterministic effect of the disturbance on selected plant outputs. The resulting cost function used to determine controller gains has two distinct parts.

The dual cost is accomplished using a result presented in Ref. 30 and developed further in this chapter. The steady-state plant state and control response can be decomposed into a deterministic component dependent only on the disturbance which satisfies a differential equation and a zero mean stochastic response due to the Guassian white noise sources. The necessary conditions for the dual cost function to have a (local) minimum are derived in this chapter. A numerical algorithm is also developed to solve the optimal disturbance minimization problem necessary conditions. The special case where the disturbance is not affected by plant states is presented. A design example using PIFCGT is discussed in Chapter 5.

A. The Windshear Model

A basic wind model relationship in the aircraft's local level plane at a position above the earth's surface for windshear was developed by C. Belcastro and A. Ostroff at the NASA Langley Research Center, Ref. 29. The NASA Langley windshear model is presented in this section. The wind shear plus steady wind affecting the longitudinal dynamics of the aircraft is modeled as

$$\begin{bmatrix} U_w \\ W_w \end{bmatrix}_e = \begin{bmatrix} U_{wc} \\ W_{wc} \end{bmatrix}_e + \begin{bmatrix} U_z \\ W_z \end{bmatrix} z_e \tag{118}$$

Defining the following variables

$$\underline{w}_e = \begin{bmatrix} U_w \\ W_w \end{bmatrix} \tag{119}$$

$$\underline{w}_{ce} = \begin{bmatrix} U_{wc} \\ W_{wc} \end{bmatrix}_e \tag{120}$$

$$s_z = \begin{bmatrix} U_z \\ W_z \end{bmatrix} \tag{121}$$

The relationship can be restated as

$$w_e = w_{ce} + s_z z_e \tag{122}$$

w_e is the wind velocity vector in the earth-fixed reference frame, w_{ce} is the constant wind velocity, s_z is the wind shear gradient vector and z_e is the vertical height of the position in the atmosphere above the earth's surface. The wind velocity in aircraft body axis is given by

$$w_b = H_\theta w_e = H_\theta w_{ce} + H_\theta s_z z_e \tag{123}$$

where

$$H_\theta = \begin{bmatrix} c\theta & -s\theta \\ s\theta & c\theta \end{bmatrix} \tag{124}$$

and θ is the aircraft Euler pitch angle. Taking the derivative of Eq. 123, yields,

$$\dot{w}_b = \dot{\theta} L_\theta w_{ce} + H_\theta \dot{w}_{ce} + \dot{\theta} L_\theta s_z z_e + H_\theta \dot{s}_z z_e + H_\theta s_z \dot{z}_e \tag{125}$$

where

$$L_\theta = \begin{bmatrix} -s\theta & -c\theta \\ c\theta & -s\theta \end{bmatrix} \tag{126}$$

Equation 125 can be simplified by factoring $\dot{\theta} L_\theta$ and substituting Eq. 123,

$$\dot{w}_b = \dot{\theta} I_\theta w_b + H_\theta s_z \dot{z}_e + H_\theta \dot{w}_{ce} + H_\theta \dot{s}_z z_e \tag{127}$$

where

$$I_\theta = \begin{bmatrix} 0 & -1 \\ 1 & 0 \end{bmatrix} \tag{128}$$

The perturbation representation of Eq. 127 is

$$\begin{aligned} \Delta\dot{w}_b = {} & \dot{\theta}_o\, I_\theta\, \Delta w_b + I_\theta\, w_{bo}\, \Delta\dot{\theta} + L_{\theta o}\, s_{zo}\, \dot{z}_{eo}\, \Delta\theta + \dot{z}_{eo}\, H_{\theta o}\, \Delta s_z \\ & + H_{\theta o}\, s_{zo}\, \Delta\dot{z}_e + L_{\theta o}\, \dot{w}_{ceo}\, \Delta\theta + H_{\theta o}\, \Delta\dot{w}_{ce} + z_e\, L_{\theta o}\, \dot{s}_{zo}\, \Delta\theta \\ & + z_{eo}\, H_{\theta o}\, \Delta\dot{s}_z + H_{\theta o}\, \dot{s}_{zo}\, \Delta z_e \end{aligned} \tag{129}$$

The o subscript indicates the variable is representing the nominal value at the desired flight condition. The vectors w_{ce} and s_z are assumed to be constant, i.e.

$$\dot{w}_{ce} = \dot{s}_z = \Delta\dot{w}_{ce} = \Delta\dot{s}_z = 0.0 \tag{130}$$

The windshear gradient perturbation vector is assumed to be 0, $\Delta s_z = 0$

Substituting Eq. 130 into Eq. 129 and simplifying, results in the following,

$$\Delta\dot{w}_b = \dot{\theta}\, I_\theta\, \Delta w_b + I_\theta\, w_{bo}\, \Delta\dot{\theta} + \dot{z}_{eo}\, L_{\theta o}\, s_{zo}\, \Delta\theta + H_{\theta o}\, s_{zo}\, \Delta\dot{z}_e \tag{131}$$

Eq. 131 can be rewritten as

$$\Delta\dot{w}_b = A_w\, \Delta w_b + H_x\, \Delta x + H_{\dot{x}}\, \Delta\dot{x} \tag{132}$$

where

$$A_w = \dot{\theta}\, I_0 \tag{133}$$

(2x2)

$$H_x = \begin{bmatrix} 0 & 0 & 0 & \dot{z}_{eo} & L_{\theta o} & s_{zo} & 0 \\ 0 & 0 & 0 & & 0 & & 0 \end{bmatrix} \quad (4x5) \tag{134}$$

$$H_{\dot{x}} = \begin{bmatrix} 0 & 0 & 0 & I_\theta & w_{bo} & H_{\theta o} & s_{zo} \\ 0 & 0 & 0 & 0 & & 0 & \end{bmatrix} \quad (4x5) \tag{135}$$

$$\Delta x^T = \begin{bmatrix} \Delta u & \Delta w & \Delta q & \Delta\theta & \Delta z_e \end{bmatrix} \tag{136}$$

Grouping the wind velocity model in Eq. 132 with the standard representation of the plant dynamics produces,

$$\begin{bmatrix} I & 0 \\ -H_{\dot{x}} & I \end{bmatrix} \begin{bmatrix} \Delta\dot{x} \\ \Delta\dot{w}_b \end{bmatrix} = \begin{bmatrix} A & D_w \\ H_x & A_w \end{bmatrix} \begin{bmatrix} \Delta x \\ \Delta w_b \end{bmatrix} + \begin{bmatrix} B \\ 0 \end{bmatrix} \Delta u \tag{137}$$

The matrix D_w is obtained from the Δu and Δw column vectors in the A matrix,

$$D_w = \begin{bmatrix} -A_u & -A_w & 0 & 0 \end{bmatrix}; \quad A = \begin{bmatrix} A_u & A_w & A_q & A_\theta & A_{ze} \end{bmatrix} \tag{138}$$

Multiplying Eq. 137 by $\begin{bmatrix} I & 0 \\ H_{\dot{x}} & I \end{bmatrix}$ produces the final plant representation

$$\begin{bmatrix} \Delta\dot{x} \\ \Delta\dot{w}_b \end{bmatrix} = \begin{bmatrix} A & D_w \\ H_x + H_{\dot{x}}A & A_w + H_{\dot{x}}D_w \end{bmatrix} \begin{bmatrix} \Delta x \\ \Delta w_b \end{bmatrix} + \begin{bmatrix} B \\ H_{\dot{x}}B \end{bmatrix} \Delta u \tag{139}$$

The wind vector, Δw_b, is affected by the plant states but not by the control states since it is easily shown that $H_{\dot{x}}B$ is a zero matrix. Representing the aircraft plus wind dynamics in discrete time, however, causes the discrete control effect matrix Γ to have entries in all locations.

B. Deterministic Disturbance Accommodation Using The Command Generator Tracker

The objective of this section is to determine the plant star trajectory when the plant output, y, is tracking a model output, y_m and the plant dynamics are affected by deterministic disturbances. The combined plant model and disturbance model are represented as follows

$$\begin{bmatrix}\Delta x\\ \Delta s\end{bmatrix}_{k+1} = \begin{bmatrix}\Phi & D_w\\ H_w & \Phi_w\end{bmatrix}\begin{bmatrix}\Delta x\\ \Delta s\end{bmatrix}_k + \begin{bmatrix}\Gamma\\ \Gamma_w\end{bmatrix}\Delta u_k \tag{140}$$

$$\Delta y_k = H_x\,\Delta x_k + H_s\,\Delta s_k \tag{141}$$

The aircraft perturbation state vector is Δx_k, the perturbation control vector is Δu_k, the disturbance vector is Δs_k and the selected perturbation outputs in which the effect of the disturbance is to be suppressed is Δy_k. The output of a command generator, Δy_m, is generated by the command model

$$\Delta x_{m,k+1} = \Phi_m\,\Delta x_{mk} + \Gamma_m\,\Delta u_m \tag{142}$$

$$\Delta y_{mk} = H_m\,\Delta x_{mk} + D_m\,\Delta u_m \tag{143}$$

The command generator state is Δx_{mk} and Δu_m is the command generator control that is assumed to be constant. The dimensions of Δy_m Δy and Δu are assumed to be equal. The aircraft output tracks the model output while suppressing the disturbance along the star trajectory. Using the same structure as in Chapter 2, i. e. a linear relationship, the star trajectory is constructed as

$$\begin{bmatrix}\Delta x^*\\ \Delta u^*\end{bmatrix}_k = \begin{bmatrix}S_{11} & S_{12}\\ S_{21} & S_{22}\end{bmatrix}\begin{bmatrix}\Delta x_{mk}\\ \Delta u_m\end{bmatrix} + \begin{bmatrix}S_{13}\\ S_{23}\end{bmatrix}\Delta s_k \tag{144}$$

Equation 144 is the solution to the tracking problem if the S_{ij} matrices exist. The unknown feedforward S_{ij} matrices can be shown to satisfy solvable algebraic relationships by expressing $\Delta\underline{x}^*_{k+1} - \Delta\underline{x}^*_k$ first using the plant dynamics, Eq. 140, then using Eq. 144 and equating the two expressions for $\Delta\underline{x}^*_{k+1} - \Delta\underline{x}^*_k$. Without going through the details, the algebraic relationships for the S_{ij} matrices are as follows:

$$\begin{bmatrix} (\Phi - I - S_{13} H_w) & (\Gamma - S_{13}\Gamma_w) \\ H & 0 \end{bmatrix} \begin{bmatrix} S_{11} & S_{12} \\ S_{21} & S_{22} \end{bmatrix} = \begin{bmatrix} S_{11}(\Phi_m - I) & S_{11}\Gamma_m \\ H_m & D_m \end{bmatrix} \tag{145}$$

$$\begin{bmatrix} \Phi & \Gamma \\ H & 0 \end{bmatrix} \begin{bmatrix} S_{13} \\ S_{23} \end{bmatrix} = \begin{bmatrix} S_{13}\Phi_w - D_w \\ -H_s \end{bmatrix} + \begin{bmatrix} S_{13} H_w & S_{13}\Gamma_w \\ 0 & 0 \end{bmatrix} \begin{bmatrix} S_{13} \\ S_{23} \end{bmatrix} \tag{146}$$

A numerical solution for S_{13} and S_{23} in Eq. 146 is obtained by inverting the quad partition matrix

$$\begin{bmatrix} \Phi & \Gamma \\ H & 0 \end{bmatrix}^{-1} = \begin{bmatrix} \Omega_{11} & \Omega_{12} \\ \Omega_{21} & \Omega_{22} \end{bmatrix} \tag{147}$$

and multiplying Eq. 146 by the inverse:

$$\begin{bmatrix} S_{13} \\ S_{23} \end{bmatrix} = \begin{bmatrix} \Omega_{11} & 0 \\ \Omega_{21} & 0 \end{bmatrix} \begin{bmatrix} S_{13} \\ S_{23} \end{bmatrix} \Phi_w + \begin{bmatrix} \Omega_{11} & 0 \\ \Omega_{21} & 0 \end{bmatrix} \begin{bmatrix} S_{13} \\ S_{23} \end{bmatrix} \begin{bmatrix} H_w & \Gamma_w \end{bmatrix} \begin{bmatrix} S_{13} \\ S_{23} \end{bmatrix}$$

$$- \begin{bmatrix} \Omega_{11} D_w + \Omega_{12} H_s \\ \Omega_{21} D_w + \Omega_{22} H_s \end{bmatrix} \tag{148}$$

Equation 148 is a generalized Riccati equation. A convergent algorithm for solving Eq. 148 has been developed and is described in Appendix A. There may be more than one solution or there may be no solution to Eq. 148. After S_{13} and S_{23} are determined, they can be substituted into Eq. 145 and the result can be numerically solved using the technique discussed in Ref. 6. The control tracking problem solution in Eq. 145 is not independent of the disturbance rejection solution because of the coupling matrices H_w and Γ_w.

Any control system of the form

$$\Delta u_k = \Delta u_k^* + K C_x (\Delta x_k - \Delta x_k^*) \tag{149}$$

can be ideally used to stabilize Φ and eliminate the steady-state disturbance in Δy_k. In the control system, K is the feedback gain and C_x is the observation matrix for the system states. Equation 149 can be rearranged as

$$\Delta u_k = \overbrace{K C_x \Delta x_k}^{u_f} + \overbrace{(S_{23} - K C_x S_{13})}^{u_a} \Delta s_k + (S_{21} - K C_x S_{11}) \Delta x_{mk} + (S_{22} - K C_x S_{12}) \Delta u_m \tag{150}$$

which is the form shown in Eq. 117. If $S_{23} - K C_x S_{13}$ is of full rank, the disturbance state, Δs_k, must be measured or observed in order to implement Eq. 150. It is evident from Eq. 150, that if K is to stabilize the plant and eliminate the disturbance in the Δy_k response without using a u_a control term, then K must satisfy the equation

$$S_{23} - K C_x S_{13} = 0 \tag{151}$$

A feedback gain which satisfies Eq. 151 does not always exist. Necessary and sufficient conditions for the existence of a gain K which satisfies Eq. 151 are given in Ref. 26 for the case where H_w and Γ_w are zero matrices.

The next section addresses the question: What is the steady-state plant response to the disturbance and white noise sources if the control system shown in Eq. 150 is implemented? The formulation includes the case of an estimator

observing $\Delta\underline{s}_k$, since the estimator dynamics can be adjoined to the aircraft dynamics to extend the state dimension of $\Delta\underline{x}$.

C. The Stochastic Star Trajectory:

The command generator tracker and the star trajectory have always been applied to deterministic models. In this section, noise processes are introduced into the models and the concept of the star trajectory is used to investigate the tracking response of the stochastic system in steady-state. The objective to determine a design technique for accommodating windshear dynamics that are driven by random noise.

The aircraft model and disturbance dynamics shown in the previous section are generalized further and represented as follows:

Discrete Perturbation Aircraft Model:

$$\Delta\underline{x}_{k+1} = \Phi\Delta\underline{x}_k + \Gamma\Delta\underline{u}_k + D_w\,\Delta\underline{s}_k + \underline{w}_k \tag{152}$$

Disturbance:

$$\Delta\underline{s}_{k+1} = \Phi_w\,\Delta\underline{s}_k + H_w\,\Delta\underline{x}_k + \Gamma_w\,\Delta\underline{u}_k + \underline{\sigma}_k \tag{153}$$

Measurement:

$$\Delta\underline{z}_k = C_x\,\Delta\underline{x}_k + C_w\,\Delta\underline{s}_k + \underline{v}_k \tag{154}$$

Control System:

$$\Delta\underline{u}_k = -K\,\Delta\underline{z}_k = -K\,C_x\,\Delta\underline{x}_k - K\,C_w\,\Delta\underline{s}_k - K\,\Delta\underline{v}_k \tag{155}$$

The zero-mean, white Gaussian noise sources in the above models have covariances:

$$E\left\{\underline{w}_k\,\underline{w}_k^T\right\} = W \tag{156}$$

$$E\left\{\underline{\sigma}_k\,\underline{\sigma}_k^T\right\} = W_s \tag{157}$$

$$E\left\{\underline{\sigma}_k\,\underline{w}_k^T\right\} = W_{sx} \tag{158}$$

$$E\left\{\underline{v}_k\,\underline{v}_k^T\right\} = V \tag{159}$$

All other cross covariances between the disturbance and measurement noise sources are assumed to be zero. The C_w matrix in Eq. 155 allows for the fact that some sensors, such as an airspeed sensor, measure a combination of the aircraft and disturbance states. The disturbance and plant process noises are allowed to be cross correlated as shown in Eq. 158.

Given the control system structure shown in Eq. 155, the steady-state response for Δx_k is assumed to satisfy the equation

$$\Delta x_k^* = S_{31}\ \Delta s_k + \begin{bmatrix} A_1 & A_2 & \cdots \end{bmatrix} \begin{bmatrix} \Delta w_k \\ \Delta w_{k+1} \\ \cdot \\ \cdot \\ \cdot \end{bmatrix} + \begin{bmatrix} B_1 & B_2 & \cdots \end{bmatrix} \begin{bmatrix} \Delta v_k \\ \Delta v_{k+1} \\ \cdot \\ \cdot \\ \cdot \end{bmatrix} + \begin{bmatrix} C_1 & C_2 & \cdots \end{bmatrix} \begin{bmatrix} \Delta\sigma_k \\ \Delta\sigma_{k+1} \\ \cdot \\ \cdot \\ \cdot \end{bmatrix} \tag{160}$$

The assumption used in Eq. 160, where an infinite sequence of unknown feed-forward matrices is used to describe the star trajectory, has been used before in Ref. 5. In the final answer for Δx_k^*, the infinite sequences will be replaced by a difference equation once the A_i, B_i, and C_i matrices are known.

The solutions for S_{31}, A's, B's, and C's are determined by computing $\Delta x_{k+1}^* - \Delta x_k^*$ as discussed in the previous section. Using the plant dynamics, the expression for $\Delta x_{k+1}^* - \Delta x_k^*$ becomes

$$\Delta x_{k+1}^* - \Delta x_k^* = (\Phi - \Gamma\ K\ C_x - I)\ \Delta x_k^* + (D_w - \Gamma\ K\ C_w)\ \Delta s_k - \Gamma\ K\ \Delta v_k + \Delta w_k \tag{161}$$

Using 153, 155, and 160 $\Delta x_{-k}^* - \Delta x_{-k}^*$ results in

$$\Delta x_{k+1} - \Delta x_k^* = S_{31}\left[(\Phi_w - \Gamma_w K C_w) - I\right]\Delta s_k + S_{31}(H_w - \Gamma_w K C_x)\Delta x_k^* - S_{14}\Gamma_w K \Delta v_k$$
$$+ S_{14}\sigma_k + \left[-A_1 \quad A_1-A_2 \quad A_2-A_3 \ \ldots\right]\begin{bmatrix}\Delta w_k\\ \Delta w_{k+1}\\ \Delta w_{k+2}\\ \vdots\end{bmatrix}$$
$$+ \left[-B_1 \quad B_1-B_2 \quad B_2-B_3 \ \ldots\right]\begin{bmatrix}\Delta v_k\\ \Delta v_{k+1}\\ \Delta v_{k+2}\\ \vdots\end{bmatrix} + \left[-C_1 \quad C_1-C_2 \quad C_2-C_3 \ \ldots\right]\begin{bmatrix}\Delta\sigma_k\\ \Delta\sigma_{k+1}\\ \Delta\sigma_{k+2}\\ \vdots\end{bmatrix} \tag{162}$$

Substituting the expression for Δx_k^* from Eq. 160 into Eqs. 161 and 162 and equating the two expressions yields solvable equations for the S_{31}, A_i, B_i, and C_i matrices. Defining the matrices

$$\Phi_c = (\Phi - \Gamma K C_x) - S_{31}(H_w - \Gamma_w K C_x) \tag{163}$$

$$\chi_c = \Gamma K - S_{31}\Gamma_w K \tag{164}$$

expressing Eq. 160 in the z-domain and substituting the solutions for the A_i, B_i, and C_i matrices into Eq. 160 yields:

$$\Delta x^* = S_{31}\Delta s - \left[\Phi_c^{-1} + \Phi_c^{-2} z + \Phi_c^{-3} z^2 + \ldots\right]\Delta w$$
$$+ \left[\Phi_c^{-1}\chi_c + \Phi_c^{-2}\chi_c z + \Phi_c^{-3}\chi_c z^2 + \ldots\right]\Delta v$$
$$+ \left[\Phi_c^{-1} S_{31} + \Phi_c^{-2} S_{31} z + \Phi_c^{-3} S_{31} z^2 + \ldots\right]\Delta\sigma \tag{165}$$

S_{31} satisfies the generalized Riccati equation

$$(\Phi - \Gamma K C_x) S_{31} + S_{31} (\Phi_w - \Gamma_w K C_w) - S_{31} (H_w - \Gamma_w K C_x) S_{31} + (D_w - \Gamma K C_w) = 0 \quad (166)$$

Equation 166 can be expressed in the form of Eq. 200 of Appendix A if $(\Phi - \Gamma K C_x)$ is invertible.

The infinite z-domain sequences in Eq.165 have the closed-form relationship

$$\left[I - z \Phi_c\right]^{-1} = \left[I + \Phi_c^{-1} z + \Phi_c^{-2} z^2 + \ldots\right] \quad (167)$$

Substituting Eq. 167 into Eq. 165 and converting back to the time domain yields

$$\Delta x_k^* = S_{31} \Delta s_k + \Delta \tilde{x}_k \quad (168)$$

$$\Delta \tilde{x}_{k+1} = \Phi_c \Delta \tilde{x}_k + \Delta w_k - S_{31} \Delta \sigma_k + \overbrace{(S_{31} \Gamma_w K - \Gamma K)}^{-\chi_c} \Delta v_k \quad (169)$$

Equations 168 and 169 are an important contribution of the report. In steady state, the closed-loop aircraft response to deterministic and stochastic disturbances can be decomposed into two components. One component, $S_{31} \Delta s_k$, shows how each state in the aircraft is affected by the disturbance states that satisfy a difference equation. The other component, $\Delta \tilde{x}_k$, shows how the white Gaussian noise sources are corrupting the system response. Equation 168 leads to a natural framework for finding the feedback gain K as discussed in the next section.

If the solution for Δx_k^* is substituted into the control system, Δu_k^* can be rewritten as

$$\Delta u_k^* = (-K C_x S_{31} - K C_w) \Delta s_k + \Delta \tilde{u}_k \quad (170)$$

$$\Delta \tilde{u}_k = - K C_x \Delta \tilde{x}_k - K \Delta v_k \quad (171)$$

In steady-state, the control response decomposes into a component dependent on Δs_k and a zero-mean component, $\Delta \tilde{u}_k$, driven by measurement noise and the zero-mean plant response, $\Delta \tilde{x}_k$.

D. Optimal Disturbance Suppression:

The objective of this section is to construct a cost function representing desirable objectives for the plant and control system shown in Eqs. 152 to 155, then minimize the cost function by finding the feedback gain K. The derivation is cumbersome if Γ_w and H_w are non-zero matrices. The matrices Γ_w and H_w are assumed to be zero for the derivation in this section. After the optimal gain is derived with Γ_w and H_w zero, the optimal gain solution with Γ_w and H_w non-zero is presented for completeness.

If Γ_w and H_w are non-zero, the feedback gain, K, can affect values in the S_{31} matrix and the response of $\Delta\tilde{x}_k$. The feedback gain cannot affect the response of Δs_k. Hence, a useful cost function with Γ_w and H_w zero for disturbance minimization is

$$J_e = E\left\{\left[\Delta\tilde{x}^T\ \Delta\tilde{u}^T\right]\begin{bmatrix} Q_1 & M \\ M^T & R \end{bmatrix}\begin{bmatrix} \Delta\tilde{x} \\ \Delta\tilde{u} \end{bmatrix}_k\right\} + \tfrac{1}{2}\,\mathrm{trace}\left\{(H_x S_{31} + H_s)^T Q_2 (H_x S_{31} + H_s)\right\} \quad (172)$$

If Δx_k were weighted in a quadratic cost function, the Δs_k component in Δx_k would add to the cost. If Δs_k is neutrally stable or unstable, then quadratically weighting Δx_k in a cost function could yield an undefined cost in steady-state.

Weighting $\Delta\tilde{x}_k$ and $\Delta\tilde{u}_k$ as shown in Eq. 172 yields a finite cost if the closed-loop plant matrix is stable, since both signals are zero-mean and do not depend on Δs_k. The second part of the cost function in Eq. 172 attempts to minimize the disturbance response in the system output as defined in Eq. 166. No restriction is placed on the first dimension of H_x and H_s in Eq. 172. The cost function represents a tradeoff between optimal stochastic performance and deterministic disturbance suppression.

Substituting Eq. 171 into the cost function produces

$$J_e = \text{trace}\left\{(Q_1 + C_x^T K^T R K C_x - M K C_x - C_x^T K^T M^T) X\right\}$$
$$+ \text{trace}\left\{K^T R K V\right\} + \tfrac{1}{2}\,\text{trace}\left\{(H_x S_{31} + H_s)^T Q_2 (H_x S_{31} + H_s)\right\} \quad (173)$$

where

$$E\left\{\underline{v}_k \ \underline{v}_k^T\right\} = V; \qquad E\left\{\underline{\tilde{x}}_k \ \underline{\tilde{x}}_k^T\right\} = X \quad (174a,b)$$

X is the covariance of the system error response and is computed using Eq. 169. The cost function, J_e, can be minimized subject to the equality constraints for X and S_{31} using Lagrange multipliers. The complete cost function is given by

$$J = J_e + J_L \quad (175)$$

where

$$J_L = \text{trace}\left\{(-X + \Phi_c X \Phi_c^T + W + \Gamma K V K^T \Gamma^T + S_{31} W_s S_{31}^T - S_{31} W_{sx} - W_{sx}^T S_{31}^T) P^T\right\} \quad (176)$$
$$+ \text{trace}\left\{(\Phi_c S_{31} + S_{31}(-\Phi_w) + D_w - \Gamma K C_w) Y^T\right\}$$

$$\Phi_c = \Phi - \Gamma K C_x \quad (177)$$

The P and Y matrices are the Lagrange multipliers.

Necessary conditions for J to have a minimum are $\partial J/\partial X = 0$, $\partial J/\partial S_{31} = 0$, $\partial J/\partial P = 0$, $\partial J/\partial Y = 0$, and $\partial J/\partial K = 0$. The five necessary conditions for optimality can be expressed as five matrix equations.

Covariance Equation for $\underline{\tilde{x}}_k$

$$X = \Phi_c X \Phi_c^T + \begin{bmatrix} I & -S_{31} \end{bmatrix} \begin{bmatrix} W & W_{sx}^T \\ W_{sx} & W_s \end{bmatrix} \begin{bmatrix} I \\ -S_{31}^T \end{bmatrix} + \Gamma K V K^T \Gamma^T \quad (178)$$

Star Trajectory Equation

$$\Phi_c S_{31} + S_{31}(-\Phi_w) = \Gamma K C_w - D_w \quad (179)$$

Cost Equation

$$P = \Phi_c^T P \Phi_c + \begin{bmatrix} I & -C_x^T K^T \end{bmatrix} \begin{bmatrix} Q_1 & M \\ M^T & R \end{bmatrix} \begin{bmatrix} I \\ -K C_x \end{bmatrix} \tag{180}$$

Complementary Star Trajectory Equation

$$\Phi_c^T Y + Y (-\Phi_w^T) = 2.0 P \left[W_{sx} - S_{31} W_s \right] - H_x^T Q_2 \left[H_s + H_x S_{31} \right] \tag{181}$$

Gain Equation

$$(R + \Gamma^T P \Gamma) K (C_x X C_x^T + V) = (\Gamma^T P \Phi + M^T) X C_x^T + \tfrac{1}{2} \Gamma^T Y (C_w^T + S_{31}^T C_x^T) \tag{182}$$

A numerical algorithm for finding a gain, K, which satisfies the necessary conditions is presented next by extending the convergent ouput feedback algorithm derived in Ref. 8:

Choose an initial K_o so that Φ_c is stable.

Choose a scalar α so that $J(K_i)$ is decreasing during the following iterations:

1. Solve Eq.179 for S_{31} using K_i.
2. Solve Eq.178 for X using K_i and S_{31} from 1.
3. Solve Eq.180 for P using K_i.
4. Solve Eq.181 for Y using K_i, S_{31} from 1 and P from 3.
5. Solve Eq.182 for K using S_{31} from 1, X from 2, P from 3 and Y from 4.
6. Update the feedback gain

$$K_{i+1} = K_i + \alpha (K - K_i) \tag{183}$$

7. If $| J(K_{i+1}) - J(K_i)| > \varepsilon$ and/or $||\partial J(K_i)/\partial K_i|| > \varepsilon$, where ε is some convergence criterion, then set i = i+1 and repeat steps 1 through 6.

Equations 178 to 181 are Lyapunov equations that can be solved using the Bartels-Stewart algorithm, Ref. 19.

If H_w and/or Γ_w are non-zero, it is no longer clear that the cost function shown in Eq. 172 represents design objectives. Alternative cost functions with H_w and Γ_w non-zero is an area of future research. If Δs_k remains uncontrollable or controlling Δs_k from Δu_k is not desired, as is the case for wind shear disturbances, then the cost function shown in Eq. 172 remains attractive. The following equations show how the problem is modified if H_w and/or Γ_w are non-zero:

First the following matrices are defined:

$$\Gamma_s = \Gamma - S_{31} \Gamma_w \tag{184}$$

$$\Phi_c = \Phi - \Gamma K C_x \tag{185}$$

$$\Gamma_c = \Gamma_w K C_x - H_w \tag{186}$$

$$\Phi_d = \Phi_w - \Gamma_w K C_w \tag{187}$$

$$\Phi_{cd} = \Phi_c + S_{31} \Gamma_c \tag{188}$$

$$\Phi_{dc} = -\Phi_d + \Gamma_c S_{31} \tag{189}$$

then the five necessary conditions can be shown to reduce to the following matrix equations

Covariance Equation for X

$$X = \Phi_{cd} X \Phi_{cd}^T + \begin{bmatrix} I & -S_{31} \end{bmatrix} \begin{bmatrix} W & W_{sx}^T \\ W_{sx} & W_s \end{bmatrix} \begin{bmatrix} I \\ -S_{31}^T \end{bmatrix} + \Gamma_s K V K \Gamma_s^T \tag{190}$$

Star Trajectory Generalized Riccati Equation

$$\Phi_c S_{31} + S_{31} (-\Phi_d) = \Gamma K C_w - D_w - S_{31} \Gamma_c S_{31} \tag{191}$$

Cost Equation

$$P = \Phi_{cd}^T P \Phi_{cd} + \begin{bmatrix} I - C_x^T K^T \end{bmatrix} \begin{bmatrix} Q_1 & M \\ M^T & R \end{bmatrix} \begin{bmatrix} I \\ -K C_x \end{bmatrix} \tag{192}$$

Complementary Star Trajectory Equation

$$\Phi_{cd}^T Y + Y \Phi_{dc}^T = 2.0\ P \left[W_{sx} - S_{31}\ W_s \right] - H_x^T Q_2 \left[H_s + H_z\ S_{31} \right] \tag{193}$$

$$- 2.0\ P\ \Phi_{cd}\ X\ \Gamma_c^T - 2.0\ P\ \Gamma_s\ K\ V\ K^T\ \Gamma_w^T \tag{193}$$

Gain Equation

$$(R + \Gamma_s^T P\ \Gamma_s)\ K\ (C_x\ X\ C_x^T + V) = (\Gamma_s^T P\ (\Phi - S_{31}\ H_w) + M^T)\ X\ C_x^T$$

$$+ \tfrac{1}{2}\ \Gamma_s^T Y\ (C_w^T + S_{31}^T\ C_x^T) \tag{194}$$

The algorithm shown for Eqs. 178 to 182 can be used to solve Eqs. 190 to 194. The primary differences are that K must be chosen so that Φ_{cd} is stable and S_{31} is the solution to a generalized Riccati equation rather than a Lyapunov equation. K stabilizes the stochastic term, $\Delta\tilde{x}$, when H_w and Γ_w are non-zero, but the total closed-loop system for Δx and Δs can be unstable or neutrally stable because of the way J_e is chosen.

6. DESIGN AND SIMULATION OF CONTROL SYSTEMS

This chapter presents digital flight control system design parameters and nonlinear 6-DOF simulations for four digital control designs. The objective of the control system is to cause a small commercial jet (Boeing 737) to capture and track a 3 deg glideslope near the terminal area. Enroute to touchdown, the SRI wind package, Ref. 31, is used to model a windshear disturbing the aircraft dynamics.

A. Design Models

The four control designs are:

SR-PIFCGT — A single rate PIFCGT design using a linear aircraft model driven by white noise sources.

MR-PIFCGT — A multi-rate PIFCGT design using a linear aircraft model driven by white noise sources.

WS-PIFCGT — A single rate PIFCGT design using a linear aircraft model combined with the windshear model. The feedback gains are computed using the algorithm in section 4D with Γ_w and H_w nonzero.

EP-PIFCGT — A single rate PIFCGT design using a linear aircraft model combined with the windshear model and the energy probe measurement. The feedback gains are computed using the algorithm in Section 4D with Γ_w and H_w nonzero.

The states in the aircraft design model and the output vector used for feedback are presented next:

Integrators

$$\Delta\xi_{hk+1} = \Delta\xi_{hk} + \Delta t \left[(\Delta\hat{h}_k - \Delta h_{m,k}) + 5\,(\Delta\dot{\hat{h}}_k - \Delta\dot{h}_{m,k}) \right]$$

$$\Delta\xi_{CAS,k+1} = \Delta\xi_{CAS,k} + \Delta t\,(\Delta CAS_k - \Delta CAS_{m,k})$$

Prefilters

$$\Delta\dot{\hat{a}}_z = -10.0\ (\Delta\hat{a}_z - \Delta a_z)$$

$$\Delta\dot{\hat{q}} = -10.0\ (\Delta\hat{q} - \Delta q)$$

Complementary Filter

$$\begin{bmatrix} \Delta\dot{\hat{h}} \\ \Delta\ddot{\hat{h}} \end{bmatrix} = \begin{bmatrix} 0 & 1 \\ 0 & 0 \end{bmatrix} \begin{bmatrix} \Delta\hat{h} \\ \Delta\dot{\hat{h}} \end{bmatrix} + \begin{bmatrix} 0.8 \\ 0.32 \end{bmatrix} \left[\Delta h - \Delta\hat{h}\right] + \begin{bmatrix} 0 \\ 1 \end{bmatrix} \Delta a_h$$

SR-PIFCGT $\quad \Delta t = 0.1$ sec

States

$$\Delta x^T = \left[\Delta u \quad \Delta w \quad \Delta q \quad \Delta\theta \quad \Delta h \quad \Delta\hat{a}_z \quad \Delta\hat{q} \quad \Delta\hat{h} \quad \Delta\dot{\hat{h}} \quad \Delta EPR \quad \Delta\delta_e \quad \Delta\xi_h \quad \Delta\xi_{CAS} \quad \Delta u_t \quad \Delta u_e\right]$$

Controls

$$\Delta u^T = \left[\Delta v_e \quad \Delta v_t\right]$$

Outputs

$$\Delta y^T = \left[\Delta\hat{a}_z \quad \Delta\hat{q} \quad \Delta CAS \quad \Delta\theta \quad \Delta\hat{h} \quad \Delta\dot{\hat{h}} \quad \Delta\xi_h \quad \Delta\xi_{CAS} \quad \Delta u_t \quad \Delta u_e\right]$$

MR-PIFCGT $\quad \Delta t_f = 0.05$ sec; $\Delta t_s = 0.1$ sec

States

$$\Delta x^T = \left[\Delta u \quad \Delta w \quad \Delta q \quad \Delta\theta \quad \Delta h \quad \Delta\hat{a}_z \quad \Delta\hat{q} \quad \Delta\hat{h} \quad \Delta\dot{\hat{h}} \quad \Delta EPR \quad \Delta\delta_e \quad \Delta\xi_h \quad \Delta\xi_{CAS} \quad \Delta u_t \quad \Delta u_e\right]$$

Controls

$$\Delta u^T = \left[\Delta v_e \quad \Delta v_t\right]$$

Fast Outputs

$$\Delta y_f^T = \left[\Delta\hat{a}_z \quad \Delta\hat{q} \quad \Delta\xi_h \quad \Delta\xi_{CAS} \quad \Delta u_t \quad \Delta u_e\right]$$

Slow outputs

$$\Delta y_s^T = \left[\Delta CAS \quad \Delta\theta \quad \Delta\hat{h} \quad \Delta\dot{\hat{h}}\right]$$

WS-PIFCGT $\Delta t = 0.1$ sec

States

$$\Delta x^T = \left[\Delta u \;\; \Delta w \;\; \Delta q \;\; \Delta\theta \;\; \Delta h \;\; \Delta\hat{a}_z \;\; \Delta\hat{q} \;\; \Delta\hat{h} \;\; \Delta\dot{\hat{h}} \;\; \Delta EPR \;\; \Delta\delta_e \;\; \Delta\xi_h \;\; \Delta\xi_{CAS} \;\; \Delta u_t \;\; \Delta u_e\right]$$

Disturbances

$$\Delta s^T = \left[\Delta U_{wb} \;\; \Delta W_{wb}\right]$$

Controls

$$\Delta u^T = \left[\Delta v_e \;\; \Delta v_t\right]$$

Outputs

$$\Delta y^T = \left[\Delta\hat{a}_z \;\; \Delta\hat{q} \;\; \Delta CAS \;\; \Delta\theta \;\; \Delta\hat{h} \;\; \Delta\dot{\hat{h}} \;\; \Delta\xi_h \;\; \Delta\xi_{CAS} \;\; \Delta u_t \;\; \Delta u_e\right]$$

EP-PIFCGT $\Delta t = 0.1$ sec

States

$$\Delta x^T = \left[\Delta EP_1 \;\; \Delta EP_2 \;\; \Delta u \;\; \Delta w \;\; \Delta q \;\; \Delta\theta \;\; \Delta h \;\; \Delta\hat{a}_z \;\; \Delta\hat{q} \;\; \Delta\hat{h} \;\; \Delta\dot{\hat{h}} \;\; \Delta EPR \;\; \Delta\delta_e \;\; \Delta\xi_h \;\; \Delta\xi_{CAS} \;\; \Delta u_t \;\; \Delta u_e\right]$$

Disturbances

$$\Delta s^T = \left[\Delta U_{wb} \;\; \Delta W_{wb}\right]$$

Controls

$$\Delta u^T = \left[\Delta v_e \;\; \Delta v_t\right]$$

Outputs

$$\Delta y^T = \left[\Delta EP \;\; \Delta\hat{a}_z \;\; \Delta\hat{q} \;\; \Delta CAS \;\; \Delta\theta \;\; \Delta\hat{h} \;\; \Delta\dot{\hat{h}} \;\; \Delta\xi_h \;\; \Delta\xi_{CAS} \;\; \Delta u_t \;\; \Delta u_e\right]$$

The aircraft model is trimmed at 69 m/s (135 kt) descending straight flight using a glideslope of 3 deg. Flaps are set to 30 deg. The weight is 85000 lbs.

The five states for the longitudinal aircraft dynamics in body axis are the body x-axis velocity, Δu, the body z-axis velocity, Δw, pitch rate, Δq, pitch Euler angle, $\Delta\theta$ and vertical height Δz. The prefilter states, $\Delta\hat{a}_z$ and $\Delta\hat{q}$, model a continuous-time prefilter used to suppress aliasing errors in the body mounted z-axis accelerometer measurement for a_z and the rate gyro measurement for q. The noisy height measurement, h, which can come from a barometric altimeter or the Microwave Landing System (MLS), is complementary filtered with the gravity corrected output of the accelerometer to yield smooth estimates for $\hat{h}$ and $\dot{\hat{h}}$. The two states, ΔEPR and $\Delta\delta_e$, model the actuators dynamics for throttle and elevator respectively, and are discussed in Ref. 32. The type 1 property for the control system is obtained using the integrator states ξ_h and ξ_{CAS}. The integrator state, $\Delta\xi_h$, integrates the height command error plus 5 times the height rate error. The integrator state, $\Delta\xi_{CAS}$, integrates the CAS command error where CAS is a calibrated airspeed measurement. The states Δu_t and Δu_e are the perturbation aircraft control states placed in the state vector because of control rate weighting.

The multi-rate control design breaks the measurements into a fast-sample-rate group and a slow-sample-rate group. The fast rate is chosen to be 20 samples/sec while the slow rate is 10 samples/sec. The integrator states and control position states must be sampled at the fast rate. The two inner-loop measurements, $\Delta\hat{a}_z$ and $\Delta\hat{q}$, are also sampled at the fast rate. The slow measurements are airspeed, pitch angle and the output of the complementary filters. The complementary filter model in Φ is not modeled at the slow rate, however. Modeling a slow rate complementary filter in Φ would cause Φ to become a periodic matrix. The complementary filter is propagated and updated at 20 iterations/sec in the nonlinear simulation. The WS-PIFCGT design uses the wind shear disturbance dynamics in the design model. The nominal values used for u_z and w_z are -0.1 m/sec/m and 0.02 m/sec/m, respectively.

The EP-PIFCGT design includes the energy probe measurement in the WS-PIFCGT measurement vector. Two states, ΔEP_1 and ΔEP_2, are added to the state vector to model the sensor dynamics described in Refs. 10 and 11.

The longitudinal command model propagated in the simulation uses a double integration of vertical acceleration to generate the vertical path trajectory. The CAS trajectory is constant,

$$\begin{bmatrix} h_m \\ \dot{h}_m \end{bmatrix}_{k+1} = \begin{bmatrix} 1 & \Delta t \\ 0 & 1 \end{bmatrix} \begin{bmatrix} h_m \\ \dot{h}_m \end{bmatrix}_k + \begin{bmatrix} \Delta t^2/2 & 0 \\ \Delta t & 0 \end{bmatrix} \begin{bmatrix} \ddot{h}_m \\ CAS_m \end{bmatrix}_k \tag{195}$$

The commands used for $\ddot{h}_m$ in the nonlinear simulation are

$$\text{If } \dot{h}_m > -8.3 \text{ and } h_m > 200 \text{ Then } \ddot{h}_m = -1.5 \quad \text{Else} \tag{196}$$

$$\text{If } h_m < 150 \text{ and } \dot{h}_m < 0 \quad \text{Then } \ddot{h}_m = 1.5 \text{ Else } \ddot{h}_m = 0.0 \tag{197}$$

The command model descends at a constant rate of descent (8.3 ft/sec) until 150 ft is reached. The descent is changed to straight and level flight after h_m reaches 150 ft. The change to straight and level flight eventually puts the command model height state at 122ft. The aircraft and command model are initialized to 700ft straight and level flight at the beginning of the simulation. The command model used to design the command generator tracker feedforward gains only uses h_m, $\dot{h}_m$ and CAS_m as discussed in Ref. 3.

The design of the control system is achieved by choosing the diagonal elements in the matrices Q, R, X, W and V iteratively until the control system has desired closed-loop properties. Adjustments are made to the elements until one set of numbers, shown in Table 1, can be used in all four design conditions.

B. Control Design Properties

Six evaluation procedures are used to determine the feedback and tracking properties of the control designs. The six evaluations are the feedback gain elements, singular value plots, Ref. 33, eigenvalue plots, Ref. 33, Bode plots for each control loop, closed-loop eigenvalues and nonlinear simulations.

The feedback gain and feedforward gain matrices are shown in Table 2. Comparing the single rate and multi-rate designs, the gain elements almost all increased in value an average of 25% in the elevator loop. The elevator loop bandwidth increased in the multi-rate design as shown by the -9.37 control gain. The multi-rate design had less of an effect on the throttle loop which has a much lower bandwidth. The two wind shear design gain elements change significantly from the case when no wind shear is modeled in three of the measurement loops: $\hat{a}_z$, $\hat{h}$, and ξ_{CAS}. One of the closed-loop poles is significantly altered (destabilized) by the wind shear dynamics and the increased gain values on these three measurements appear to improve system robustness to wind shear disturbances. The throttle loop bandwidth increases in the presence of the wind shear dynamics as evidence by the -3.63 and -4.9 δ_T control gains.

The closed-loop eigenvalues for the designs are obtained from the discrete system linear matrices. Each eigenvalue inside the unit circle in the z-domain is mapped to the left-half plane using

$$\lambda_z = a + jb = me^{j\theta} \tag{198}$$

$$\lambda_s = \frac{1}{\Delta t} \ln \lambda_z = \frac{m}{\Delta t} + j \frac{\theta}{\Delta t} \tag{199}$$

The three single rate designs are evaluated with and without the wind shear dynamics. The SR-PIFCGT closed-loop eigenvalues shown in Table 3 have adequate damping and stability without the wind shear system. The wind shear dynamics introduce two poles into the system; one is neutrally stable while the other is

slightly unstable. Windshear as a phenomenon only occurs for a specific period of time. The control system's objective is to maintain control over the aircraft dynamics and track the command model. The primary change in the closed-loop eigenvalues is that the pole most associated with the phugoid motion ($\omega_n = 0.35$, $\xi = 0.49$) changes damping to $\xi = 0.19$, i.e., the phugoid motion destablizes. Increasing the nominal values for the wind shear gradients further destabilizes the phugoid mode.

The new capability provided by the theoretical derivation in Section 5D allows the design plant model to contain the unstable coupled windshear dynamics. The WS-PIFCGT closed-loop eigenvalues are presented in Table 4. The closed-loop model without wind shear has good damping ratios on complex modes ($\xi > 0.5$) with the windshear model, the phugoid mode destabilizes but has better damping than the mode in Table 3 ($\xi = 0.33$ verses $\xi = 0.19$). The energy probe further aids in stabilizing the phugoid mode as shown in Table 5 ($\xi = 0.40$).

The closed-loop mapped eigenvalues for the multi-rate design are shown in Table 6. Despite a significant change in feedback gains between single and multi-rate designs, the closed-loop eigenvalues for the single rate and multi-rate designs are similiar. The multi-rate and single rate designs use the same quadratic weights. The extra three poles in Table 6 are caused by the hold circuits in the system model.

The frequency domain methods for evaluating the single rate control designs result in the plots shown in Figs. 1 to 6 and Table 7. Frequency domain analysis of the multi-rate design is not within the scope of this effort. The minimum singular value of the return difference matrix, as discussed in Ref. 33, is a conservative indication of closed-loop plant robustness to unstructured perturbations in the plant dynamics. A small singular value means there is a small plant perturbation (physically unrealizable perturbations are allowed)

that can destabilize the plant. The three singular value plots all indicate potentially poor designs. Reference 33 investigated singular values and demonstrated that eigenvalue analysis of the return difference matrix, although a not guranteed indication of robustness, provides a clear picture of the possible robustness boundary. The eigenvalues of the return difference matrix are bounded below by the minimum singular value and above by the maximum singular value. The true multivariable plant robustness should be bounded between the minimum singular value and the minimum eigenvalue of the return difference matrix.

The eigenvalue plots in Figs. 1 to 3 indicate a much more robust design then the singular value plots and compare favorably to the information provided by the Bode plots. The smallest eigenvalue is near $\omega = 3.5$ rad/sec in all three design. Specific values are shown in Table 7. The frequency for the smallest eigenvalue is near the frequency for the short period modes shown in Tables 3 to 5. Another effect evident from the eigenvalue and singular value plots in Fig. 3 is that the energy probe sensor increases plant robustness in the low frequency region, $\omega < 1$, where plant alterations due to windshear are likely to occur.

The Bode plots in Figs. 4 to 6 provide useful information concerning the bandwidth and robustness of each loop, individually. The bandwidth (the frequency at which the gain remains below -6 db) for throttle is between 0.5 rads/sec and 0.25 rads/sec. The designs using the windshear dynamics have lower throttle bandwidth. The bandwidth for the elevator is between 2 and 3 rads/sec. All phase margins are better than 65 degs and gain margins are better than -10 db.

C. Nonlinear Simlations

Nonlinear six degree-of-freedom simulations of the control systems for a glideslope capture and track are shown in Figs. 7 to 9 . Windshear, gust disturbances and measurement noise are inactive in the simulation. The captures are

smooth with little overshoot both at the beginning and end of the simulation where the aircraft returns to straight and level flight. The best performance is provided by the multi-rate design which has smoother surface motion and better CAS control.

The next four simulations in Figs. 10 to 13 show the four control designs capturing and tracking the glideslope in the presence of windshear. The longitudinal, horizontal and vertical shears are shown in Fig. 16 and correspond to the windshear in the SRI package known as the Philadelphia/Allegheny windshear. The aircraft encounters an increasing headwind. The headwind decreases gradually then dramatically into a tailwind. The tailwind changes back to zero. Coincident with the change from a headwind to a tailwind, the aircraft encounters a downward vertical wind of 20kt. The large drop in airspeed causes the control systems to briefly saturate throttle (at 60 deg) and pitch the aircraft up to 8 deg.

The best windshear response is provided by the WS-PIFCGT design. The airspeed deviations are smaller and the aircraft pitches up the least (6 deg). The WS-PIFCGT design also maintains the largest separation between the aircraft and the ground in the critical time period between 75 and 85 secs into the simulation. The MR-PIFCGT design has the largest deviations in airspeed and height during the windshear. The EP-PIFCGT design using the energy probe sensor for feedback encountered small elevator and throttle oscillations when throttle surpassed 30 degrees.

A 1 kt gust is added to the nonlinear simulations in Figs. 14 and 15. The effect of the gusts is primarily evident in the throttle response. The tracking is relatively unaffected by the gust response.

7. SUMMARY AND RECOMMENDATIONS

A summary of the results in this report are:

- Optimal output feedback is successfully used to design a single rate control system using the proportional integral filter structure.
- The optimal output feedback approach and optimal output feedback algorithm are extended to use the hierarchical control design approach with minimal change to the output feedback design model matrices. Unwanted states and observations encountered as each loop is designed are made uncontrollable and unobservable and stabilized if the mode is not stable.
- An optimal multi-rate output feedback synthesis problem is formulated and necessary conditions for an optimal solution are derived. An algorithm to solve for the constant gain solution is presented. The algorithm is programmed and designs are made comparing the multi-rate and single rate designs. The PIF structure is extended to use multi-rate output feedback. The PIF feedforward gain is shown to be periodic in time.
- The command generator tracker is extended to accommodate disturbances which are affected by the plant dynamics. The extension causes one of the Lyapunov equations encountered in the usual command generator tracker to become a generalized Riccati equation. A globally convergent algorithm for solving the generalized Riccati equation is developed.
- A new and novel approach is developed to accommodate windshear in the presence of noise. The command generator tracker is extended to the stochastic environment. The steady-state plant response is decomposed into the stochastic and deterministic components. A novel cost function

is constructed which suppresses the effect of disturbances, stabilizes the stochastic plant response and does not require a measurement of the disturbance state. The disturbance and plant dynamics can be coupled. An algorithm which computes the (local) optimal gain is developed, has been programmed and is used to determine a PIFCGT control system.

- Design and simulations showed that the multi-rate design (which uses faster measurements on some sensors) performs best for the quadratic weights chosen when no disturbances are present. The design using the new disturbance accommodation synthesis approach performs best when the aircraft is simulated flying through a windshear. The windshear design using the energy probe also performs well except for small oscillations that occur during the severe part of the windshear simulations.

Recommendations

- The command generator tracker can be extended to the multi-rate case.
- The multi-rate command generator tracker would allow the computation of the multi-rate frequency response by extending the approach developed in Ref. 30.
- The multirate problem can be extended to include the case of many models with one controller as discussed in Ref. 17.
- The solution in Section 5B has application beyond disturbance suppression. The solution in Section 5B solves a feedback decoupling problem. Consider the lateral dynamics of the aircraft where it is desirable to decouple the roll and sideslip response. Partioning the plant states into two groups and identifing one group as Δx and the other group as Δs, the feedforward solution yields a control system for decoupling the $H\Delta x$ response from the Δs states. $H\Delta x$ can be sideslip and Δs can be the roll state. Any rolling motion would not affect sideslip.

APPENDIX A

A Convergent Algorithm for a Generalized Riccati Equation:

A generalized Riccati equation has the following form:

$$X = A\,X\,B + A\,X\,C\,X + D \tag{200}$$

where X is an unknown matrix. If A were invertible then Eq. 200 could be rewritten as

$$0 = F\,X + X\,B + X\,C\,X + G \tag{201}$$

which resembles the continuous-time Riccati equation obtained in the optimal regulator problem.

Define the function f(X) as

$$f(X) = A\,X\,B + A\,X\,C\,X + D \tag{202}$$

and define the direction, d, at X as

$$d = A\,d\,B + A\,d\,C + A\,X\,C\,d + (f(X)-X) \tag{203}$$

Define the matrix, E, as

$$E = (I - A\,X\,C)^{-1} \tag{204}$$

the direction, d, satisfies the Lyapunov equation

$$d = E\,A\,d\,(B + C) + E\,(f(X)-X) \tag{205}$$

The globally convergent algorithm for computing X is

1. Choose a starting value for X, usually $X_o = 0$.
2. Compute d_k in Eq. 205 using X_k.
3. Choose α_k according to

$$\alpha_k = \min\left\{1.0, \frac{1}{2}\,\frac{\| f(X_k) - X_k \|}{\| A\,d_k\,C\,d_k \|}\right\} \tag{206}$$

4. Update X_k using

$$X_{k+1} = X_k + \alpha_k d_k \tag{207}$$

5. If $\|f(X_k) - X_k\|$ is small, stop, otherwise increment k and go back to 1.

REFERENCES

1. Downing, D. R., Bryant, W. H. and Ostroff, A. J.: "Flight Test of a VTOL Digital Autoland System Along Complex Trajectories", Proc. of the 1979 AIAA Guidance and Control Conference, Boulder, CO, August 1979.

2. Broussard, J. R.: "Design, Implementation and Flight Testing of PIF Autopilots for General Aviation Aircraft", NASA CR-3709, July 1983.

3. Broussard, J. R.; and Halyo, N.: Investigation, Development, and Application of Optimal Output Feedback Theory. Volume II. NASA CR-3829, 1984.

4. Halyo, N.: "Development of a Digital Guidance and Control Law for Steep Approach Automatic Landings Using Modern Control Techniques", NASA CR-3074, February 1979.

5. O'Brien, M. J. and Broussard, J. R.: "Feedforward Control to Track the Output of a Forced Model", The 17th IEEE Conference on Decision and Control, San Diego, CA, January 1979.

6. Berry, P. W., Broussard, J. R., and Gully, S. W.: "Validation of High Angle of Attack Methods," ONR-CR215-237-3, September 1979.

7. Maybeck, P. S.: Stochastic Models, Estimation and Control, Vol. 3, Academic Press, New York, NY, 1982.

8. Halyo, N.; and Broussard, J. R.: Investigation, Development, and Application of Optimal Output Feedback Theory. Volume I. NASA CR-3828, 1984.

9. Sandell, N. R., Varaiya, P., Athans, M., and Safonov, M. G.: "Survey of Decentralized Control Methods for Large Scale Systems", IEEE Trans. on Automatic Control, Vol. AC-23, 1978, pp. 108-128.

10. Ostroff, A. J., Hueschen, R. M., Hellbaum, R. F. and Creedon, J. F.: "Flight Evaluation of a Simple Total Energy-Rate System with Potential Wind-Shear Application", NASA TP-1854, May 1981.

11. Nicks, Oran W.: Aircraft Total Energy Sensor. NASA TM X-73928, 1976.

12. Dorato, P., Louis, A. H.: "Optimal Linear Regulators: The Discrete-Time Case," IEEE Trans. Auto Control, Vol. AC-16, No. 6, December 1971.

13. Kwakernaak, H.; and Sivan, R.: Linear Optimal Control Systems. John Wiley & Sons, Inc., c.1972.

14. Doyle, J. C., and Stein, G.: "Multivariable Feedback Design, Concepts for a Classical/Modern Synthesis". IEEE Trans. Auto. Control, Vol. AC-26, No. 1, Feb. 1981, pp. 4-16.

15. Broussard, J. R. and Halyo, N.: "Active Flutter Suppression Using Optimal Output Feedback Digital Controllers", NASA CR-165939, May 1982.

16. Caglayan, A. K., Halyo, N., and Broussard, J. R.: "The Use of the Optimal Output Feedback Algorithm in Integrated Control System Design", NAECON, Dayton, Ohio, May 17-19, 1983.

17. Halyo, N.: and Broussard, J. R.: Algorithms for Output Feedback, Multiple Model and Decentralized Control Problems. NASA Aircraft Controls Research - 1983, NASA CP-2296, 1984, pp. 281-304.

18. Glasson, D. P.: "A New Technique for Multirate Digital Control Design and Sample Rate Selection", Journal of Guidance and Control, Vol. 5, No. 4, July - August 1982.

19. Armstrong, E. S.: ORACLS - A Design System for Linear Multivariable Control, Marcel Dekker, Inc., New York, c.1980.

20. Halyo, N., and Foulkes, R. E., "On the Quadratic Sampled-Data Regulator with Unstable Random Disturbances", IEEE SMC Cos. Proc., 1974 International Conf., on Syst., Man and Cybern., pp. 99-103, Oct. 1974.

21. Johnson, C. D.: "Accommodation of External Distrubance in Linear Regulator and Servomechanism Problems", IEEE Trans. Auto. Control, Vol. AC-16, 1971, pp. 635-644.

22. Johnson, C. D.: "Discrete-Time Disturbance-Accommodating Control Theory with Applications to Missile Digital Control", Journal of Guidance and Control, Vol. 4, No. 2, March-April 1981, pp. 116-125.

23. Levin, V. and Kreindler, E.: "Use of Disturbance Estimator for Disturbance Suppression", IEEE Trans. Auto. Control, Vol. AC-21, 1976, pp. 776-778.

24. Davison, E. J.; "The Output Control of Linear Time-Invariant Multivariable Systems with Unmeasurable Arbitrary Disturbances", IEEE Trans. Auto. Control, Vol. AC-17, 1972, pp. 621-629.

25. Wonham, W. M.: Linear Multivariable Control: A Geometric Approach, New York, Springer-Verlag, 1979.

26. Bhattacharyyo, S. P.: "Disturbance Rejection In Linear Systems", Int. J. Sys. Sci., Vol. 5, No. 7, 1974, pp. 633-639.

27. Shah, S. L. Seborg, D. E., and Fisher, D. G.: "Disturbance Localization in Linear Systems by Eigenvector Assigment", Int. J. of Control, Vol. 6, 1977, pp. 853-869.

28. Willems, J. L.: "Disturbance Isolation in Linear Feedback Systems", Int. J. Systems Sci., Vol. 6, 1975, pp. 233-238.

29. Belcastro, Christine M.; and Ostroff, Aaron J.: Total Energy-Rate Feedback for Automatic Glide-Slope Tracking During Wind-Shear Penetration. NASA TP-2412, May 1985.

30. Broussard, J. R.: "Computation of Differential Equation Particular Solutions with Application to Sigma Plots", IEEE Trans. on Automatic Control, Vol. AC-29, 1984, pp. 457-459.

31. Dieudonne, J. E.: "Comments on a Proposed Standard Wind Hazard Environment and Its Use in Real Time Aircraft Simulation", AIAA 17th Aerospace Science Meeting, New Orleans, LA, January 1979, AIAA paper 79-0324.

32. Broussard, J. R. and Stallman, S. T.: "Modification and Verification of an ACSL Simulation of the ATOPS B-737 Research Aircraft", NASA CR-166049, February 1983.

33. Mukhopadhyay, V. and Newsom, J. R.: "Application of Matrix Singular Value Properties for Evaluating Gain and Phase Margins of Multi-loop Systems", Proc. of the AIAA Guidance and Control Conference, San Diego, CA, August 1982.

TABLE 1. DESIGN PARAMETERS FOR THE CONTROL DESIGNS
(UNITS ARE FT. AND DEG)

X + W States	W Matrix Diagonal Elements	Q Matrix Diagonal Elements	Additional Q Weights
u	100.00	0.0016	$\dot{w}$ 3.5
w	25.0	0.16	
q	0.01	0.0081	
θ	0.01	0.0081	
h	100.0	0.04	
a_z	0.25	0.0	
q	40.0	0.0	
h	64.0	0.0	
$\dot{h}$	10.24	0.0	
EPR	1.0	0.0	
δ_e	1.0	0.0	
ξ_h	0.0	0.0009	
ξ_{CAS}	0.0	0.004	
u_t	16.0	0.09	
u_e	4.0	0.01	
EP1	1.0	0.0	
EP2	1.0	0.0	

R Matrix Diagonal Elements		V Matrix Diagonal Elements	
v_t	0.09	$\hat{a}_z$	0
v_e	0.04	$\hat{q}$	0
		CAS	9.0
		θ	9.0
		$\hat{h}$	0
		$\dot{\hat{h}}$	0
		ξ_h	0
		ξ_{CAS}	0
		u_t	0
		u_e	0
		EP	0

TABLE 2. FEEDBACK GAINS FOR THE CONTROL SYSTEMS

CONTROL	STATE FEEDBACK GAINS							CONTROL DESIGN
	E_p	$\hat{a}_z$	$\hat{q}$	CAS	θ	$\hat{h}$	$\dot{\hat{h}}$	
v_T	-	-6.33	-0.566	-2.18	-0.47	-0.57	-2.69	SINGLE RATE
v_e	-	1.65	4.23	1.91	6.69	0.76	1.72	DESIGN
v_T	-	-9.38	-0.37	-2.10	0.171	-0.923	-3.10	SINGLE RATE
v_e	-	5.14	4.80	1.91	6.88	1.06	4.09	WINDSHEAR DESIGN
v_T	-1.35	-9.86	-0.90	-2.05	1.14	-1.06	-4.97	SINGLE RATE
v_e	1.14	4.69	4.08	2.67	7.56	1.08	4.92	WINDSHEAR DESIGN WITH ENERGY PROBE
v_T	-	-6.92	-0.41	-2.24	-0.367	-0.628	-2.86	MULTI-RATE
v_e	-	2.56	5.5	2.39	8.22	0.99	2.27	DESIGN

TABLE 2. FEEDBACK GAINS FOR THE CONTROL SYSTEMS (CONTINUED)

CONTROL	INTEGRATOR GAINS ξ_1	ξ_2	CONTROL DESIGN
v_T	-0.075	-0.11	SINGLE RATE
v_e	0.064	0.003	DESIGN
v_T	-0.086	-0.184	SINGLE RATE
v_e	0.099	0.060	WINDSHEAR DESIGN
v_T	-0.196	-0.26	SINGLE RATE
v_e	UNAVAILABLE		WINDSHEAR DESIGN WITH ENERGY PROBE
v_T	-0.077	-0.11	MULTI-RATE
v_e	0.083	0.0078	DESIGN

CONTROL	CONTROL GAINS δ_T	δ_e	CONTROL DESIGN
v_T	-2.59	-1.0	SINGLE RATE
v_e	1.31	1.76	DESIGN
v_T	-3.63	-0.75	SINGLE RATE
v_e	2.37	-8.53	WINDSHEAR DESIGN
v_T	-4.9	0.174	SINGLE RATE
v_e	3.75	-7.1	WINDSHEAR DESIGN WITH ENERGY PROBE
v_T	-2.64	-0.631	MULTI-RATE
v_e	1.67	-9.37	DESIGN

TABLE 2. FEEDBACK GAINS FOR THE CONTROL SYSTEMS (CONCLUDED)

CONTROL	FEEDFORWARD GAIN $\dot{h}_m$	FEEDFORWARD GAIN V_m	CONTROL DESIGN
v_T	5.4	1.4	SINGLE RATE
v_e	-3.4	-0.039	DESIGN
v_T	7.73	0.785	SINGLE RATE
v_e	-6.59	0.157	WINDSHEAR DESIGN
v_T	7.89	0.373	SINGLE RATE
v_e	-6.59	0.157	WINDSHEAR DESIGN WITH ENERGY PROBE
			MULTI-RATE DESIGN
v_T	-0.064	-0.016	$-K_\xi B$
v_e	0.032	-0.0033	
v_T	2.95	2.19	$-K_s C_s A_{12}$
v_e	-4.21	-1.34	
v_T	1.65	-1.26	$-K_\xi A - K_f C_f A_{12} - K_u A_{22}$
v_e	0.75	1.26	

TABLE 3. CLOSED LOOP MAPPED EIGENVALUES FOR THE SINGLE RATE DESIGN (SR-PIFCGT)

DESIGN CONDITION WITHOUT WINDSHEAR			DESIGN CONDITION WITH WINDSHEAR			IDENTIFIABLE MODE
REAL	ω_n (rad/sec)	ζ	REAL	ω_n (rad/sec)	ζ	
	21.3	0.84		21.3	0.84	
-10.0			-10.0			
- 4.7			- 4.7			
	2.60	0.58		2.60	0.58	SHORT PERIOD
	0.84	0.98		0.82	0.99	
	0.52	0.68		0.63	0.69	
	0.35	0.49		0.369	0.19	PHUGOID
	0.079	0.64		0.063	0.90	
-0.08			-0.13			
			0.0			
			0.04			

TABLE 4. CLOSED-LOOP MAPPED EIGENVALUES FOR THE SINGLE RATE DESIGN WITH WINDSHEAR (WS-PIFCGT)

DESIGN CONDITION WITHOUT WINDSHEAR			DESIGN CONDITION WITH WINDSHEAR			IDENTIFIABLE MODE
REAL	ω_n (rad/sec)	ζ	REAL	ω_n (rad/sec)	ζ	
	22.77	0.71		22.77	0.71	
-10.0			-10.0			
- 4.3			- 4.3			
	3.1	0.57		3.1	0.58	SHORT PERIOD
	1.00	0.76		0.97	0.73	
	0.59	0.68		0.59	0.80	
	0.26	0.67		0.42	0.33	PHUGOID
	0.081	0.51		0.075	0.67	
-0.088			-0.088			
			0.0			
			0.035			

TABLE 5. CLOSED-LOOP MAPPED EIGENVALUES FOR THE SINGLE RATE WINDSHEAR DESIGN WITH THE ENERGY PROBE (EP-PIFCGT)

DESIGN CONDITION WITHOUT WINDSHEAR			DESIGN CONDITION WITHOUT WINDSHEAR			IDENTIFIABLE MODE
REAL	ω_n (rad/sec)	ζ	REAL	ω_n (rad/sec)	ζ	
	22.13	0.71		22.13	0.71	
-10.0			-10.0			
- 4.5			- 4.5			
	3.74	0.56		3.74	0.57	SHORT PERIOD
	1.65	0.89		1.64	0.91	
	0.90	0.55		0.88	0.55	
				0.57	0.77	
	0.21	0.74		0.37	0.40	PHUGOID
	0.08	0.41		0.072	0.57	
-0.13			-0.08			
			0.0			
			0.039			

TABLE 6. CLOSED-LOOP MAPPED EIGENVALUES FOR THE MULTI-RATE CONTROL DESIGN

DESIGN CONDITION WITHOUT WINDSHEAR			IDENTIFIABLE MODE
REAL	ω_n (rad/sec)	ζ	
	370	0.99	
	366	0.99	
	325	0.99	
	20.6	0.96	
-10.0			
- 5.2			
	2.6	0.57	SHORT PERIOD
	0.82	0.95	
	0.52	0.69	
	0.34	0.50	PHUGOID
	0.080	0.66	
-0.075			

TABLE 7. FREQUENCY DOMAIN PROPERTIES OF THE CONTROL DESIGNS
(ω is in rad/sec)

CONTROL DESIGN	MINIMUM SINGULAR VALUE		MINIMUM EIGENVALUE		THROTTLE				ELEVATOR			
					GAIN MARGIN		PHASE MARGIN		GAIN MARGIN		PHASE MARGIN	
	db	ω	db	ω	db	ω	deg	ω	db	ω	deg	ω
SR-PIFCGT	-15.07	0.4	-2.8	3.3	-18.0	1.4	84	0.15	-13.0	4.6	80	0.45
WS-PIFCGT	-12.8	0.9	-3.7	3.3	-20.0	1.7	70	0.1	-40.0	4.3	80	0.63
EP-PIFCGT	-14.1	0.1	-3.5	3.9	-20.8	1.7	84	0.15	-10.0	4.7	69	0.57

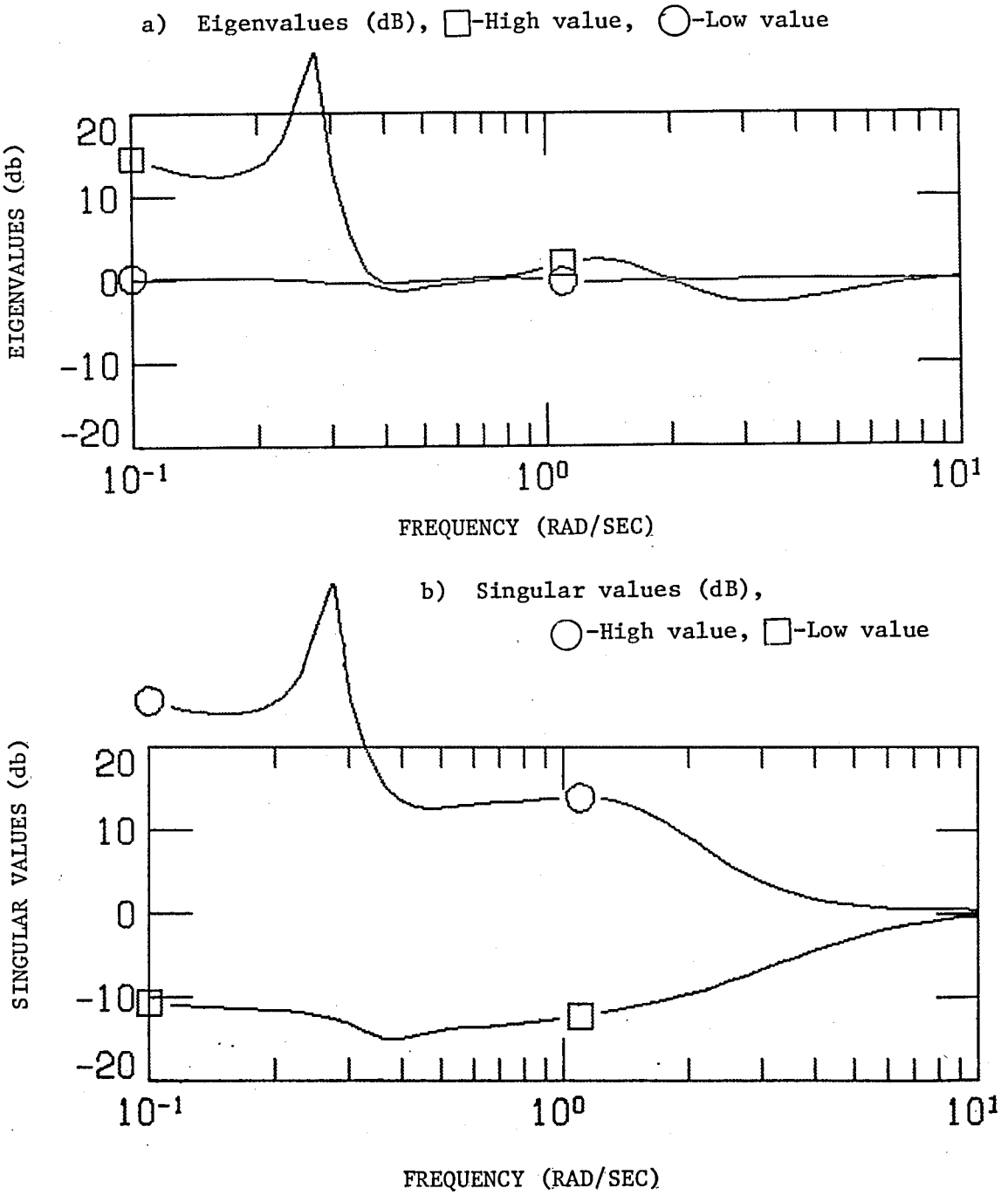

FIGURE 1. SINGULAR VALUE AND EIGENVALUE PLOTS FOR THE SINGLE RATE DESIGN (SR-PIFCGT).

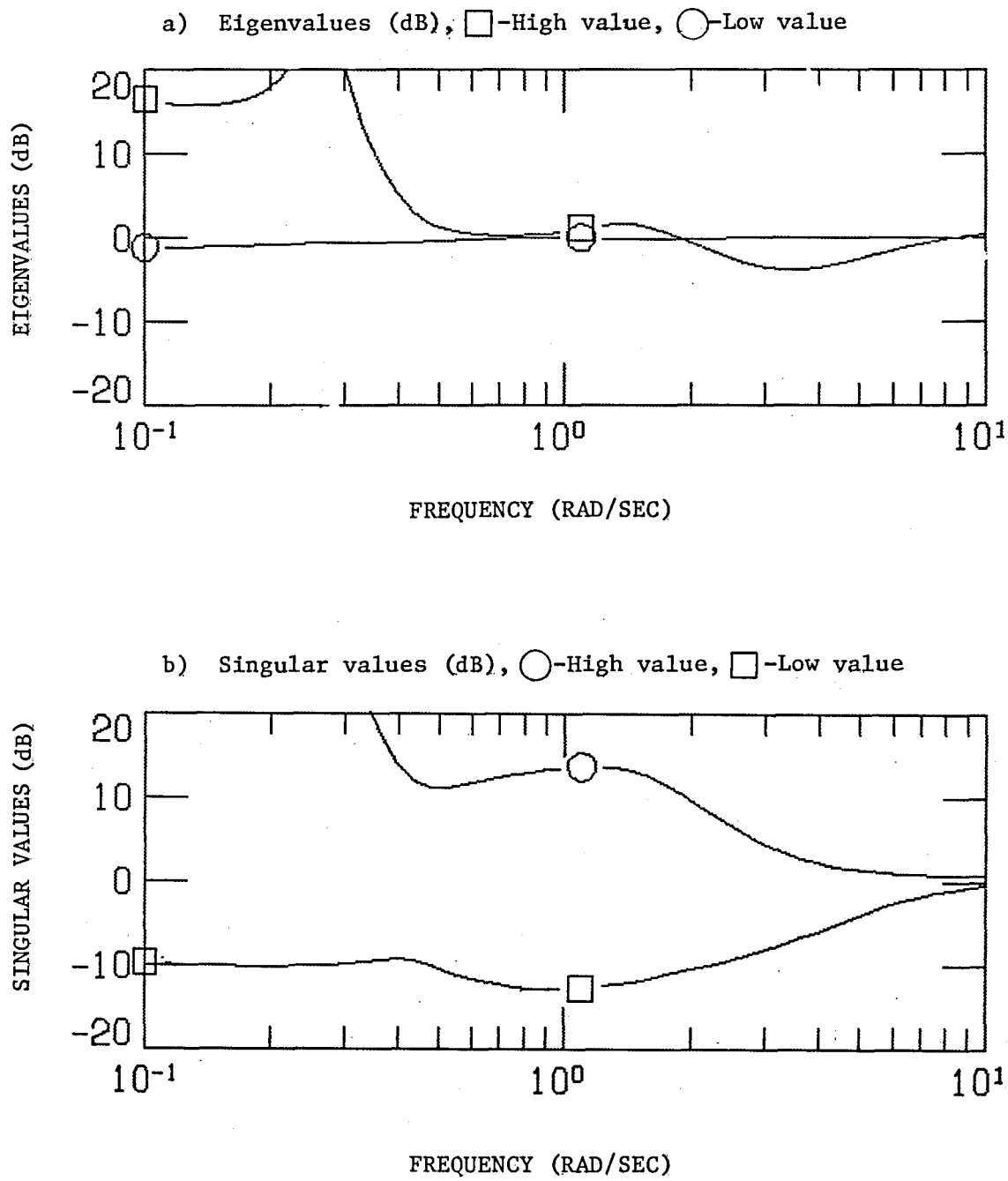

FIGURE 2. SINGULAR VALUE AND EIGENVALUE PLOTS FOR THE SINGLE RATE WINDSHEAR DESIGN (WS-PIFCGT).

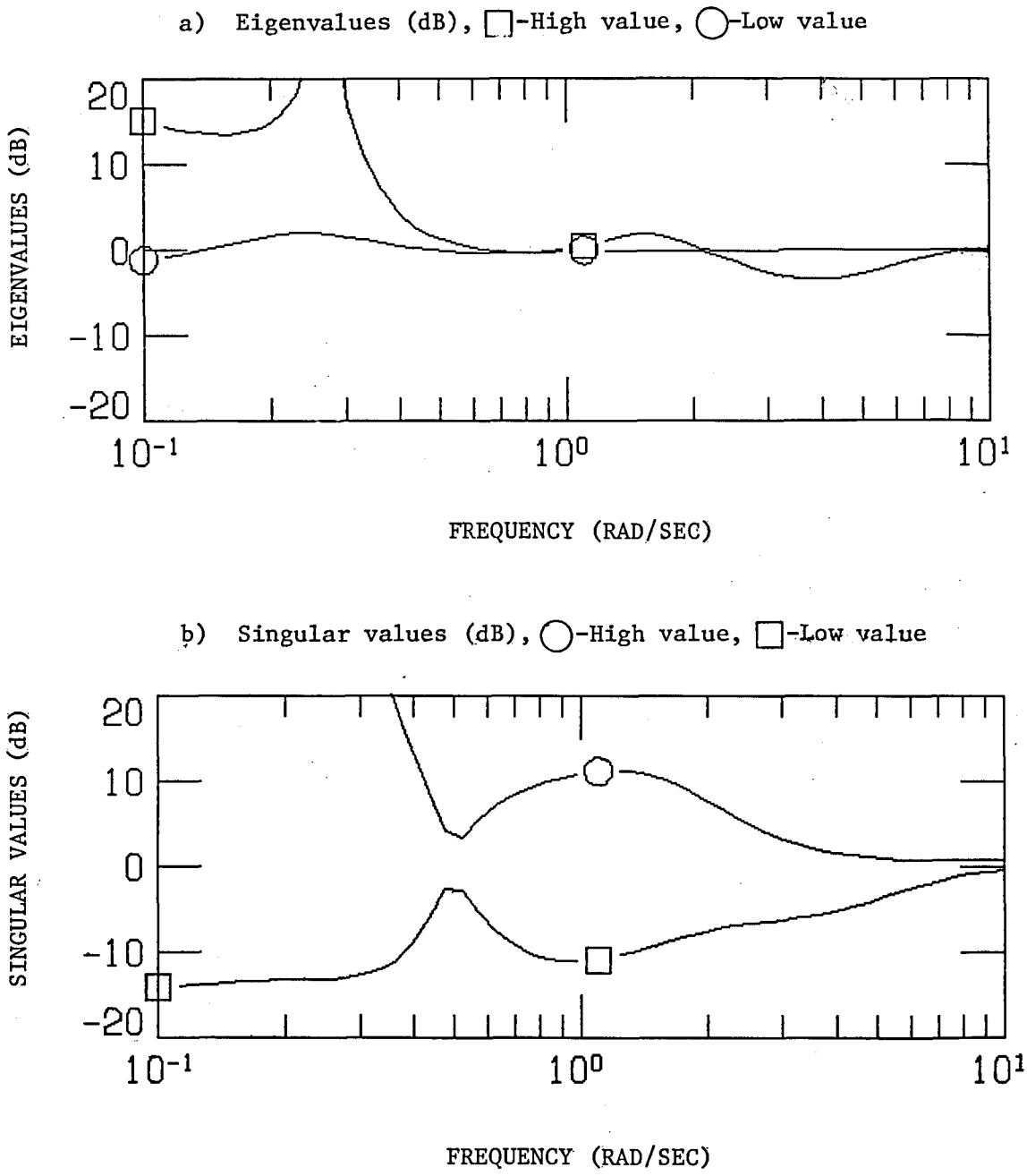

FIGURE 3. SINGULAR VALUE AND EIGENVALUE PLOTS FOR THE SINGLE RATE WINDSHEAR DESIGN WITH THE ENERGY PROBE (EP-PIFCGT)

a) Throttle-Loop Open,○-Gain, □-Phase

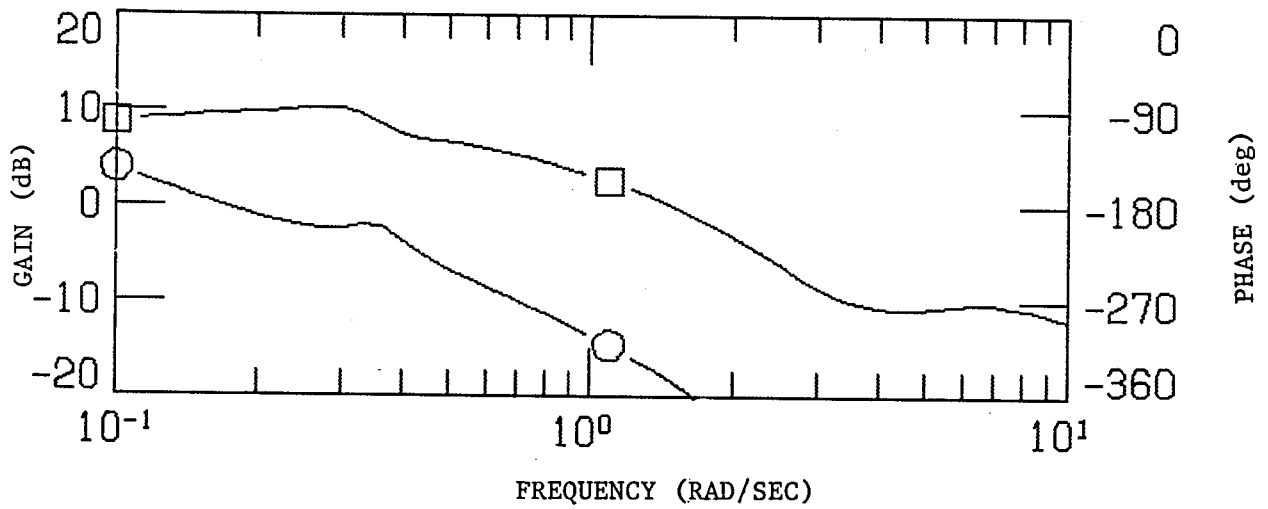

b) Elevator-Loop Open,○-Gain,□-Phase

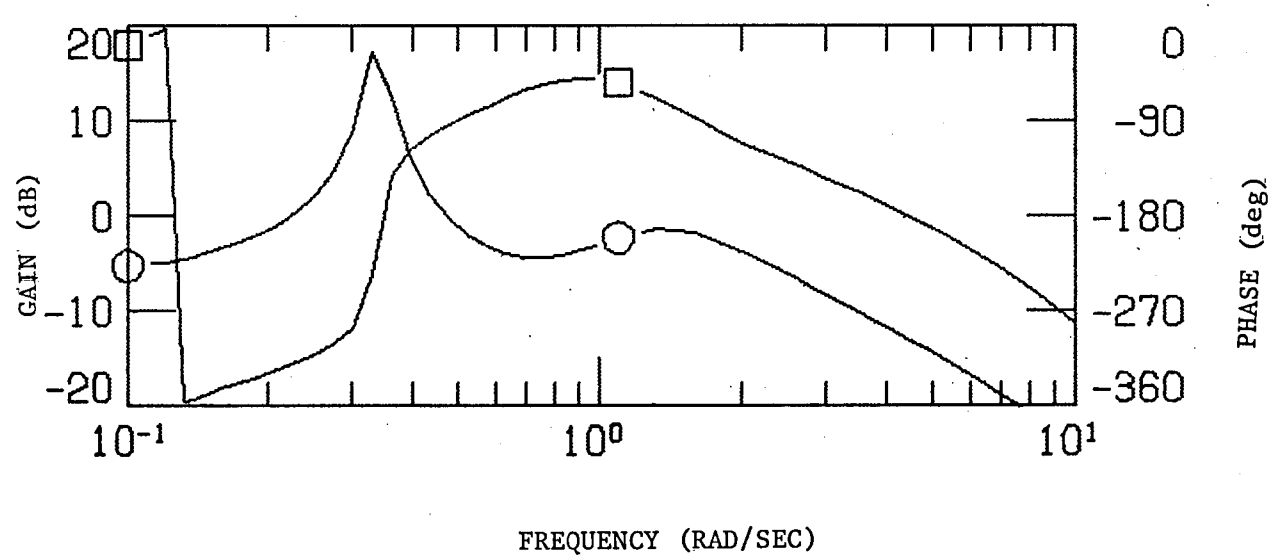

FIGURE 4. BODE PLOTS FOR THE SINGLE RATE DESIGN (SR-PIFCGT)

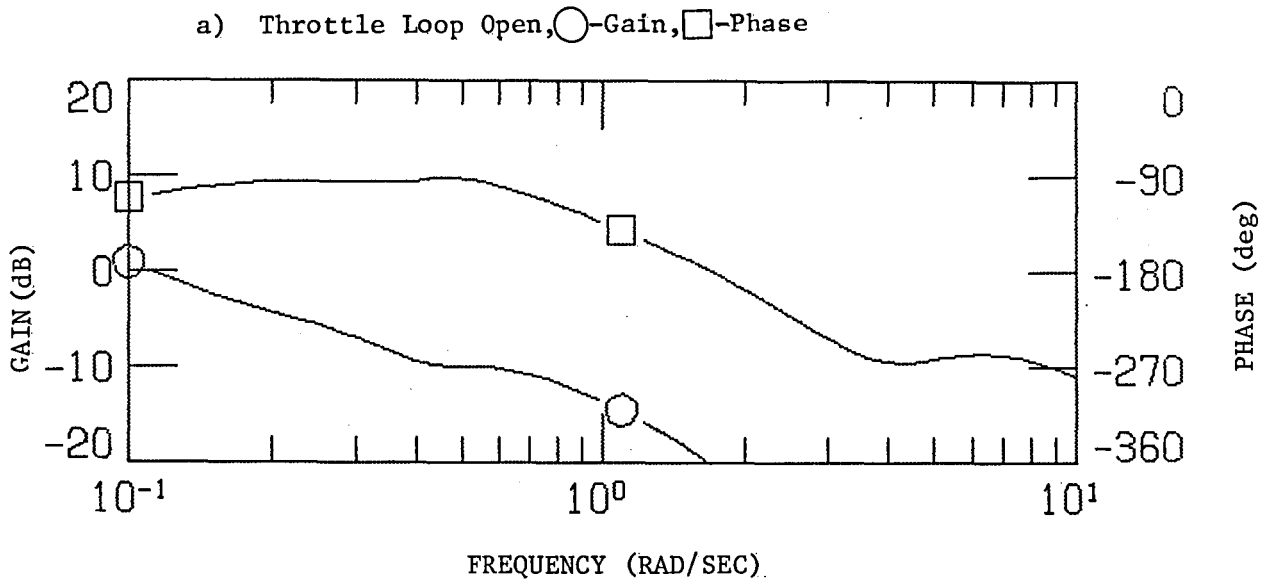

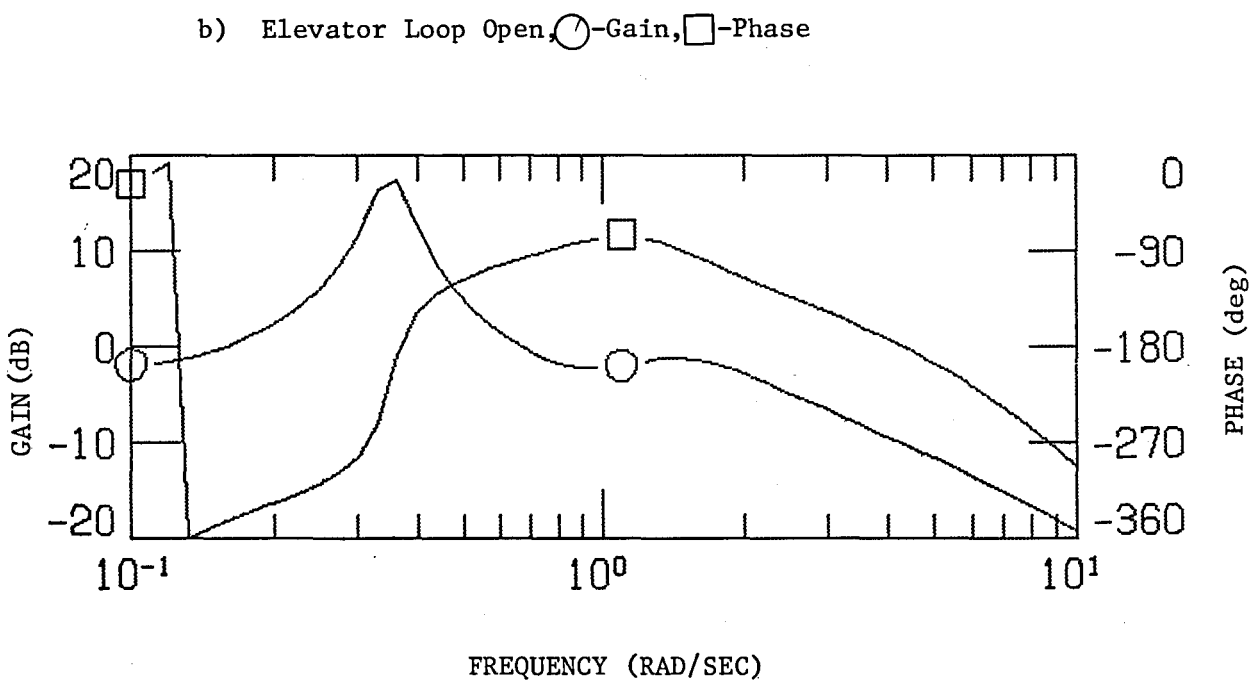

FIGURE 5. BODE PLOTS FOR THE SINGLE RATE WINDSHEAR DESIGN (WS-PIFCGT)

a) Throttle Loop Open,◯-Gain, □-Phase

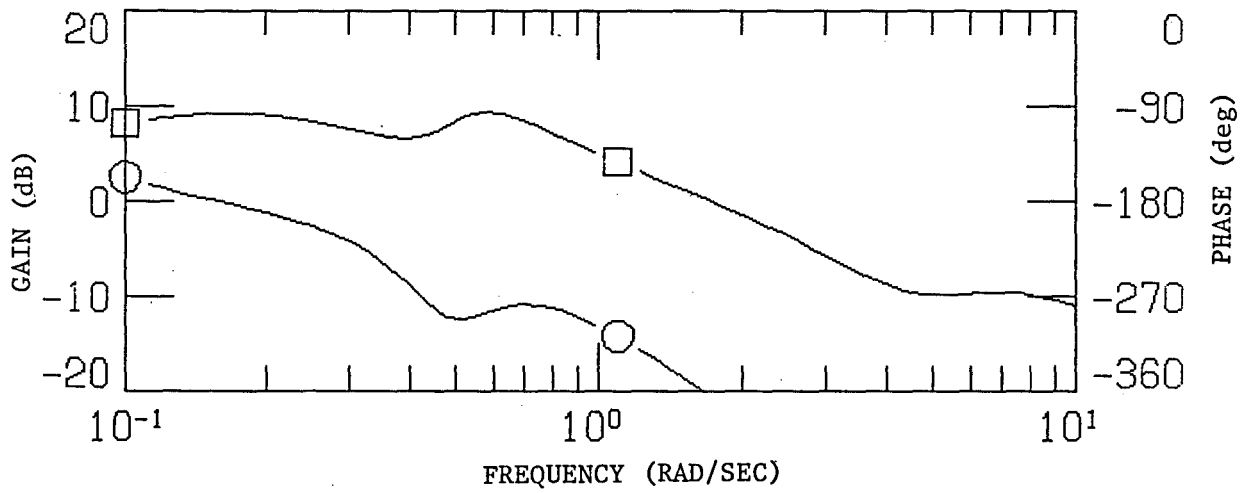

b) Elevator Loop Open,◯-Gain,□-Phase

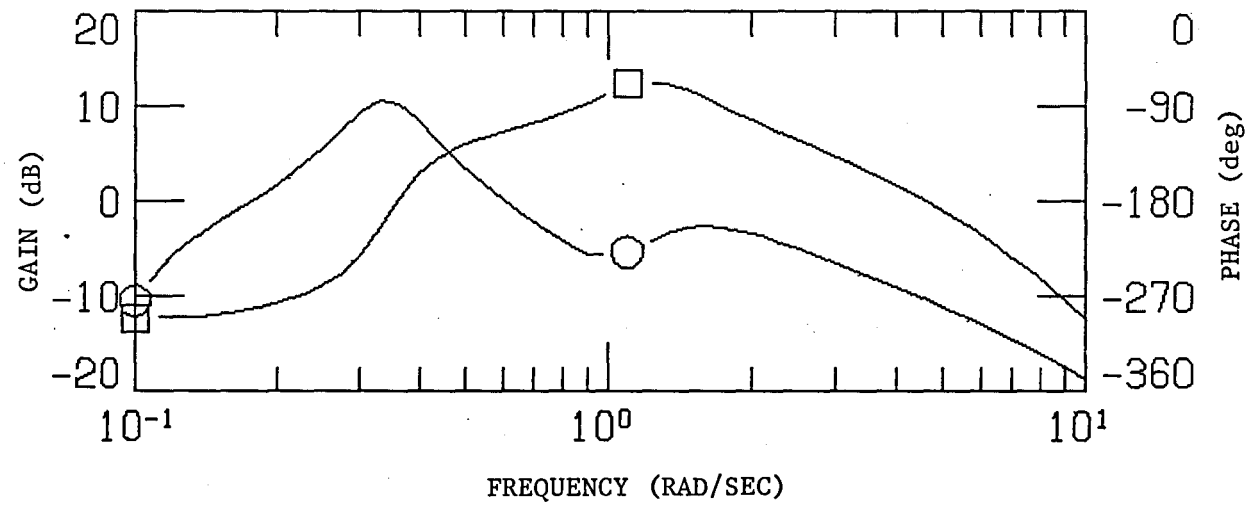

FIGURE 6. BODE PLOTS FOR THE SINGLE RATE WINDSHEAR DESIGN WITH THE ENERGY PROBE. (EP-PIFCGT)

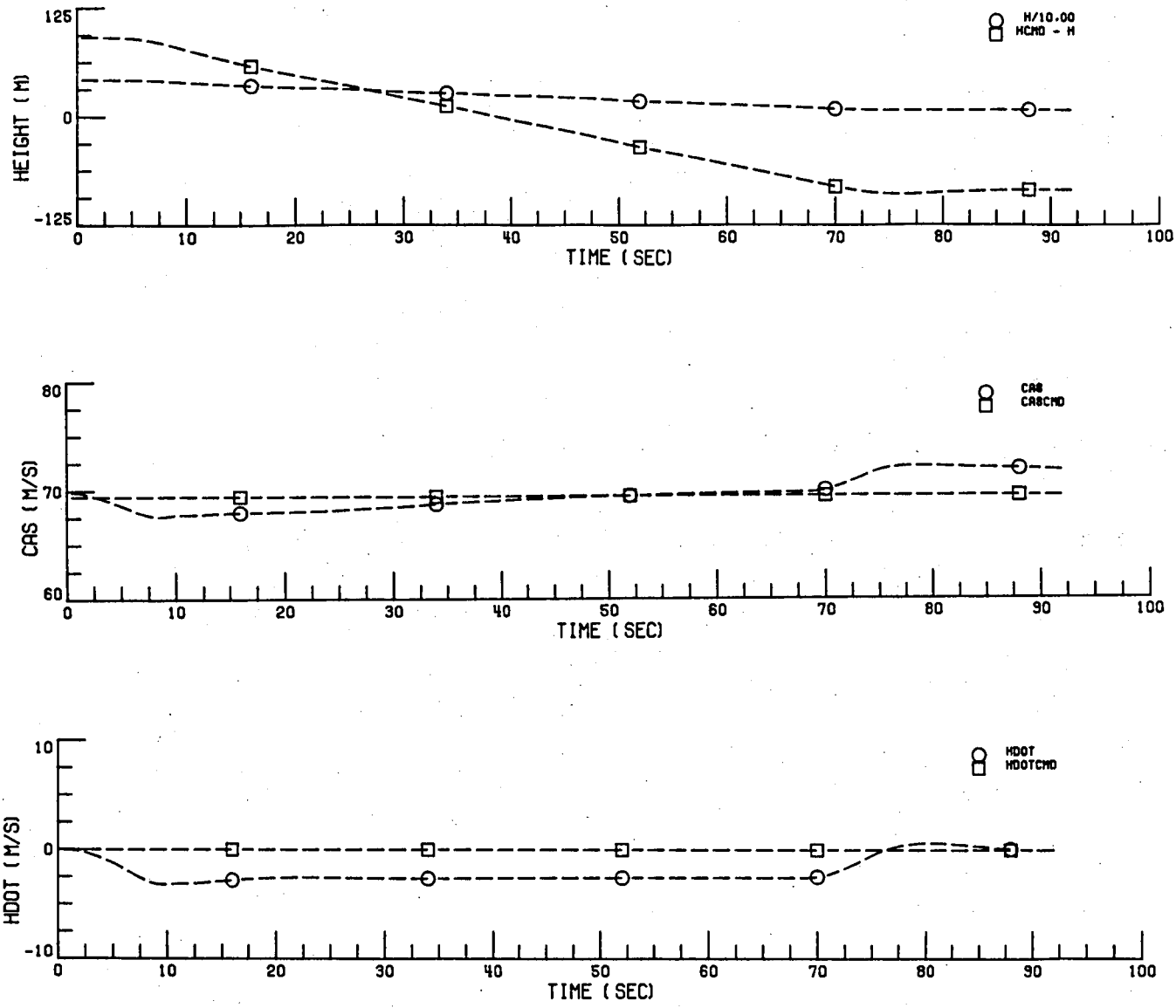

FIGURE 7. SR-PIFCGT GLIDESLOPE CAPTURE AND TRACK WITH NO WINDSHEAR AND NO GUSTS

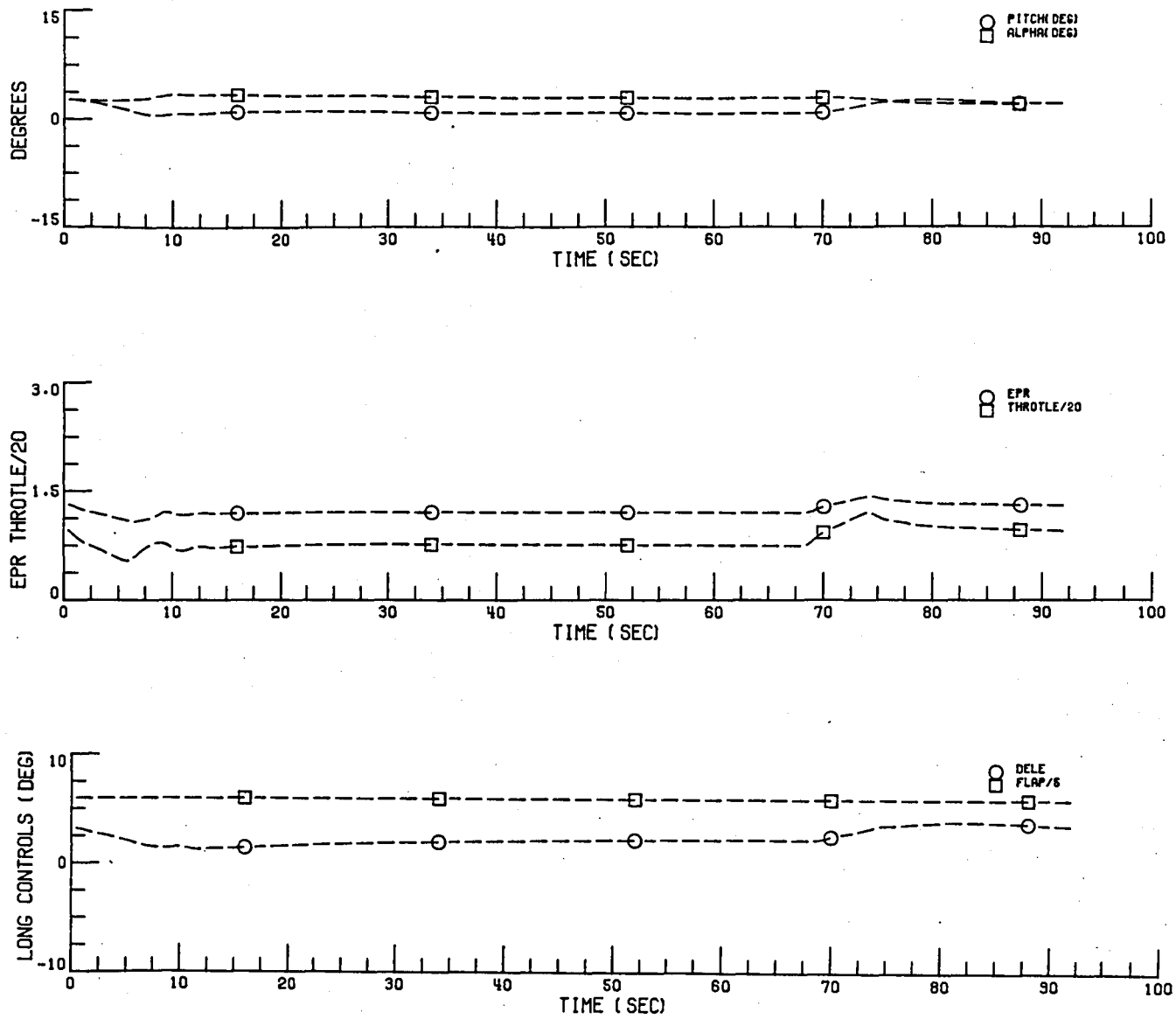

FIGURE 7. SR-PIFCGT GLIDESLOPE CAPTURE AND TRACK WITH NO WINDSHEAR AND NO GUSTS (CONCLUDED)

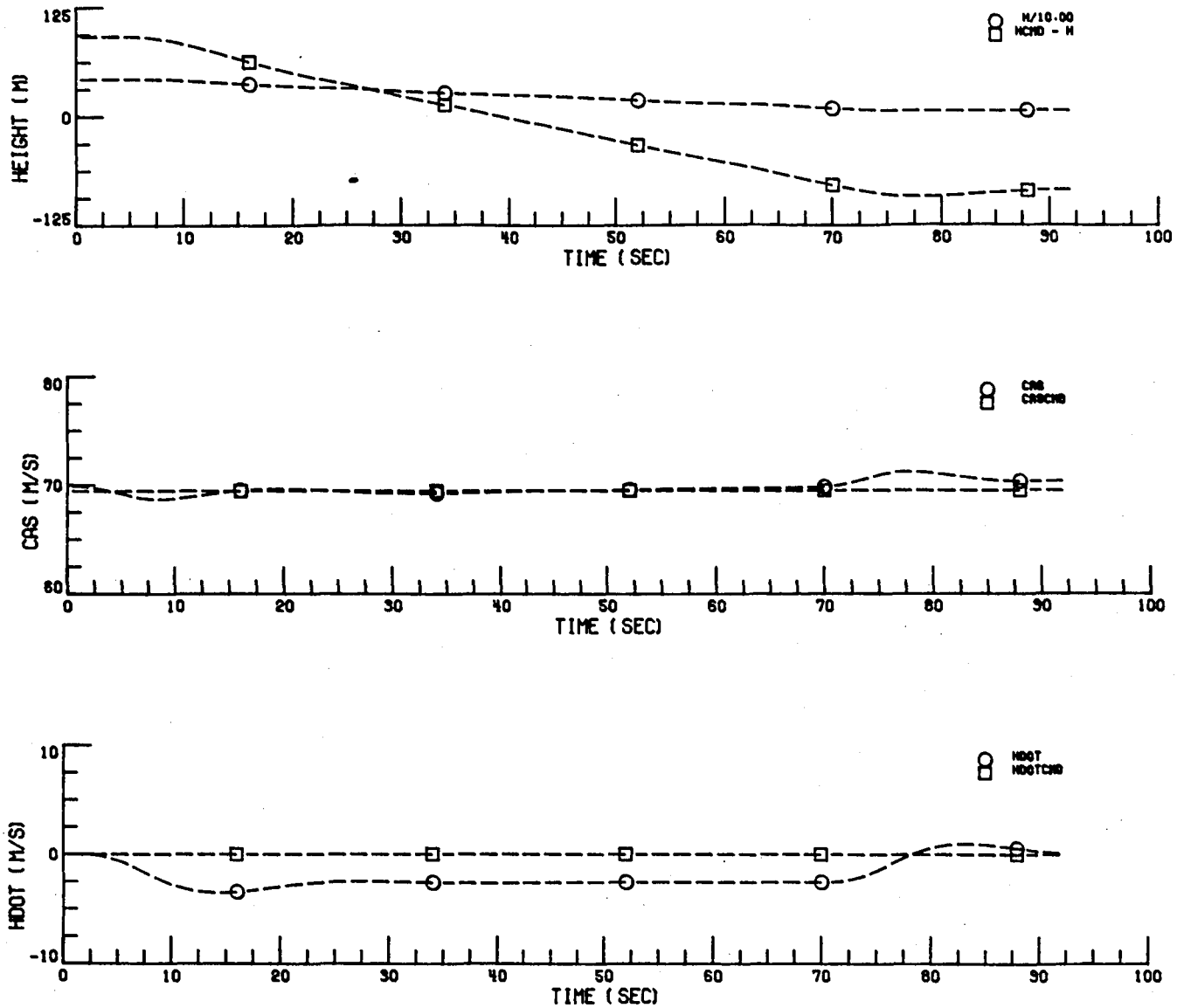

FIGURE 8. MR-PIFCGT GLIDESLOPE CAPTURE AND TRACK WITH NO WINDSHEAR AND NO GUSTS

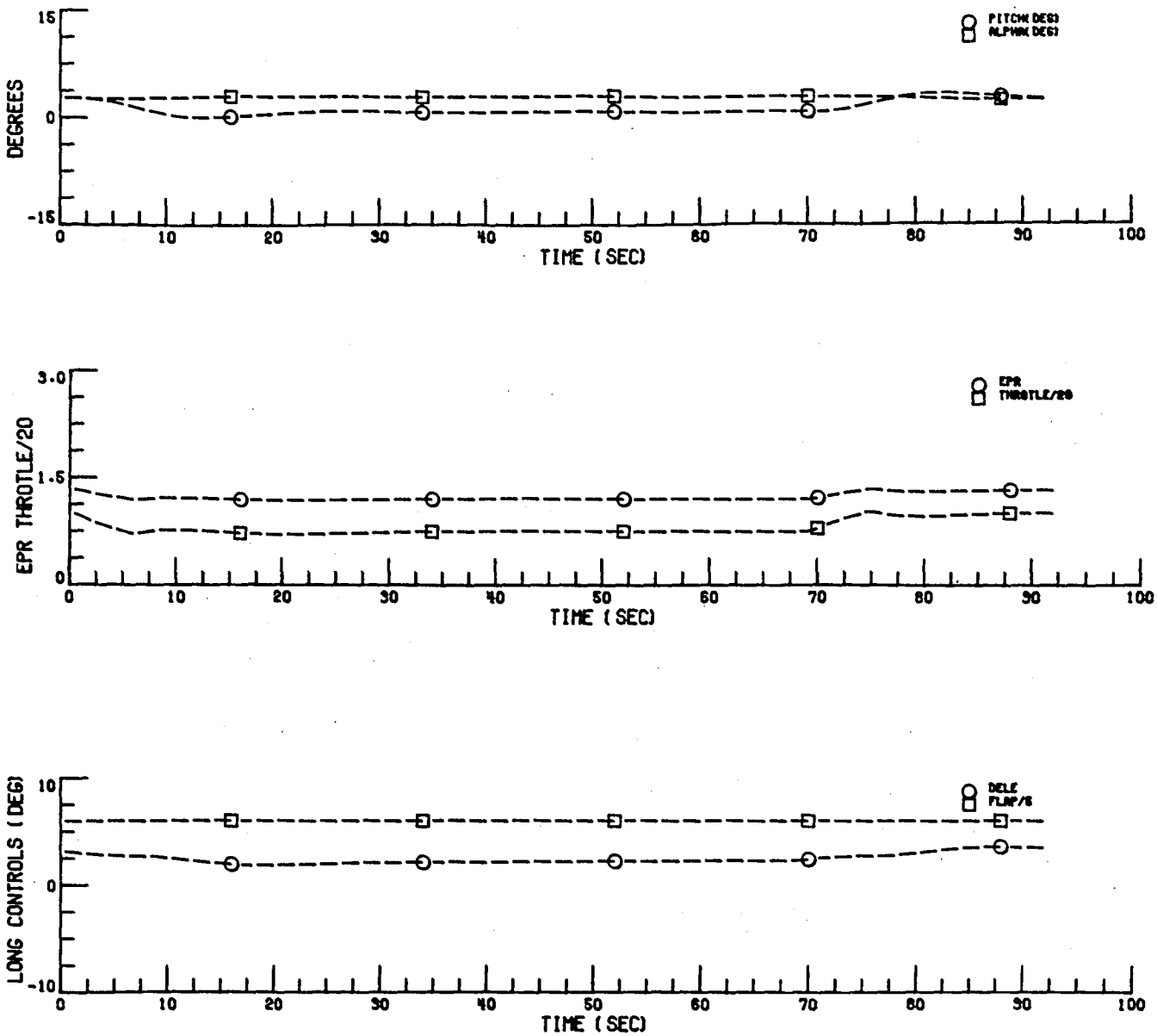

FIGURE 8. MR-PIFCGT GLIDESLOPE CAPTURE AND TRACK WITH NO WINDSHEAR AND NO GUSTS (CONCLUDED)

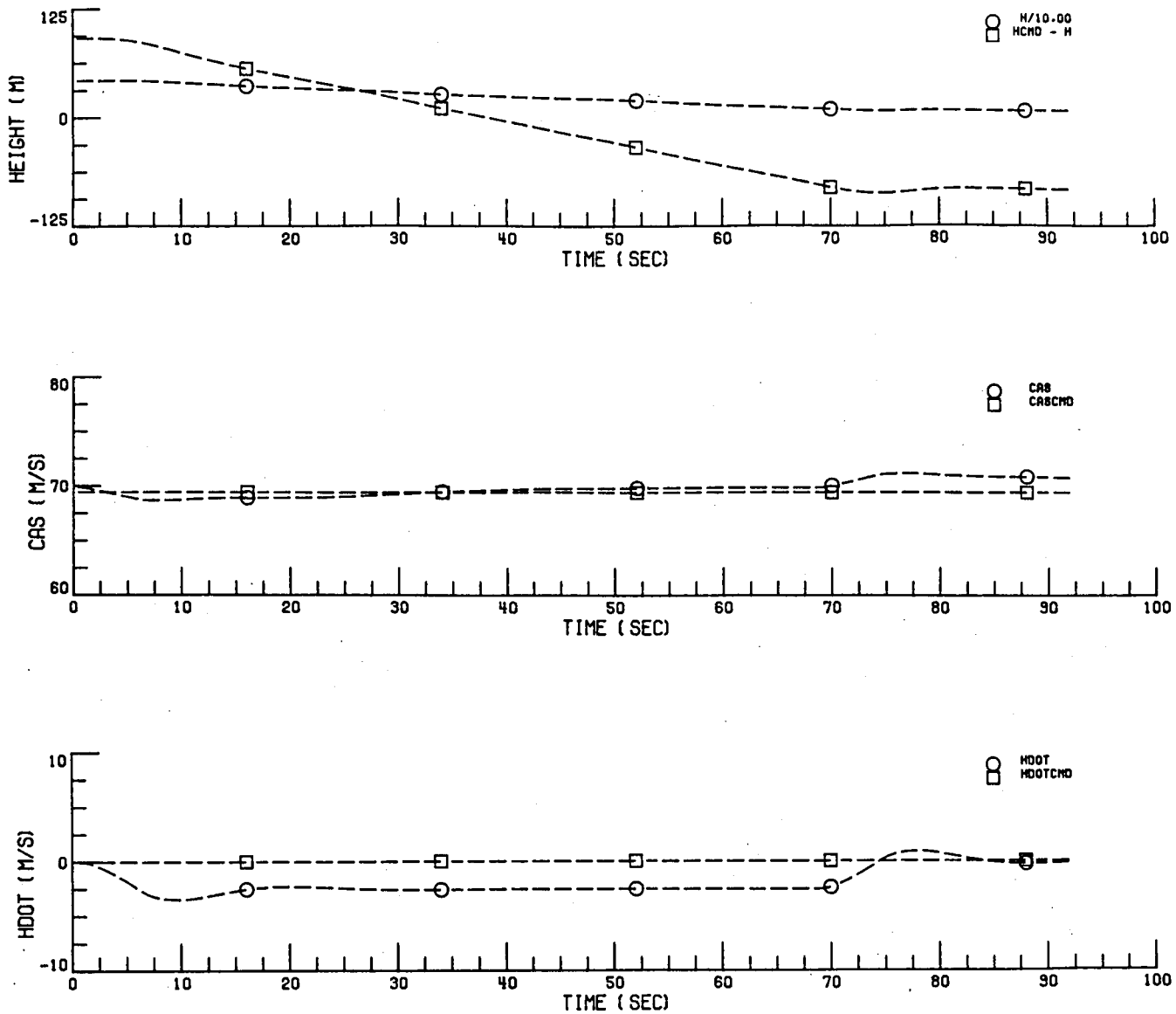

FIGURE 9. WS-PIFCGT GLIDESLOPE CAPTURE AND TRACK WITH NO WINDSHEAR AND NO GUSTS

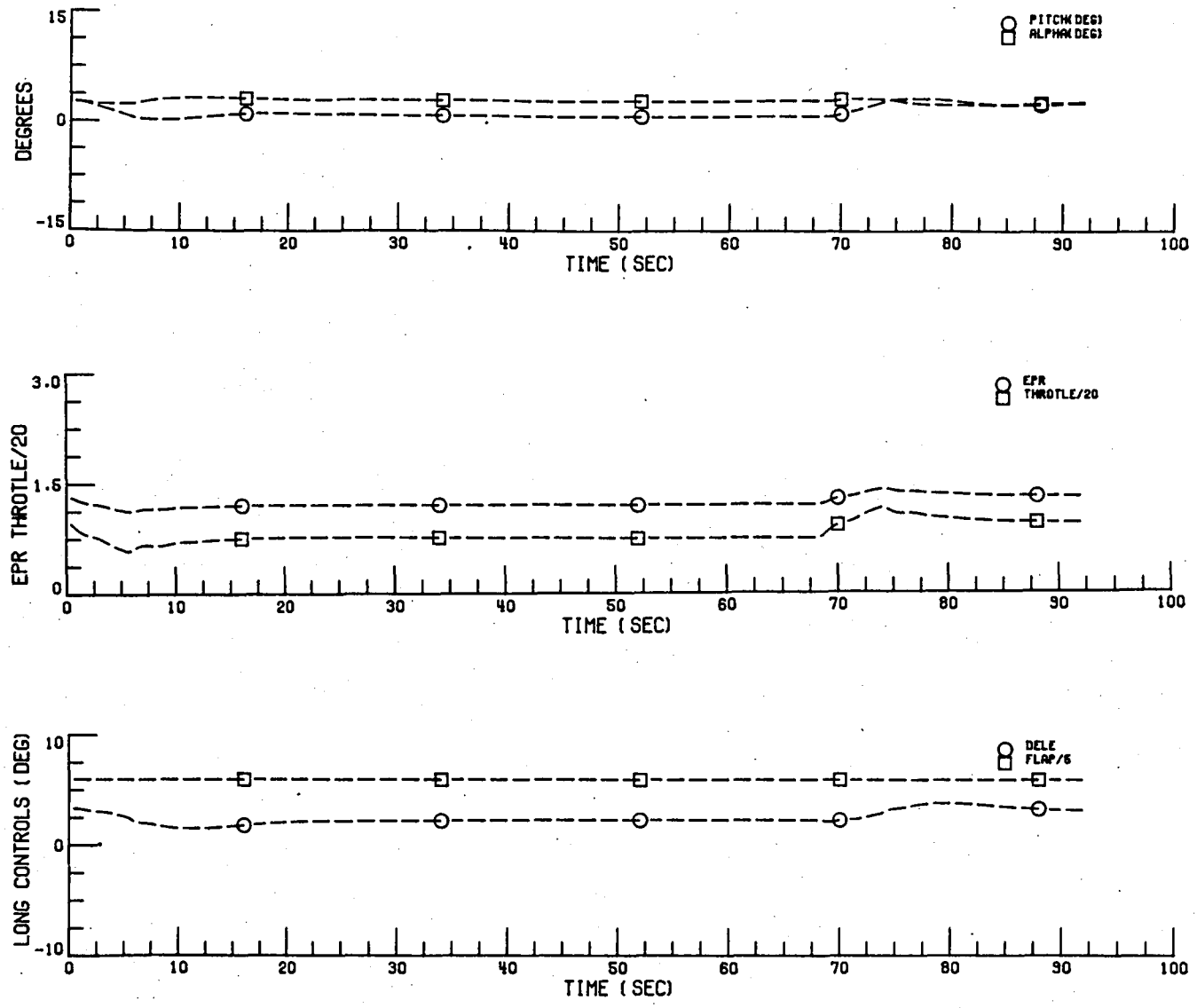

FIGURE 9. WS-PIFCGT GLIDESLOPE CAPTURE AND TRACK WITH NO WINDSHEAR AND NO GUSTS (CONCLUDED)

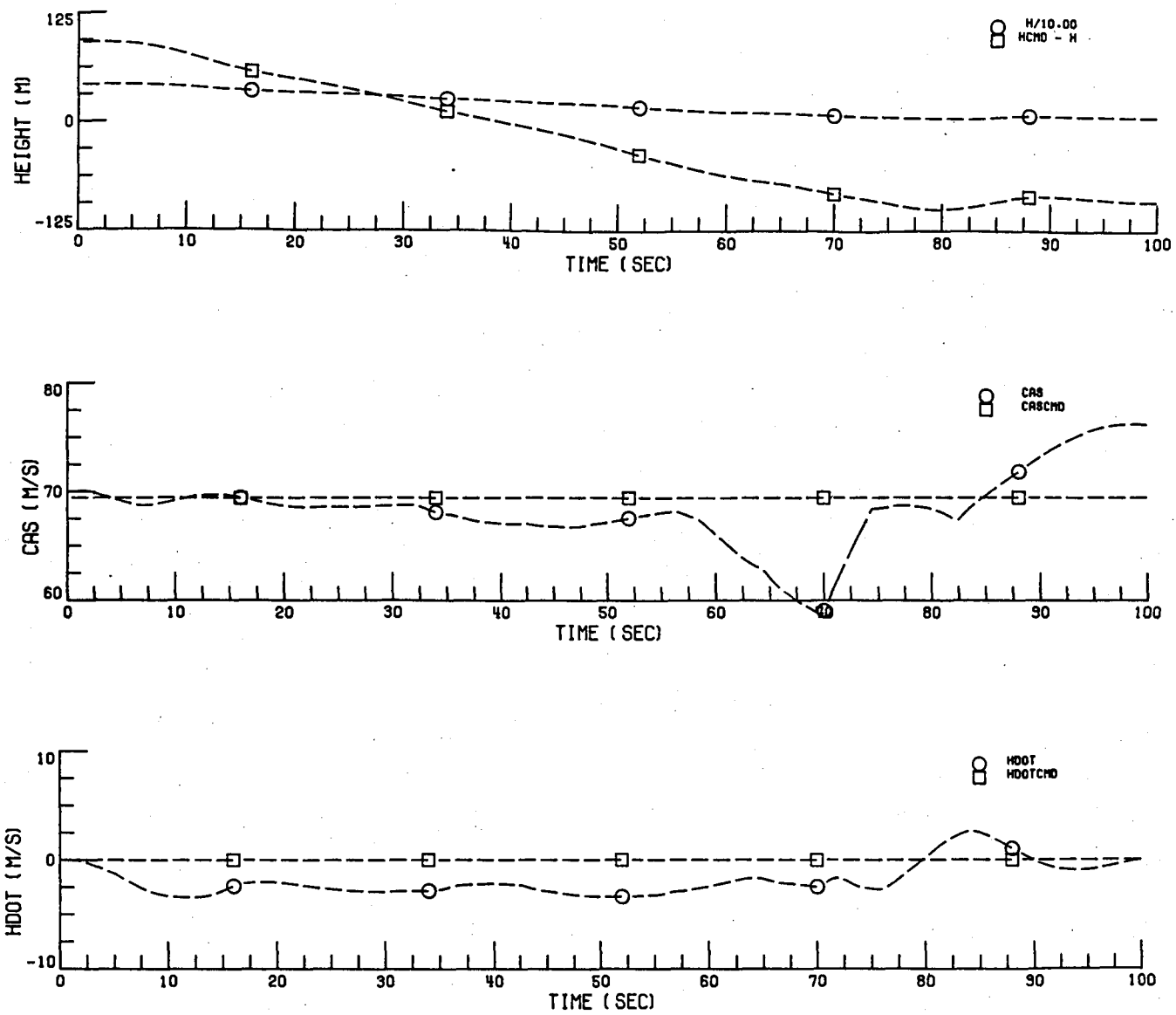

FIGURE 10. SR-PIFCGT GLIDESLOPE CAPTURE AND TRACK WITH WINDSHEAR AND NO GUSTS

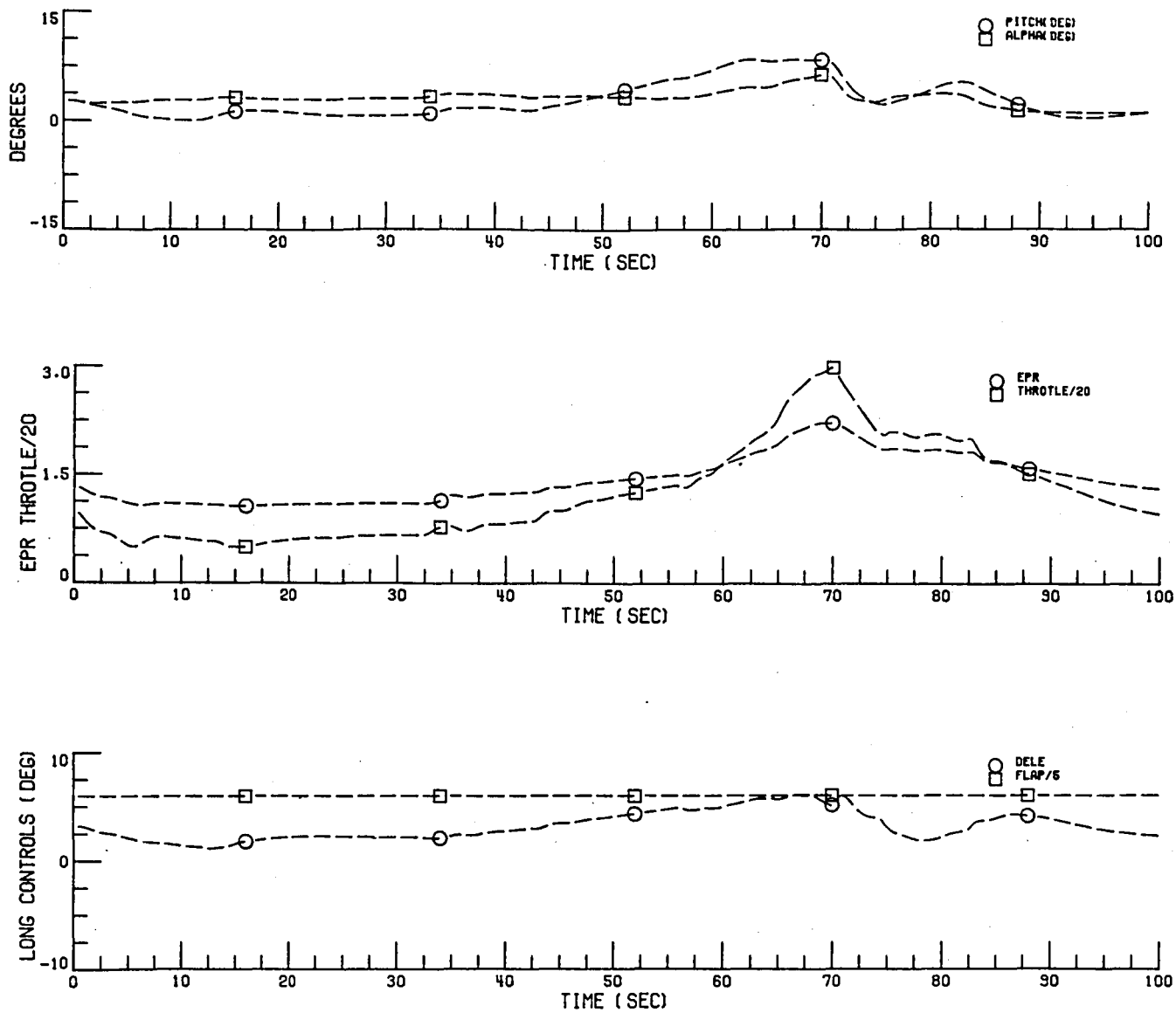

FIGURE 10. SR-PIFCGT GLIDESLOPE CAPTURE AND TRACK WITH WINDSHEAR AND NO GUSTS (CONCLUDED)

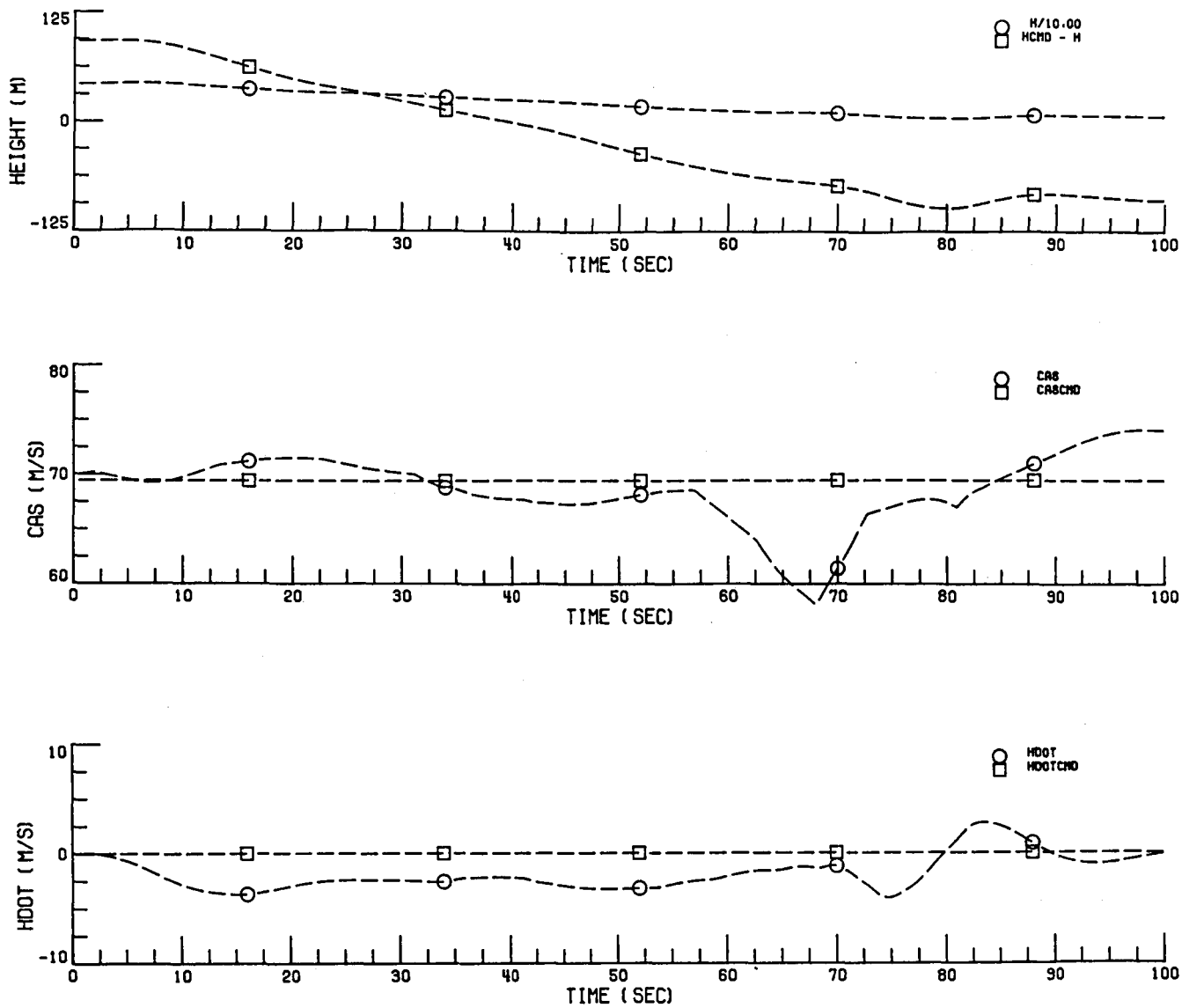

FIGURE 11. MR-PIFCGT GLIDESLOPE CAPTURE AND TRACK WITH WINDSHEAR AND NO GUSTS

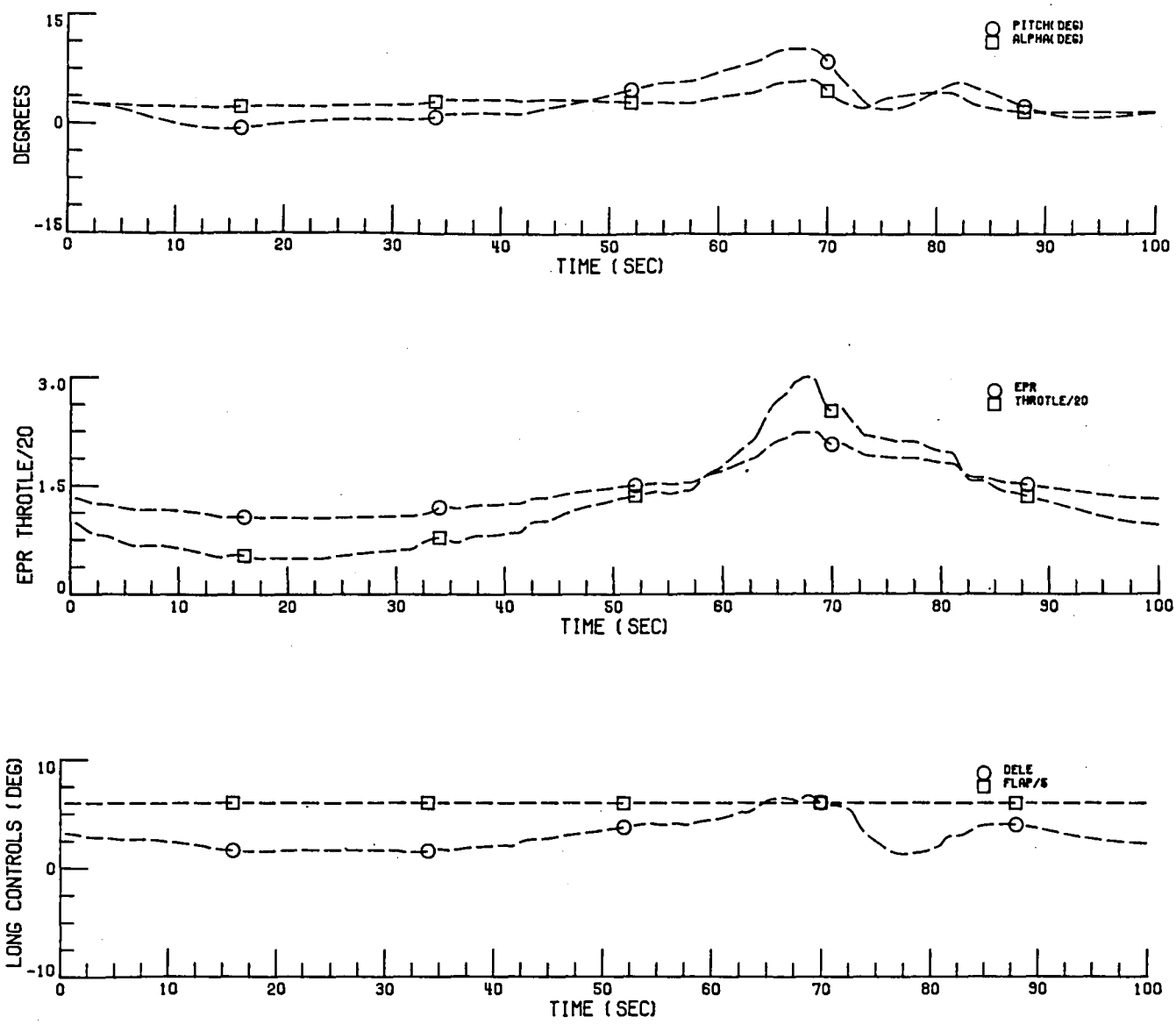

FIGURE 11. MR-PIFCGT GLIDESLOPE CAPTURE AND TRACK WITH WINDSHEAR AND NO GUSTS (CONCLUDED)

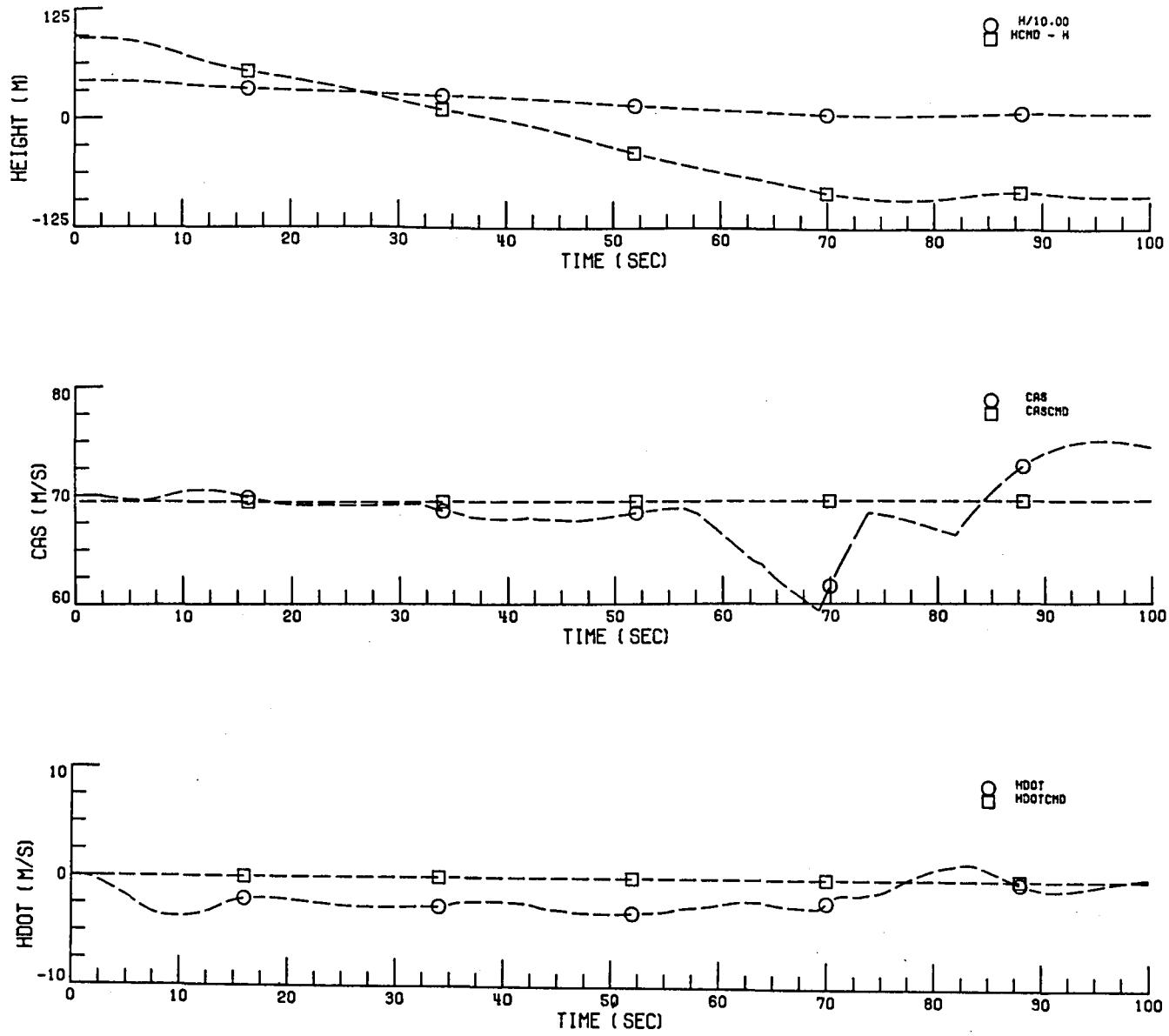

FIGURE 12. WS-PIFCGT GLIDESLOPE CAPTURE AND TRACK WITH WINDSHEAR AND NO GUSTS

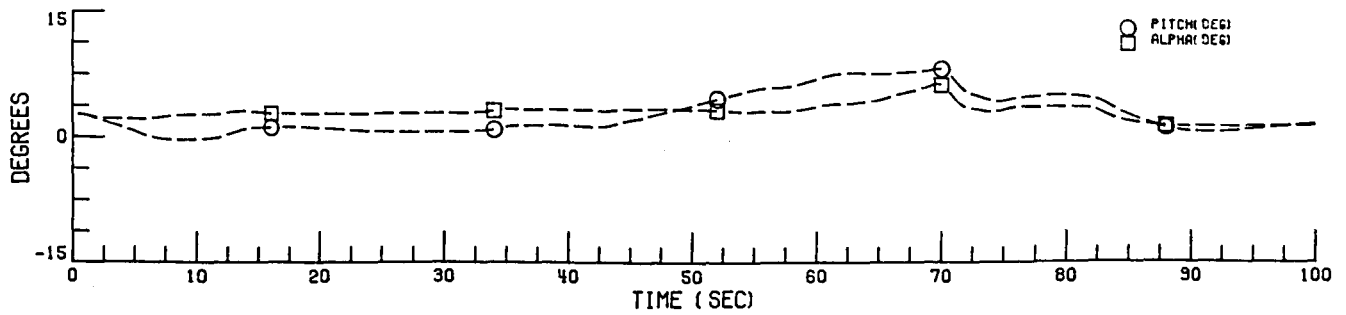

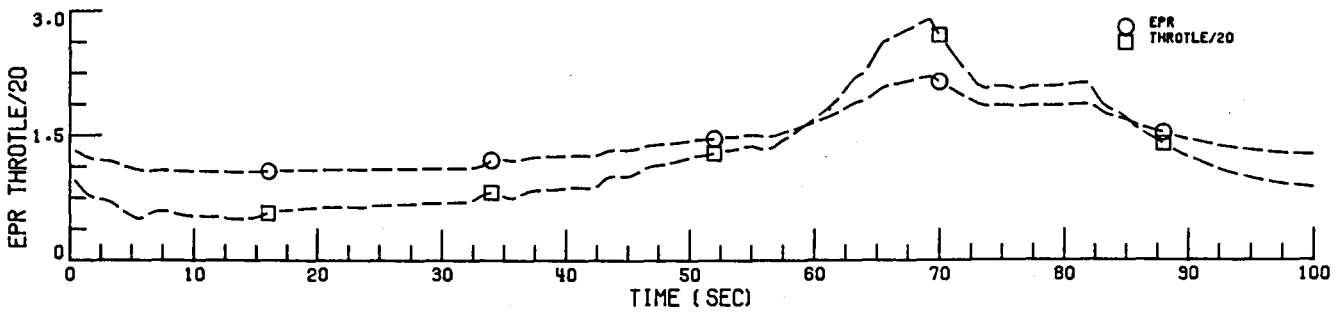

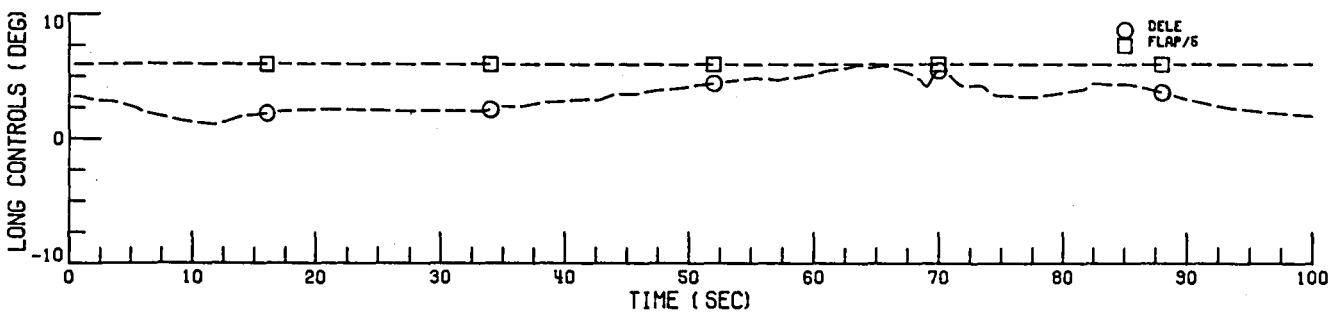

FIGURE 12. WS-PIFCGT GLIDESLOPE CAPTURE AND TRACK WITH WINDSHEAR AND NO GUSTS (CONCLUDED)

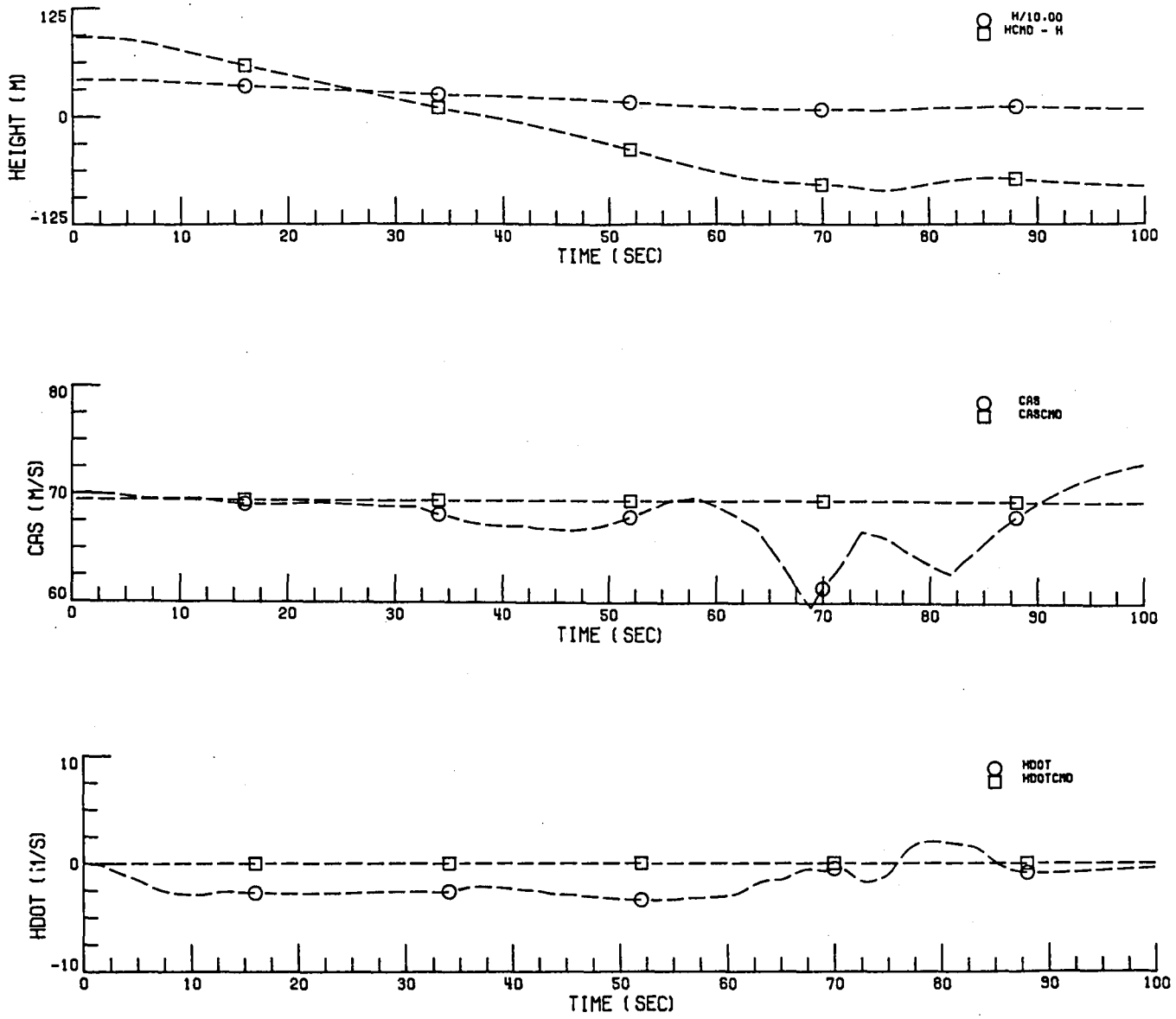

FIGURE 13. EP-PIFCGT GLIDESLOPE CAPTURE AND TRACK WITH WINDSHEAR AND NO GUSTS

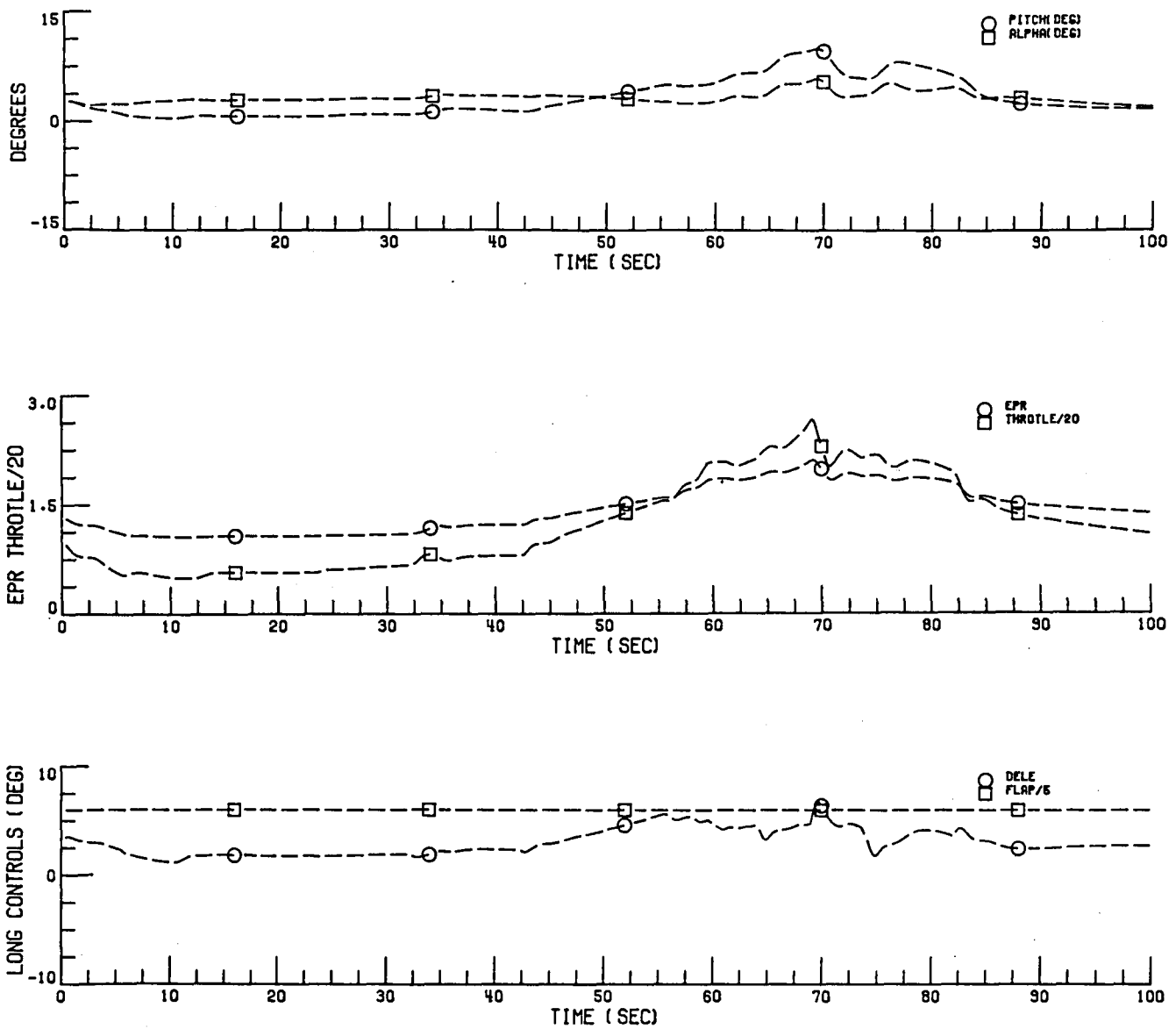

FIGURE 13. EP-PIFCGT GLIDESLOPE CAPTURE AND TRACK WITH WINDSHEAR AND NO GUSTS (CONCLUDED)

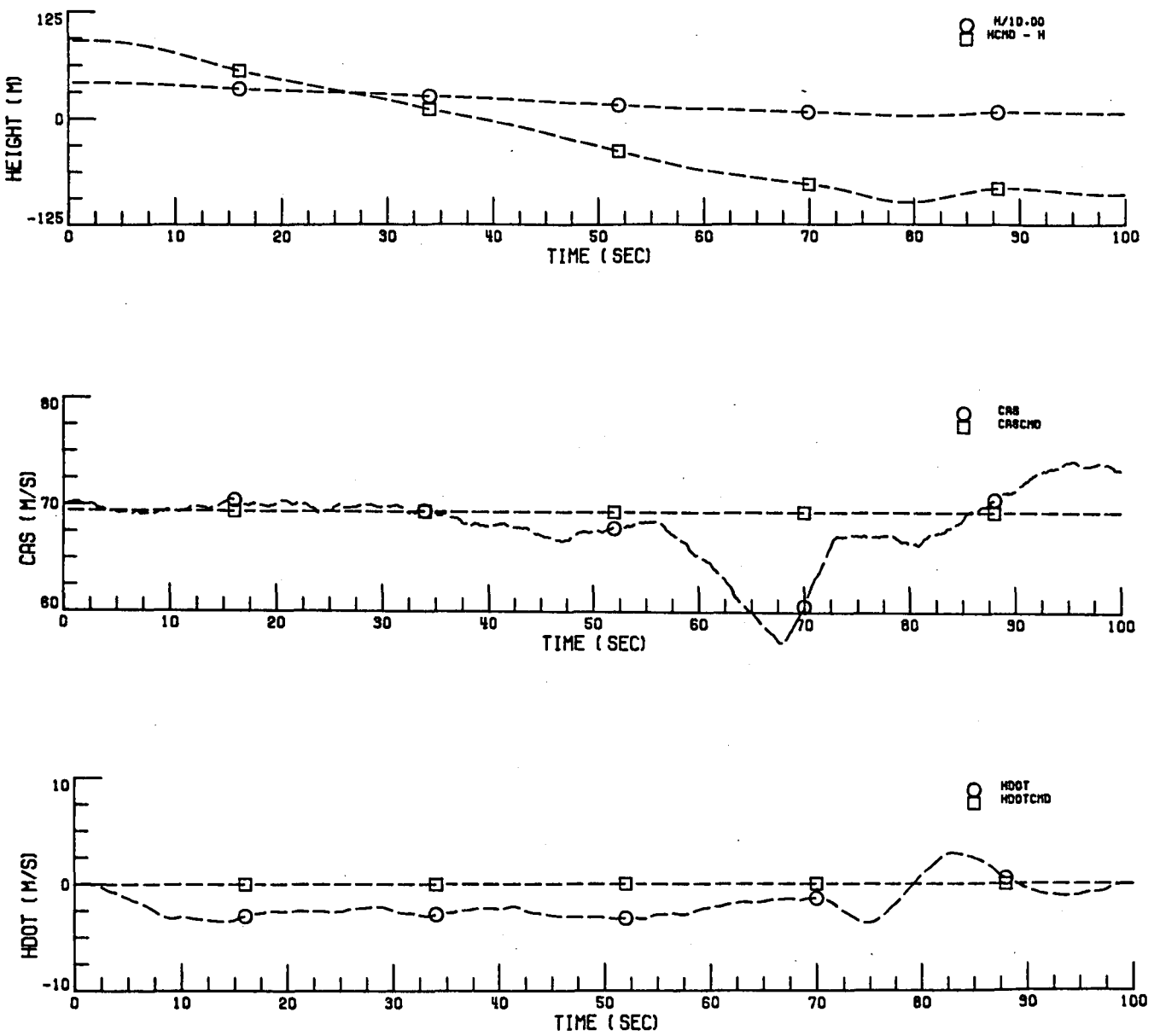

FIGURE 14. SR-PIFCGT GLIDESLOPE CAPTURE AND TRACK WITH WINDSHEAR AND A 1kt GUST

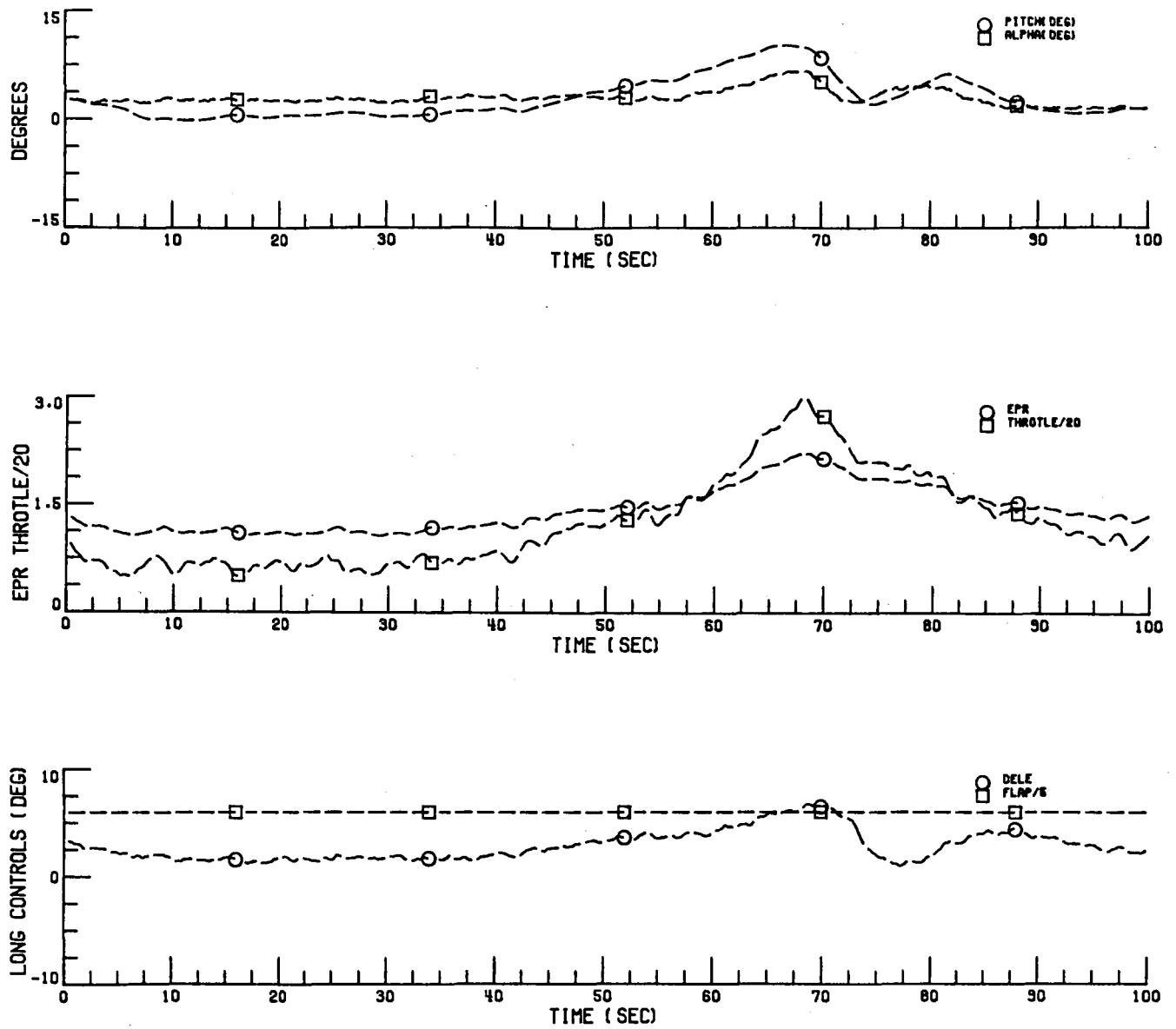

FIGURE 14. SR-PIFCGT GLIDESLOPE CAPTURE AND TRACK WITH WINDSHEAR AND A 1kt GUSTS (CONCLUDED)

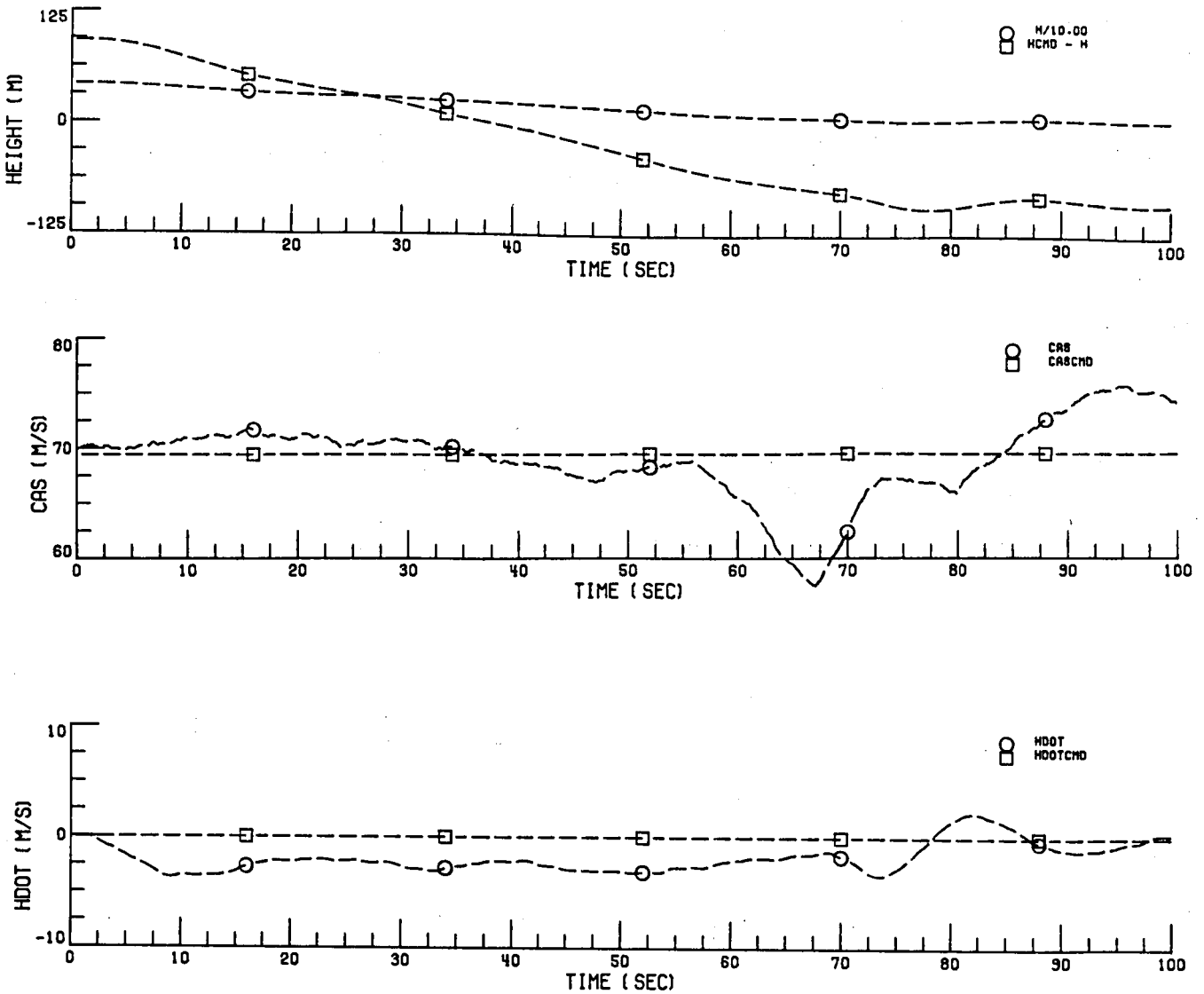

FIGURE 15. MR-PIFCGT GLIDESLOPE CAPTURE AND TRACK WITH WINDSHEAR AND A 1kt GUST

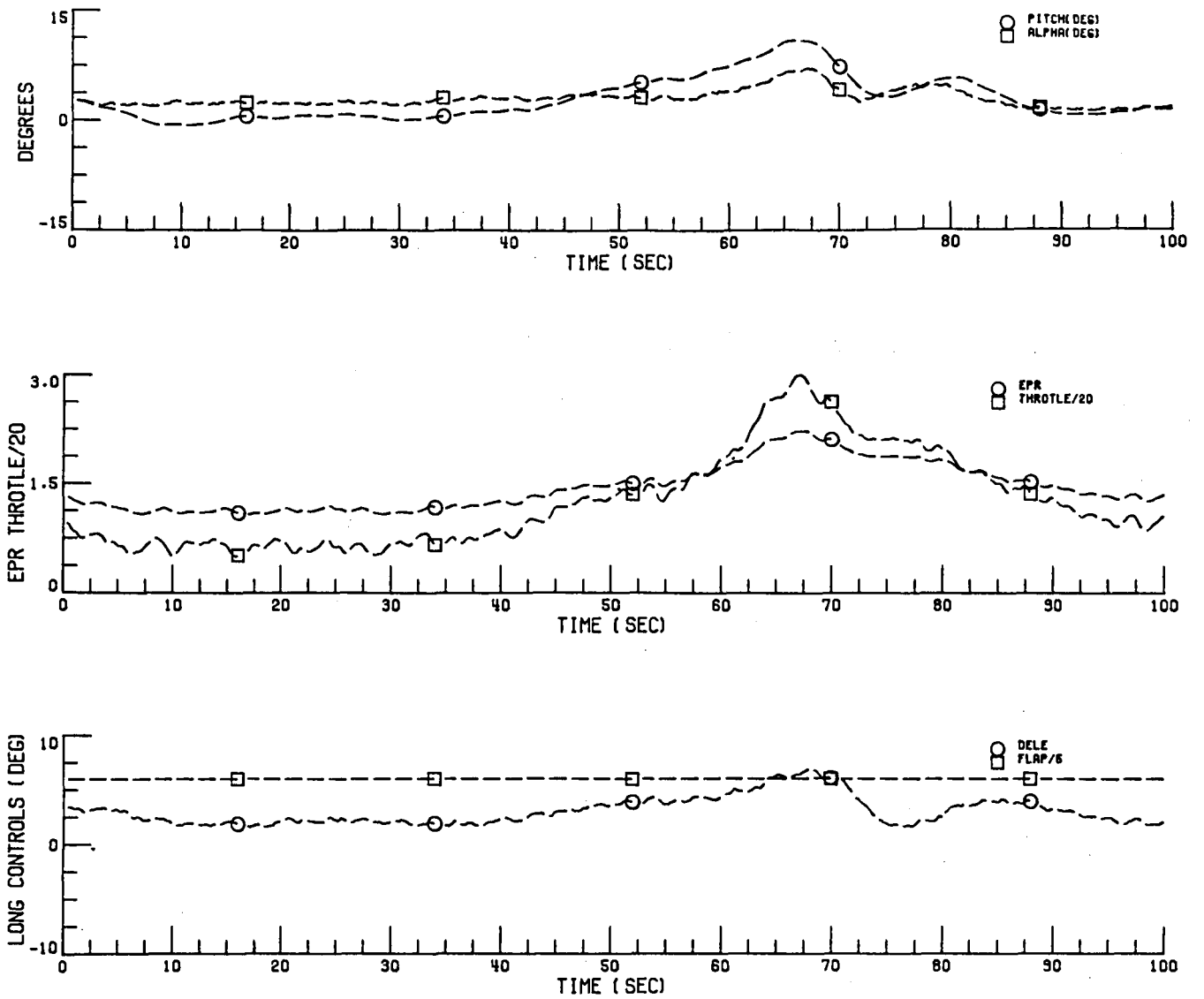

FIGURE 15. MR-PIFCGT GLIDESLOPE CAPTURE AND TRACK WITH WINDSHEAR AND A 1kt GUST (CONCLUDED)

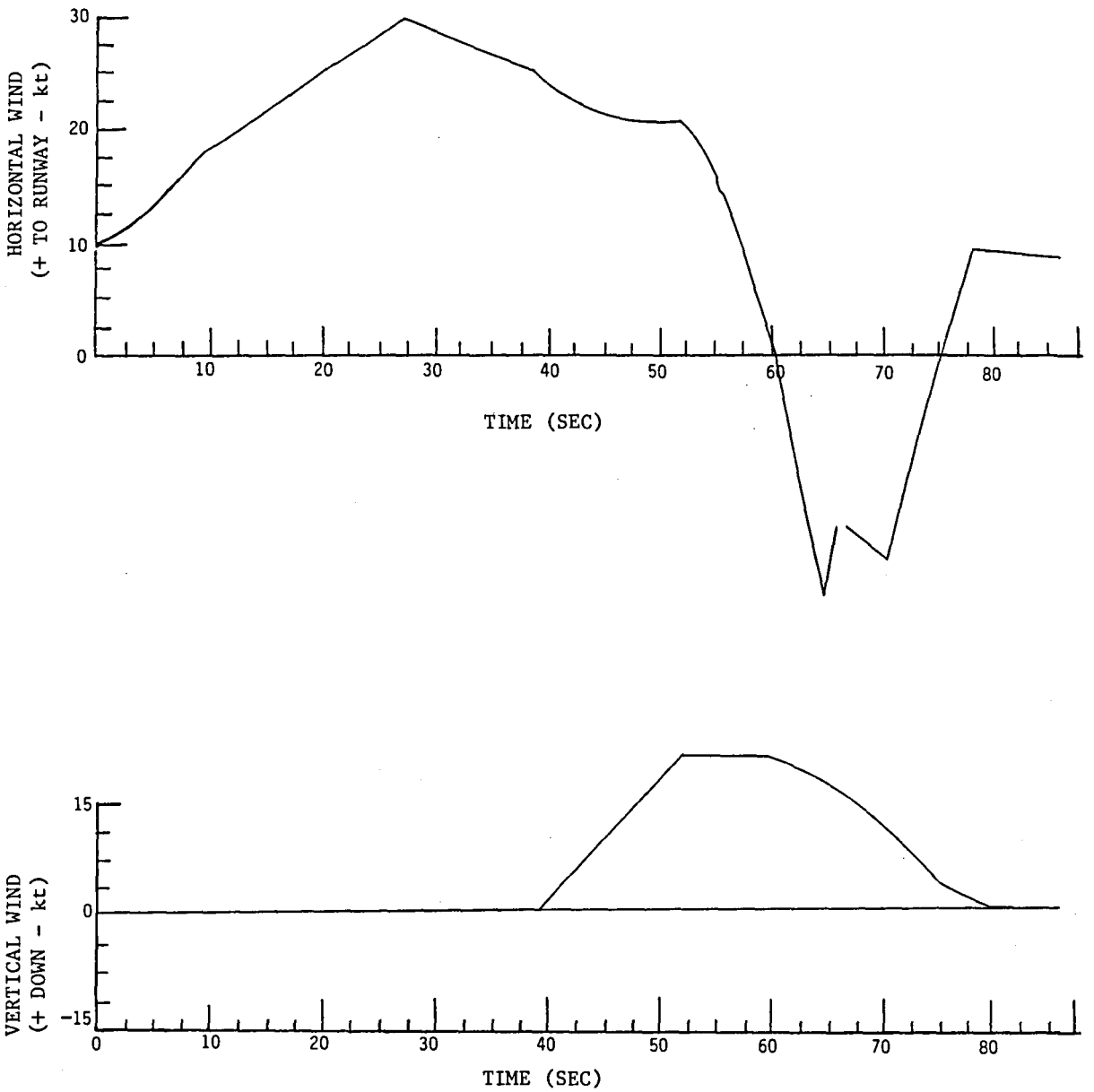

FIGURE 16. HORIZONTAL VERTICAL WINDSHEARS AFFECTING THE AIRCRAFT DYNAMICS

1. Report No.	2. Government Accession No.	3. Recipient's Catalog No.
NASA CR-3968		

4. Title and Subtitle	5. Report Date
Extensions to PIFCGT: Multirate Output Feedback and Optimal Disturbance Suppression	March 1986
	6. Performing Organization Code
7. Author(s)	8. Performing Organization Report No.
John R. Broussard	IR 684105
	10. Work Unit No.
9. Performing Organization Name and Address	11. Contract or Grant No.
Information & Control Systems, Incorporated 28 Research Drive Hampton, VA 23666	NAS1-17493
	13. Type of Report and Period Covered
12. Sponsoring Agency Name and Address	Contractor Report
National Aeronautics and Space Administration Washington, DC 20546	14. Sponsoring Agency Code 505-45-33-04

15. Supplementary Notes

Langley Technical Monitor: Richard M. Hueschen

16. Abstract

This report contains the theoretical development and the practical application of new control synthesis procedures for digital flight control systems. The new theoretical developments are the solution to the problem of optimal disturbance suppression in the presence of windshear. Control synthesis is accomplished using a linear quadratic cost function, the command generator tracker for trajectory following and the proportional-integral-filter control structure for practical implementation. Extensions are made to the optimal output feedback algorithm for computing feedback gains so that the multi-rate and optimal disturbance control designs are computed and compared for the Advanced Transport Operating System (ATOPS). The performance of the designs is demonstrated using closed-loop poles, frequency domain multi-input sigma and eigenvalue plots and detailed nonlinear 6-DOF aircraft simulations in the terminal area in the presence of windshear.

17. Key Words (Suggested by Author(s))	18. Distribution Statement
Optimal Control - Theory Optimal Control - Application Digital Flight Control System Multirate Control, Output Feedback Disturbance Accommodation	Unclassified - Unlimited Subject Category 08

19. Security Classif. (of this report)	20. Security Classif. (of this page)	21. No. of Pages	22. Price
Unclassified	Unclassified	122	A06

For sale by the National Technical Information Service, Springfield, Virginia 22161

NASA-Langley, 1986

End of Document